The role of the influenza A virus genotype on NF-κB function and phosphorylation networks

INAUGURALDISSERTATION

zur Erlangung des Doktorgrades der Naturwissenschaften

(Doctor rerum naturalium - Dr. rer. nat.)

angefertigt am Biochemischen Institut

des Fachbereich Medizin und dem Fachbereich Biologie und Chemie

der Justus-Liebig-Universität Gießen

vorgelegt von

Sharmistha Dam

Giessen, January 2018

Dekan: Prof. Dr. Volker Wissemann

Institut für Botanik

Fachbereich Biologie und Chemie

Justus-Liebig-Universität Gießen

1. Gutachter: Prof. Dr. Michael U. Martin

Institut für Immunologie

Fachbereich Biologie und Chemie

Justus-Liebig-Universität Gießen

2. Gutachter: Prof. Dr. M. Lienhard Schmitz

Biochemisches Institut

Fachbereich Medizin

Justus-Liebig-Universität Gießen

EIDESSTATTLICHE ERKLÄRUNG

Ich erkläre: Ich habe die vorgelegte Dissertation selbständig und ohne unerlaubte fremde Hilfe und nur mit den Hilfen angefertigt, die ich in der Dissertation angegeben habe. Alle Textstellen, die wörtlich oder sinngemäß aus veröffentlichten Schriften entnommen sind, und alle Angaben, die auf mündlichen Auskünften beruhen, sind als solche kenntlich gemacht. Bei den von mir durchgeführten und in der Dissertation erwähnten Untersuchungen habe ich die Grundsätze guter wissenschaftlicher Praxis, wie sie in der „Satzung der Justus-Liebig-Universität Gießen zur Sicherung guter wissenschaftlicher Praxis“ niedergelegt sind, eingehalten.

Sharmistha Dam

Giessen, den 04.01.2018

Table of Contents

List of abbreviations

°C : Degree Celsius

µg : Microgram

µl : Microliter

µM : Micromolar

aa : Amino acids

AIV : Avian influenza virus

Amp : Ampicillin

bp : Base pairs

BSA : Bovine serum albumin

cDNA : Complementary DNA

cm : Centimeter

CRISPR : Clustered regularly interspaced short palindromic repeat

C-terminal : Carboxyl-terminal

ddH2O : Deionized distilled water

DMEM : Dulbecco's Modified Eagle's medium

DMSO : Dimethyl sulfoxide

DNA : Deoxyribonucleic acid

dNTP : Deoxynucleoside triphosphate

DTT : Dithiothreitol

E : Glutamic acid

E.coli : *Escherichia coli*

ECL : Enhanced chemiluminescence

EDTA : Ethylenediamine tetraacetic acid

FCS : Fetal calf serum

FFU : Foci forming unit(s)

g : Acceleration of gravity

g : gram

h : hour(s)

HA : Hemagglutinin

HPAIV : Highly pathogenic avian influenza virus

HRP : Horse reddish peroxidase

IκB : Inhibitor of NF-κB

IFN : Interferon

IFNβ : Interferon beta

IKK : IκB kinase

IKKε : IκB kinase epsilon

IL : Interleukin

IRF3 : Interferon regulatory factor 3

IV : Influenza virus

IVA : Influenza virus A

kb : Kilo base pairs

kDa : Kilo Dalton

L : Liter

LPAIV : Low pathogenic avian influenza virus

M : Molar

M1 : Matrix protein 1

M2 : Matrix protein 2

mg : Milligram

min : Minute(s)

ml : Milliliter

MLE-15 : Mouse lung epithelial cell 15

mM : Millimolar

MOI : Multiplicity of infection

mRNA : Messenger RNA

NA : Neuraminidase

NCR : Non-coding region

NEMO : NF-κB essential modulator

NEP/NS2 : Nuclear export factor

NP : Nucleocapsidprotein

NS1 : Nonstructural protein

nt : Nucleotide(s)

N-terminus : NH2 terminus of protein

OD : Optical density

p.i. : Post infection

P/S : Penicillin/streptomycin

PA : Polymerase acidic protein

PAGE : Polyacrylamide gel electrophoresis

PB1 : Polymerase basic protein 1

PB1-F2 : Polymerase basic protein 1-F2

PB2 : Polymerase basic protein 2

PBS : Phosphate buffered saline

Pol I : RNA polymerase I

Pol II : RNA polymerase II

PolyA : Polyadenylic acid

RdRp : RNA-dependent RNA-polymerase

RNA : Ribonucleic acid

rpm : Rounds per minute

rRNA : Ribosomal ribonucleic acid

RT-PCR : Reverse transcriptase-polymerase chain reaction

Ser : Serine

SDS : Sodium dodecyl sulfate

TEMED : N,N,N',N'-tetramethylethylenediamine

Thr : Threonine

Tween 20 : Polyoxyethylenesorbiten monolaurate

Tyr : Tyrosine

U : Units

V : Volt

v/v : Volume percentage

vRNA : Viral RNA

w/v : Weight percentage

wt :Wild-type

1 Introduction

1.1 Influenza viruses (IVs)

IVs were first isolated by Wilson Smith in 1933 (Smith, 1933). Four different types of IVs are known: influenza virus A (IAV), influenza virus B (IBV), influenza virus C (ICV) and influenza virus D (IDV) (Ferguson et al., 2015; Palese and Young, 1982). They have different host ranges, genome organization, and morphology. IAV and IBV cause seasonal epidemics of disease in human almost every winter. IBV and ICV are diverged from the IAV lineage and circulate almost exclusively in humans. IDV is the new addition to this virus family that is only known to affect cattle (Ferguson et al., 2015).

1.2 IAV

Compared to other types of IVs, IAV is the most virulent pathogen for human. IAVs infect not only humans but also other species such as ducks, chickens, pigs, whales, horses and seals (Ito, 2000). Wild aquatic birds are the natural host of this type of IV, which can cause pandemic and epidemic outbreaks. IAV infection can be life threatening. IAV have different subtypes according to the antigenicity of the two surface glycoproteins of the virus;18 known types of haemagglutinin (HA) and 11 known types of neuraminidase (NA) proteins, in total 198 different combinations of these proteins are possible (Ozawa and Kawaoka, 2011). For example, the H7N7 virus designates an influenza A subtype that has a type7 HA protein and a type7 NA protein.

1.2.1 IAV transmission

IAVs can be transmitted from their natural host to humans in different ways. Humans can get an infection when they come in direct contact with infected species or are being contaminated

by an infected object or inhale virus particles (Carrat et al., 2008). But IAVs can infect humans also indirectly by transmission from aquatic wild birds to domestic birds and further transmission to pigs or humans. Pigs are considered as mixing vessels as they can be infected by human and avian IAVs, potentially allowing the production of reassorted viruses (Ma et al., 2009). This inter-species-transmission is schematically shown in Fig. 1.

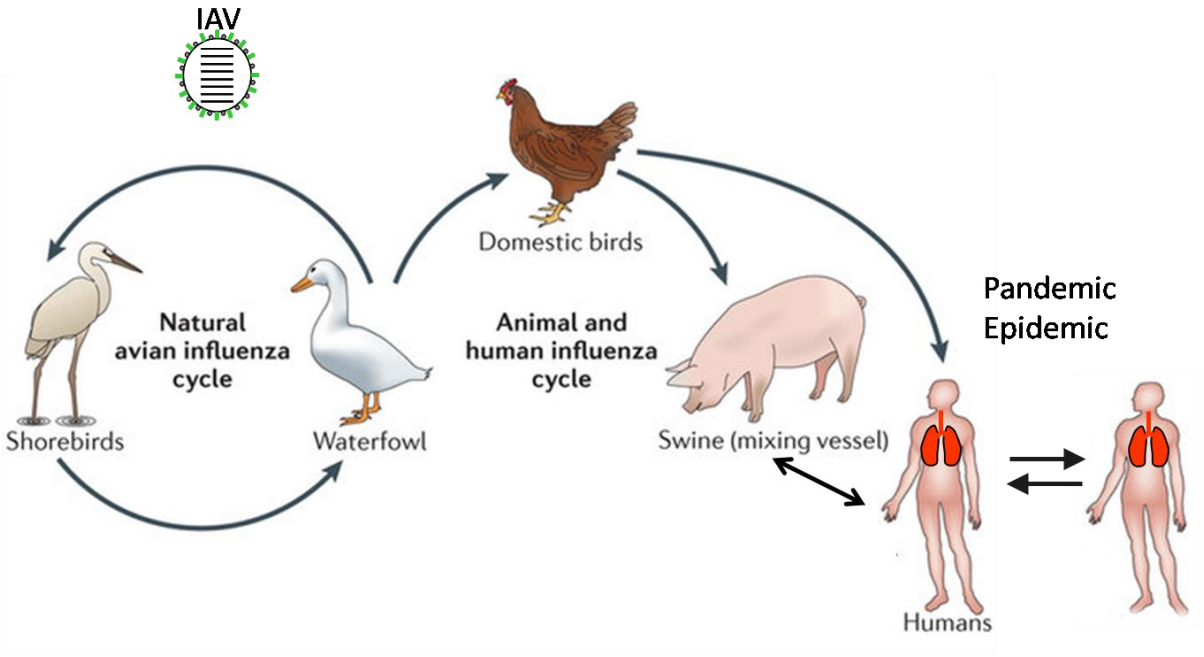

Figure 1: Animal and human IAV transmission cycle. Wild aquatic birds are the natural reservoir of avian IAVs. IAVs can be transmitted to a broad variety of other hosts, including domestic birds, pigs, and humans. Both avian and human viruses can infect swines and might produce reassorted virus. This reassorted virus can eventually infect humans and birds and lead to the generation of pandemic viruses. The representation is modified from (Shi et al., 2014).

1.2.2 Morphology of IAVs

IAVs are enveloped viruses with single stranded RNA genome of negative polarity (Lamb, 2001). IAV possess 8 genome segments (Table 1) that code for at least 10 viral proteins. The infectious particle of IAV is called virion. IAV virions are spherical in shape and have a diameter of 80 to 120 nm, but they have the ability to change their shape and size in response to environmental conditions (Lamb, 2001). These changes in size and shape are dependent on the viral strain and on the cell type used for propagation (Manz et al., 2013).

1.2.3 IAV structure and protein functions

The IAV envelope is made up from a lipid bilayer, which is derived from the host cell membrane when a new virus particle is formed. This virus particle is composed of two different kind of spike-like structures on the outside, which are known as structural glycoproteins HA and NA. In the virion the number of HA molecules is five times higher than the number of NA molecules (Kawaoka, 2007). HA forms trimers which have a cylinder-like shape whereas the NA forms tetramers assembling into a mushroom-like shape (Skehel and Wiley, 2000). HA functions to allow SA receptor binding and membrane fusion to promote the viral entry, whereas NA plays an important role in the virus budding process (Nayak et al., 2004). HA is synthesized as a precursor molecule (HA0). HA0 is glycosylated and cleaved into the HA1 and HA2 subunits. These subunits are joined by a disulfide bond (Jiang et al., 2010). The HA cleavage is important to activate the fusion activity of the HA leading to membrane fusion between the viral envelop and the host cell membrane and is therefore necessary for viral infectivity (Skehel and Wiley, 2000). HA and NA are antigens that can be recognized by the immune system. Antibodies against the HA (and partially against NA) can lead to protection against viral infection. The approved antiviral drugs Relenza® and Tamiflu® are functioning as NA inhibitors (Tuna et al., 2012).

The smallest genome segment of IAV encodes two major proteins. The matrix protein 1 (M1) is encoded protein by unspliced messenger RNA (mRNA). The spliced mRNA encodes matrix protein 2 (M2), as well as other minor proteins, the matrix protein 3 (M3) and matrix protein 42 (M42) (Wise et al., 2012). M1 underlies the inner surface of the viral envelope. It is the most abundant protein and is very important for virus replication (Shaw, 2013). The M1 has an important functional role for the import and export of the viral ribonucleo protein complexes (RNPs, see below). Beneath the viral envelope, the M1 protein forms a stiff layer to provide strength and rigidity to the lipid bilayer (Huang et al., 2001). M2 is a tetrameric

membrane protein with ion channel activity. During entry it allows protons to enter from the endosome into the viral particle. In this process the interaction between the RNPs and the M1 protein is resolved. M2 activity can be blocked by the antiviral drugs Amantadine and Rimantadine (Sugrue et al., 1990). The function of the M3 protein is not yet known. The M42 protein is only found in very few IAV strains and it is known to compensate the function of a defective M2 (Wise et al., 2012).

The heteromeric viral RNA (vRNA)-dependent RNA-polymerase (RdRp) of IAV consists of three subunits: polymerase 1 (PB1), polymerase 2 (PB2), and polymerase (PA). This complex is responsible for transcription and replication of vRNA. Together with nucleocapsid protein (NP) and the vRNA, it forms the viral RNP (vRNP) complex, which is responsible for the transcription and replication of the vRNA genome (Shaw, 2013). The PB2 subunit can bind to the cap structure of host cell mRNA and initiates genome transcription. At the N-terminal end, PB2 has a PB1 binding site (Guilligay et al., 2008). The PB1 segment encodes for polymerase subunit PB1, as well as for PB1-F2, and PB1-N40 by using different reading frames from the same RNA segment. Next to PB2, this is the second largest protein of IAV. PB1 interacts with PA for its nuclear localization (Fodor and Smith, 2004). The PB1-F2 protein plays a role in pathogenesis and virulence of IAV and it effects apoptosis of immune cells, virus replication, and in facilitating secondary bacterial infections (Krumbholz et al., 2011). The PB1-N40 protein can directly interact with the polymerase complex and is probably involved in transcription and replication of vRNA (Tauber et al., 2012). The PA protein is a polymerase subunit with an endonuclease activity and responsible for cleavage of host mRNAs (Dias et al., 2009). PA-X is the short form of PA, which is translated from the same mRNA, but by ribosomal frame shifting. PA and PA-X share the same N-terminal domain, while PA-X has a shorter C-terminal domain. PA-X can modify the host cell response and the severity of the infection (Jagger et al., 2012). PA-N155 and PA-N182

proteins were recently discovered. They are also translated from 11th and 13th AUG codons, which are highly conserved among PA mRNA of IAV, but the precise functions of these proteins are still not known (Muramoto et al., 2013). The NP is an abundant element of the RNP complex, which is translated from the fifth largest viral mRNA. It is a monomer and encapsidates the viral genome, is needed for vRNA transcription as well as in IAV replication and packaging (Portela and Digard, 2002).

The nonstructural protein 1 (NS1) and the nuclear export protein or nonstructural protein 2 (NEP/NS2) are encoded by the NS segment, which is the smallest vRNA of IAV. The amount of NEP/NS2 protein in the virion is very low, but this protein helps in the export of RNP complexes from the nucleus. NS1 has a huge impact on the viral replication and pathogenicity by counteracting the cellular/innate immune responses, such as lowering type-I IFN production and the activity of many interferon-induced genes. In addition it inhibits nuclear export and processing of cellular mRNAs (Hale et al., 2009).

RNA segments	bp	Proteins	aa	
Polymerase (basic) 2	2341	PB2	759	Virion components
Polymerase (basic) 1	2341	PB1	757	
Polymerase (acidic)	2233	PA	716	
Hemagglutinin	1775	HA	565	
Nucleoprotein	1565	NP	498	
Neuraminidase	1413	NA	454	
Matrix	1027	M1	252	
		M2	97	
Nonstructural	890	NEP/NS 2	121	
		NS1	230	Infected cells

Table 1: IAV genome segments and proteins. RNA segments of IAV and corresponding proteins are mentioned above, bp refers to basepair of the RNA segments and aa refers to amino acid of the protein segments. Modified from (Pleschka, 2013).

1.2.4 IAV lifecycle

The IAV lifecycle is divided into 5 different stages: 1) Receptor binding and cell entry; 2) Membrane fusion and uncoating of the viral core; 3) Posttranslational processing of viral proteins and virus assembly; 4) Genome packaging and virus release; 5) Cleavage activation of HA and viral infectivity and spread. The lifecycle is schematically displayed in Fig 2.

1.2.4.1. Receptor binding and cell entry

The viral HA initiates the replication process by recognizing and binding to sialic acid (SA) residues of glycoproteins or glycolipids on the cell surface. The receptor binding domain of the HA1 subunit binds to the receptor, which either possess: α (2,3)- or α (2,6)-galactose SA linkages (Colman, 1998). The α (2,6)-SA linkage is preferentially recognized by IAV with a tropism to human cells, whereas the avian-type IAV recognize α (2,3)-SA linkages, which are preferentially found on avian cell surfaces. Pigs have receptors harboring both types of linkages between SA and galactose, explaining why they are very vulnerable to infection by human and avian viruses (Shaw, 2013; Skehel and Wiley, 2000).

Upon virus-receptor binding, the attached viral particle undergoes receptor-mediated endocytosis. In this process, virus particles are taken up by the host cell plasma membrane. Within the endosomal vesicles the virus particles are exposed to the endosomal lumen. Normally, substances which are engulfed by endocytosis are travelling through the endosomal compartment and finally reach lysosomes where they degraded by hydrolytic enzymes. The viral particle avoids this degradation through the fusion of the viral envelope with the endosomal membrane, allowing the viral genome contained in the RNPs to access the cell cytosol (Matlin et al., 1981; Rust et al., 2004; Smith and Helenius, 2004).

1.2.4.2. Membrane fusion and uncoating of the viral core

In the late stage of the endocytosis, the pH of the endosome is comparatively low (pH 5-6). This subsequently mediates a conformational change in the cleaved HA. This is the most important step in virus infection (Stegmann et al., 1987). The HA1 receptor binding domain is maintained, but the N-terminal conformation of the HA2, which consists of the fusion peptide, is strongly altered. Now the exposed fusion peptide inserts itself into the endosomal membrane, leading to direct contact and fusion between the viral envelope and endosomal, cell-derived membrane (Huang et al., 2003b; Skehel and Wiley, 2002). The increased proton concentration within the endosomal vesicle results in a passive inflow of protons into the viral core via the M2 ion channel (Pinto and Lamb, 2006). The low pH within the virions allows the vRNP to dissociate from the M1 protein, which enwraps the vRNPs within the viral particle, releasing the vRNPs into the host cell cytoplasm (Boulo et al., 2007; Pinto and Lamb, 2006; Shaw, 2013). To allow viral genome transcription and replication, the cellular nuclear import machinery transports the vRNPs into the nucleus via Importin α and Importin β (Boulo et al., 2007).

1.2.4.3. Posttranslational processing of viral proteins and virus assembly

Once the vRNP complex is transported into the nucleus, the negative-sense vRNAs are transcribed to positive-sense mRNAs by the transcriptase activity of the RdRp (Lamb, 2001). The transcriptase, in a process called as 'cap snatching', snatches short cap regions from cellular mRNAs which serve as primers to start viral mRNA synthesis. This cap region is essential for efficient binding of virus-encoded mRNA to the ribosomes. The replication of the vRNAs is started by making a complementary positive sense RNA copy (cRNAs), and subsequently, the cRNA is used as a template to synthesize more vRNA. These freshly synthesized genome segments then travel back to the cytoplasm for the production of new virus particles.

Following the synthesis of the viral proteins and virus replication, the viral envelope proteins HA, NA and M2 proceed through the endoplasmic reticulum where the proteins are glycosylated, and oligomerize into trimers (HA) and tetramers (NA and M2) (Braakman et al., 1991). Subsequently, these proteins are transferred into the Golgi apparatus and trans-Golgi network where palmitoylation of cysteine residues occurs for HA and M2 (Shaw and Palese, 2013). After passage through the trans-Golgi network they reach the cell membrane. The mature HA, NA and M2 proteins are then clustered into the lipid rafts of the host cell membrane (Braakman et al., 1991; Doms et al., 1993). The pH inside the trans-Golgi network is slightly acidic, therefore a fusion-activating conformational change would likely be induced in the HA. The M2 protein, which is amply expressed in infected cells, temporarily balances the pH within the trans-Golgi network, so that HA is transported safely to the cell surface (Ciampor et al., 1992). The synthesis and oligomerization of viral core proteins occurs completely in the cytoplasm. In the nucleus NP and the RdRp components interact with newly synthesized vRNA to form RNPs. These RNPs are transported back to the nucleus to encapsidate the newly synthesized vRNA and cRNA transcripts (Paterson and Fodor, 2012).

1.2.4.4. Genome packaging and virus release

The M1 protein in association with the packaged vRNPs, interacts with the HA, NA and M2 proteins (Chen et al., 2008). This interactions function as a budding signal (Nayak et al., 2009). After budding, the viral HA attaches to the host cell receptor. At this moment, NA´s enzymatic activity cleaves the bond between the SA receptor on the host cell membrane and the HA spikes and allows virus release from the infected cell (Shaw, 2013).

1.2.4.5. Cleavage activation of HA and viral pathogenicity

HA0 is cleaved by a cellular trypsin-like protease into HA1 and HA2, a step that is important for the membrane fusion activity of the HA (Carr and Kim, 1993; Skehel and Wiley, 2000;

Wilson et al., 1981). The trypsin-like protease is expressed in epithelial cells of the respiratory tract, thus limiting the infection to the respiratory tract. HAs of low-pathogenic avian influenza viruses (LPAIV) have a monobasic cleavage site and highly pathogenic avian influenza viruses (HPAIV) have a multibasic cleavage site. As a result, these HAs from HPAIV can be cleaved by intracellular furin-like proteases, which are expressed in many cell types. This leads to infections of the whole body resulting in lethal systemic infections (Steinhauer, 1999).

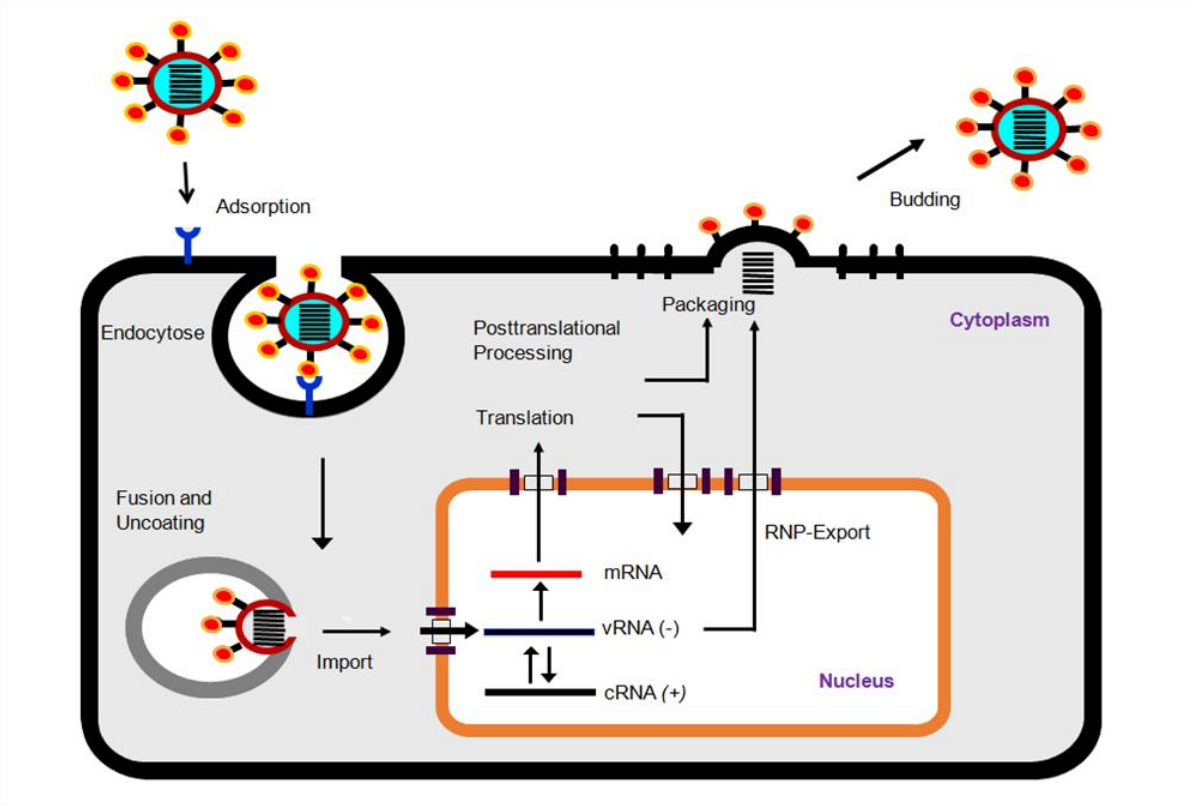

Figure 2: Schematic representation of IAV replication cycle. In the first step HA spikes bind to SA containing receptors on the cell surface. The virion is then engulfed into the cell by endocytosis. After fusion and uncoating of the virion, the viral genome is imported into the nucleus. Transcription and replication of the vRNA take place in the nucleus. Viral mRNA is exported from nucleus to cytoplasm where translation takes place. After translation, some proteins like NP, PB1, PB2, and PA go back to the nucleus to help in the replication process. After translation and post-translational modification (PTM), HA and NA are transported to the cell surface. At the last stage of virus replication cycle, vRNPs are exported out of the nucleus, packaged into new virions and then released from the membrane by the cleaving effect of NA. Modified from (Pleschka, 2013).

1.2.5 Reassortment of IAVs

RNA viruses are more prone to mutation because RNA mutations are not corrected by proofreading enzymes and segmented RNA genomes can be mixed and reassorted. In a IAV-infected cell, each vRNA segment enters the nucleus. In the nucleus they are copied several times to produce new vRNA genomes for new infectious virions. The newly produced vRNA segments packaged in the RNPs are exported to the cytoplasm and then incorporated in to new virus particles and released from of the cell by a process called budding. When a cell is infected with two or more different IAVs, the RNA segments of these viruses are copied in the nucleus. Co-infection with two (or more) IAVs can produce the parental viruses as well as different reassortant viruses which inherit RNA segments from the parental strains (Trifonov et al., 2009). This process is illustrated in the Fig. 3.

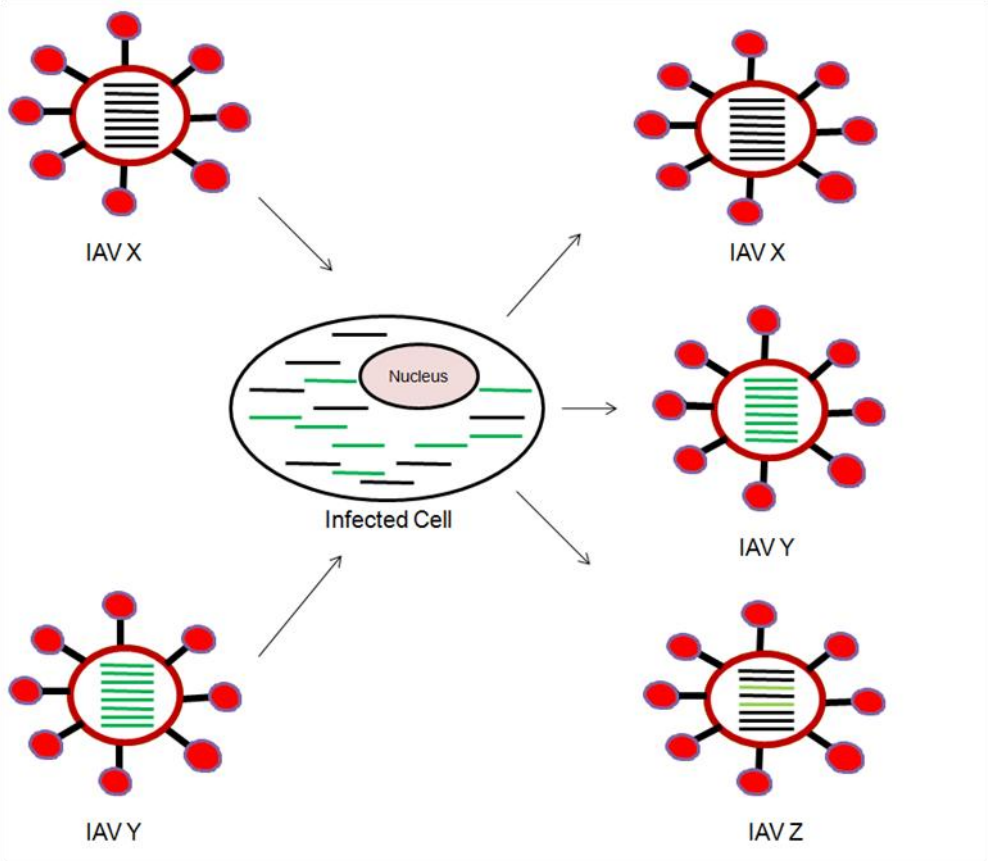

Figure 3: Reassortment events occurring with different IAV viruses. A cell is co-infected with two IAV strains (IAV X and IAV Y). The infected cell produces both parental viruses as well as a reassortant IAV Z which inherits two RNA segments from the IAV Y strain and the remainder from the IAV X strain. Modified from (Trifonov et al., 2009).

1.2.6 Reverse genetics as a tool to investigate the impact of the IAV genome on its infectivity and life cycle

The natural process of IAV reassortment can be recapitulated in the lab to produce recombinant IAVs with various combination of viral genome segments via reverse genetics. These genetically defined viruses are then compared for their replication, virulence, pathogenicity, host range and transmissibility (Li and Chen, 2014; Ma et al., 2015; Taubenberger and Kash, 2011; Wendel et al., 2015). This is a method of transcribing vRNAs into cDNAs which are cloned into a set of DNA plasmids, from which new vRNAs can be transcribed, encoding the viral mRNAs to rescue an entire and genetically accessible infectious virus. Specific primers can be used to target the conserved region at 3' and 5' ends of the viral segment to produce the full-length cDNA (Desselberger et al., 1980; Hoffmann et al., 2001). Afterwards, the amplified cDNAs are cloned into specific plasmid systems with (i) a polymerase I (PolI) promoter and terminator to produce vRNA-like transcripts and (ii) a polymerase II (PolII) promoter and a polyadenylation signal to produce the viral mRNA transcripts encoding the corresponding viral proteins, as schematically shown in Fig. 4 (Crescenzo-Chaigne and van der Werf, 2007). In the last few years, several efficient reverse genetics systems for IVs have been developed which allow the generation of recombinant IAVs, IBVs and ICVs (Hoffmann et al., 2002a; Hoffmann et al., 2002b; Mostafa et al., 2015; Subbarao et al., 2003).

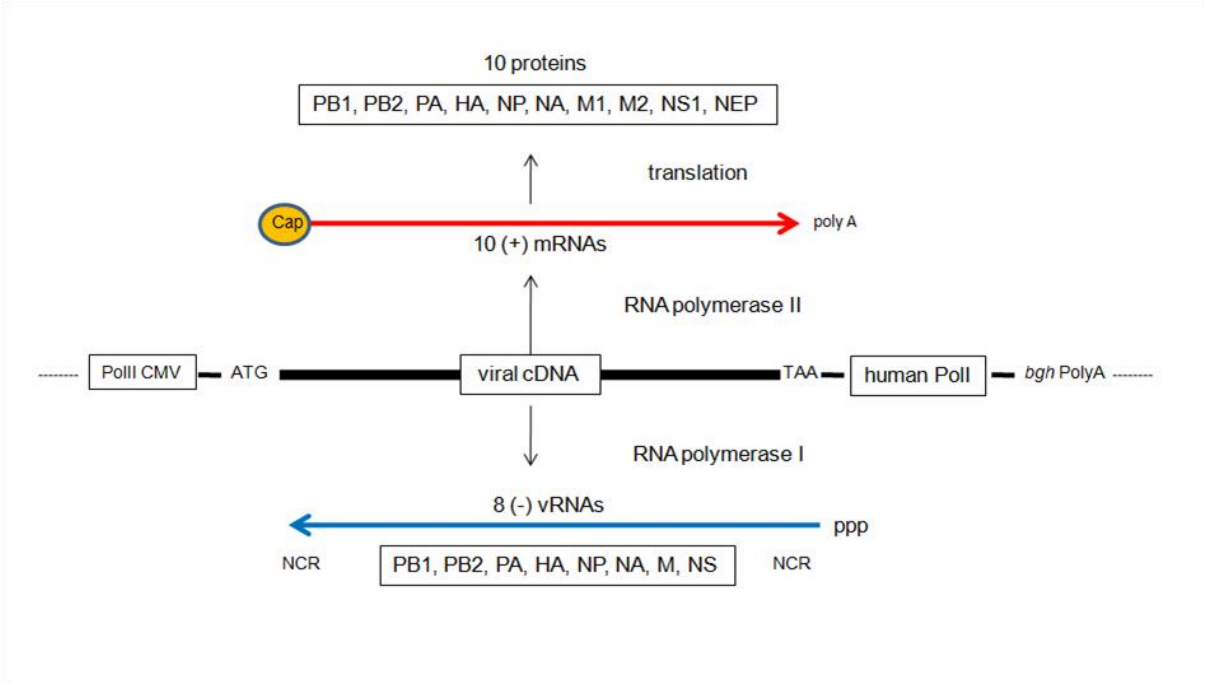

Figure 4: Reverse genetics by bi-directional transcription for the synthesis of vRNA and mRNA. The vRNA-like transcripts were synthesized using human polymerase I and terminated with Pol I terminator. mRNA transcripts of the 8 viral segments are generated using the Polymerase II promoter of the human cytomegalovirus (PolII CMV) and the polyadenylation site as a termination signal (*bgh*PolyA). The essential viral proteins are translated from the corresponding mRNA transcripts. Modified from (Hoffmann et al., 2000).

1.2.7 Antigenic drift and shift

Antigenic diversity of IAV can increase in two different ways: antigenic drift and antigenic shift. Antigenic drift occurs in the HA and NA and can cause seasonal epidemics. For example, the yearly Flu vaccine contains proteins of three different virus strains which keep changing every year. After vaccination the body can produce antibodies against these three virus strains. If one of these three strains infects the body, the newly produced antibodies mask the HA antigen and prevent HA attachment and infection. Nevertheless, the IAV genome is prone to mutation. Due to mutations the HA gene changes and the HA antigen that it encodes for, can change its shape. If the HA antigen changes its shape the antibody that was made against the previous HA cannot match and protect the body from the infection. Antigenic drift leads to a constant change in the antigenic epitopes of the virus, which can

cause severe infection. Pre-existing immunity from previous virus infections or vaccination can sometimes impair such viruses (Bush et al., 1999; Plotkin and Dushoff, 2003).

By antigenic shift at least two different strains of a IAV combine to form a new subtype, having a mixture of the surface antigens (HA and NA) of the two original strains. Antigenic shift affects the HA and NA segments and leads suddenly to drastically different antigenic properties, which can cause pandemics if there is no pre-existing immune protection within a population (Wright, 2013). For example, if a pig gets infected with a human IAV and an avian IAV at the same time, due to an antigenic shift a new virus can be produced that has most of the genes from the human IAV, but a HA or NA from the avian IAV. If the resulting new virus infects humans it can spread from human to human and an influenza pandemic can occur. In the resulting new virus possesses avian HA or NA proteins which never seen before in human upon IAV infection, and therefore most the people have no immune protection from previous infection or vaccination. The 2009 pandemic was caused by a reassortant H1N1 virus with a unique genome reorganization. The PB2 and PA segments were from a North American avian virus, the PB1 segment from a human H3N2 virus, the NA and M segments were from an Eurasian avian-like swine virus, and the HA, NP, NS segments were from the classical swine H1N1 virus (Garten et al., 2009; Medina and Garcia-Sastre, 2011).

1.3 A murine model system for studying IAV infection

Adaptation of a highly pathogenic avian IAV to a mammalian host was previously studied using two H7N7 type IAV strains: SC35 and its mouse-adapted version SC35M. The origin of SC35 is the IAV strain A/Seal/Massachusetts/1/80 (H7N7), which was serially passaged in chicken embryo cells. Due to acquisition of a multibasic cleavage site in its HA (Li et al., 1990), it became 100% lethal for chicken, but not in mice. Passaging of SC35 in mice led to

the generation of the mouse-adapted variant SC35M (Scheiblauer et al., 1995). SC35 is highly pathogenic for chicken but low pathogenic for mice, whereas SC35M is highly pathogenic for both chicken and mice. Therefore these two viruses are a suitable system to identify the molecular basis of host change and enhanced virulence in mammals. The main differences in the genome of SC35 and SC35M are found in the polymerase proteins (PB2, PB1, and PA) and NP. SC35M has considerably higher polymerase activity in mammalian cells than SC35, which can potentially explain the increased virulence in mice (Gabriel et al., 2005).

1.4 IAV-induced signaling events

IAV-encoded viral proteins where shown to interact with more than 1000 host cell proteins (Konig et al., 2010) and use host cell signaling and transport systems to ensure their own replication. IAV infection results in the activation or repression of different host cell signaling pathways within the infected cell (Julkunen et al., 2000; Ludwig et al., 2003), which either facilitate or antagonize virus replication. Different pathways are activated depending on the time of the virus infection (early or late) (Ludwig et al., 2003). The main target of IAV infection is the lung epithelium. Dendritic cells and macrophages are staying quite close to the lung epithelium. Upon infection, these immune cells produce remarkably higher amounts of inflammatory cytokines such as tumor necrosis factor α (TNFα) and type I interferon (IFN). These cytokines can also activate various signaling cascades in lung epithelial cells.

1.4.1 The PI3K/Akt signaling pathway

Like many other pathways the PI3K/Akt signaling pathway also consists of many activators, inhibitors, effectors and secondary messengers. Because of many loops and branches (GSK3, FoxO, mTORC1), this is one of the most complex pathways. The Phosphoinositide 3-kinase (PI3K) has two subunits (regulatory (p85) and enzymatic (p110)), each subunit exists in several isoforms (Ehrhardt et al., 2007). The active enzyme exhibits both a protein kinase and a lipid kinase activity (Dhand et al., 1994). The PI3K/Akt pathway can be activated by three different ways. Two pathways begin with the activation of the receptor belonging to the family of receptor tyrosine kinase (RTK) by an extracellular growth factor (Lemmon and Schlessinger, 2010). Binding to the receptor leads to the dimerization of the receptor monomers and heterologous autophosphorylation of the monomers. Depending on the receptor, different cellular proteins may bind to its phosphorylated domain. The insulin receptor substrate-1 (IRS-1) binds to the insulin like growth factor-1 (IGF-1) receptor. Receptor bound IRS-1 serves as a binding and activation site of PI3K (Lemmon and Schlessinger, 2010). In addition, PI3K may bind directly to a phophorylated tyrosine (Tyr) kinase. A completely different mechanism of PI3K activation begins with the small membrane bound GTPase RAS. By binding to an active GTP-bound Ras, PI3K is activated (Castellano and Downward, 2011).

At the next level of the pathway, the secondary messenger phosphatidylinositol (3,4,5) trisphosphate (PIP3) is formed. This leads to the activation of serine/threonine (Ser/Thr) kinase Akt (also known as protein kinase B; PKB). The active PI3K migrates to the inner side of the cell membrane and binds to phosphatidylinositol (4,5) bisphosphate (PIP2), which is the regular component of the membrane. PIP2 is anchored by its two fatty acids in the lipid layer of the membrane. PI3K is able to phosphorylates PIP2 to PIP3 (Fig 5) (Schramp et al.,

2012). PIP3 can now activate the kinase Akt, which is named after its homologous protein in retrovirus Akt8 (Carpten et al., 2007).

The Akt Ser/Thr kinase activated by PIP3 is a proto-onco protein with many substrates and effects. The best-known effect of this pathway is the inhibition of apoptosis (Hemmings and Restuccia, 2012). Activated Akt binds to BAX and hinders its ability to form holes in the outer mitochondrial membrane. In the absence of Akt, these holes lead to the apoptosis via the caspase cascade (Yamaguchi and Wang, 2001). The cascade begins with the activation of the protein Rheb, which activates the mechanistic target of rampamycin (mTOR). mTOR itself interacts with and activates the translation factor S6K by binding to the large subunit of the ribosome (Ersahin et al., 2015). S6K activates the translation of mRNA into protein. In addition, Akt may lower the concentration of the protein FoxO (Forkhead box O) by phosphorylating FoxO. Phosphorylated FoxO is a substrate of ubiquitin ligases which allows destruction of ubuquitinated FoxO by proteosomal degradation. In this way Akt prevents the tumor suppressor protein FoxO from inhibiting proliferation (Das et al., 2016).

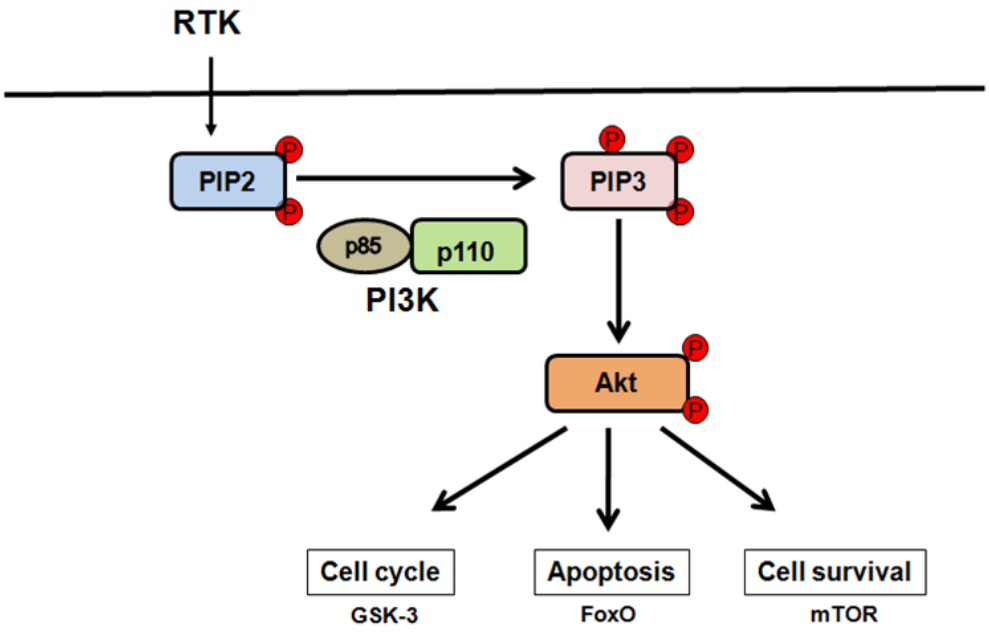

Figure 5: Schematic representation of PI3K/Akt pathway. The PI3K is activated through receptor-binding RTKs, resulting in phosphorylation of PIP2. PIP3 subsequently serves as a second messenger allowing the binding of pleckstrin homology domain-containing proteins like Akt. Akt contributes in the regulation of cellular processes like cell cycle, cell growth and apoptosis by phosphorylating further proteins. Modified from (Diehl and Schaal, 2013).

1.4.1.1 Role of PI3K/Akt signaling on IAV infection

The PI3K/Akt pathway is known to be activated via IAV infection (Neri et al., 2002; Vanhaesebroeck et al., 2005). In virus-infected cells PI3K is also involved in double-stranded RNA (dsRNA)-induced activation of the antiviral transcription factor interferon-regulatory factor 3 (IRF3) (Sarkar et al., 2004), pointing at a function in the defense mechanism against viral infection. Interestingly, IAV misuses the PI3K/Akt pathway for a virus-supportive function to regulate the viral entry (Ehrhardt et al., 2006). In the early stage of IAV infection, activation of Akt was observed, but a much stronger activation was detected in later stages of the replication cycle. Inhibiting PI3K by using a small molecule inhibitor revealed that in addition to entry, PI3K further regulates also later stages of replication (Ehrhardt et al., 2006).

It was also shown that at the late stage of IAV infection, the NS1 protein binds to the SH2 domain of the p85 subunit and activates PI3K, which leads to prevention of cell death (Neri et al., 2002). Thus inhibition of Akt kinase activity in host cells may have therapeutic advantages for IAV infection by inhibiting viral entry and replication (Hirata et al., 2014).

1.4.2 MAPK signaling

Mitogen-activated protein kinase (MAPK) signaling cascades can convert several extracellular signals to cellular responses, such as cell differentiation, proliferation, and apoptosis in eukaryotes from yeast to human (Keshet and Seger, 2010; Qi and Elion, 2005; Raman et al., 2007). Four different MAPK signaling pathways are well studied: These are extracellular signal-regulated kinases 1 and 2 (ERK1/2), c-jun N-terminal and stress-activated protein kinases (JNK/SAPK), p38 MAPK as well as ERK5 (Iyoda et al., 2003). Each cascade is activated by specific stimulus and leads to the activation of the specific MAPK following the activation of a MAPK kinase kinase (MAPKKK) and a MAPK kinase (MAPKK).

A TEY motif is present in the activation segment of the ERK family members and can be subdivided into two groups: the classic ERKs that consist mainly of a kinase domain (ERK1 and ERK2) and ERK5 that contains an extended sequence in the C-terminus of the kinase domain (Zhang and Dong, 2007). The ERK pathway begins with the binding of a ligand like epidermal growth factor (EGF) to the extracellular part of the membrane bound receptor belonging to the family of RTKs (Shaul and Seger, 2007). Ligand binding leads to the dimerization of two the subunits of the RTK. At the cell inner side of the RTK, specific domains catalyze phosphorylation of the receptor itself. Growth factor receptor bound protein 2 (GRB2) can bind to the phosphorylated RTK. The protein Son of Sevenless (SOS) is able to bind to the membrane bound protein rat sarcoma (Ras). SOS catalyzes the exchange of Ras

bound guanosinediphosphate (GDP) to guanosine triphosphate (GTP) and this exchange leads to the activation of Ras. GTP-bound active Ras is able to bind several effector proteins such as B-Raf. (Castellano and Downward, 2011). Active B-Raf phosphorylates and activates MEK1/2, which in turn phosphorylates and activates ERK1/2 (Fig 6A) (Garnett and Marais, 2004). Finally the kinase cascade leads to the activation of transcription factors such as activator protein 1 (AP1) family transcription factors. ERK5 is also known as big MAPK1 (BMK1), because it is double in size than the other MAPKs (Lee et al., 1995). Upon stimulation , MEKK2 and MEKK3 (members of the MAPKKK family) activate MEK5 (specific MAPKK for ERK5). ERK5 is phosphorylated and activated by MEK5 (Fig 6B), and then the activated ERK5 phosphorylates substrates such as myocyte enhancer factor 2 (MEF2) (Kato et al., 1997).

A TPY motif is present in the activation segment of the JNK family members including JNK1, JNK2 and JNK3 (Morrison, 2012). The JNK pathway can be activated by oxidative stress, DNA damage and other kind of environmental stress and inflammatory cytokines. Small GTPases of the Rho family are involved in the initiation of the signal cascade to JNK (Johnson and Nakamura, 2007). Membrane bound kinase MEKK1/4 or mixed lineage kinases (MLK2/3) can phosphorylate and activate MKK4/7, the SAPK/JNK kinase. On the other hand, the germinal center kinase (GCK) family in a GTPase-independent manner can also activate and phosphorylate MKK4/7. SAPK/JNK can be activated by MKK4/7 and translocate to nucleus to regulate the activity of several transcription factors (Fig 6C) (Rincon and Davis, 2009).

A TGY motif is present in the activation segment of the p38 family members (α,β,γ,δ) (Morrison, 2012). p38 pathway regulates different cellular functions such as inflammation, apoptosis and the cell cycle. This pathway is also activated by the same kind of stimuli as SAPK/JNK (Cuadrado and Nebreda, 2010). The MAPKKKs for this pathway are MLK2/3

and MEKK1-4. Theses MAPKKKs phosphorylates and activates MAPKK (MLK3/6) (Fig 6D). Important substrates of p38 signaling include the downstream kinases as well as several transcription factors including activating transcription factor-2 (ATF-2), myocyte enhance factor-2 (MEF-2).

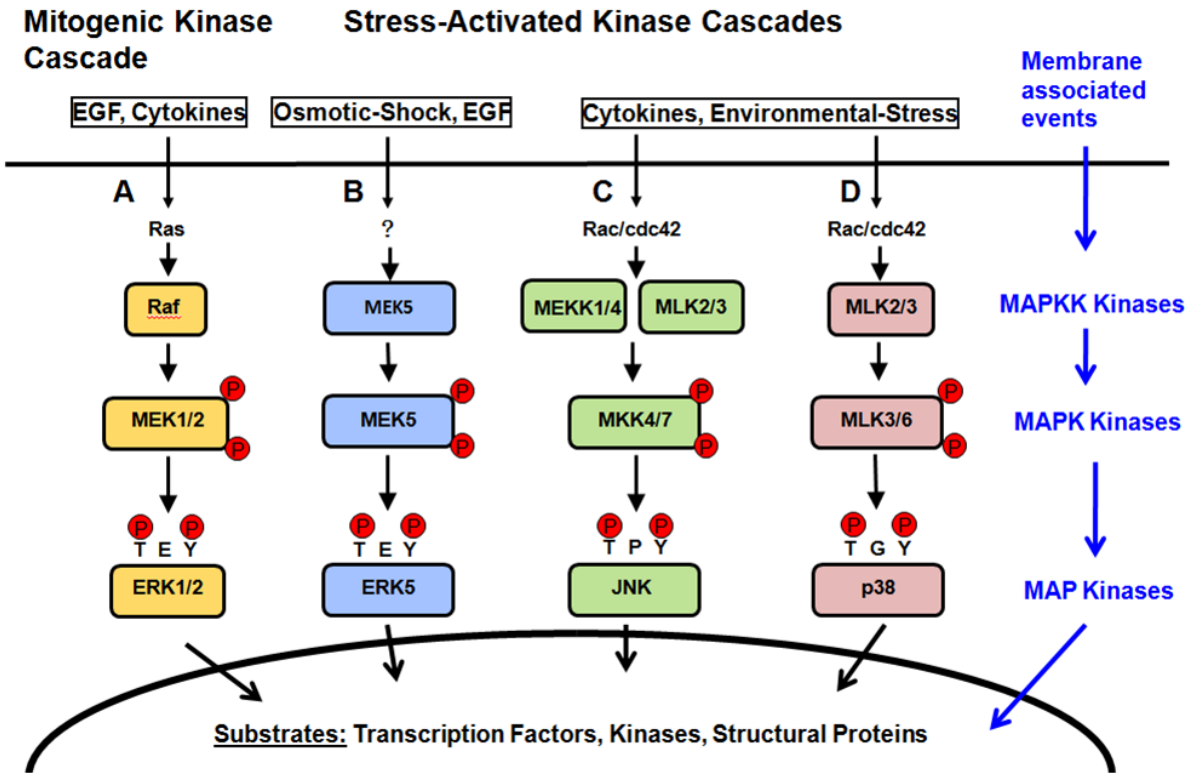

Figure 6: Schematic representation of four different MAPK signaling pathways. These are **(A)** ERK1/2, **(B)** ERK5, **(C)** JNK and **(D**) p38. These cascades belong to either mitogen- or stress-activated kinase cascades. They can be activated by many factors such as growth factors and cytokines, stress, osmotic shock and epidermal growth factor (EGF). Protein kinases of the MAPKKK class may be activated by small regulatory GTPases such as Ras, Rac, Cdc42 or other protein kinases. These cascades have a stepwise activation in common. MAPKK (MEK1/2, MKK4/7, MLK3/6, MEK5) is activated by MAPKKK. MAPK (ERK, JNK; p38, ERK5) that is activated by dual phosphorylation through a MAPKK kinase. MLK: mixed lineage kinase; ERK: extracellular signal-regulated: kinase; JNK: Jun-N-terminal kinase; MEK: MAP/ERK kinase; MEKK: MEK kinase; Ras: Rat sarcoma, Rac: Ras related C3 botulinum toxin substrate 1, Cdc42: cell division cycle 42. Modified from (Pleschka, 2008).

1.4.2.1 Role of MAPK signaling in IAV infection

IAV infection leads to the activation of all four kinds of MAPK signaling pathways (Kujime et al., 2000; Pleschka et al., 2001). Activation of p38 signaling significantly increases vRNP transport trafficking and viral replication. In a previous study, it has been shown that p38 and JNK inhibitors can reduce the expression of the chemokine RANTES in IAV infected cells (Kujime et al., 2000). During the early phase of infection, JNK phosphorylates and stimulates AP1. JNK activation is instigated by RNA accumulation produced by the viral RdRp. JNKs enhance the transcriptional activity of AP1 (Ludwig et al., 2001). AP1 is important for the expression of interferon β (IFNβ) and other antiviral cytokines (Stark et al., 1998). Inhibition of JNK signaling by expression of a dominant negative MKK7 mutant resulted in defective IFNβ transcription and increased virus replication (Ludwig et al., 2001). Several papers already showed that inhibition in p38 MAPK can reduce virus titer *in vitro* (Kujime et al., 2000; Lee et al., 2005). One interesting finding showed that inhibition of p38 *in vivo* can reduce the virus replication as well as the expression of IFNβ when infected with the highly pathogenic avian IAV (Borgeling et al., 2014). IAV infection also increased ERK signaling for efficient nuclear export of RNPs. MEK inhibition can block this pathway, which will result in decreased RNP export and virus growth, but it does not interfere with viral protein synthesis (Pleschka et al., 2001). ERK1/2 has an important role in pro-inflammatory cytokine production. The ERK5 pathway is also activated upon successful viral infection. However, activation of ERK5 or activator MEK5 by expression of dominant negative mutants, antisense or shRNA constructs did not affect the efficiency of virus replication nor the antiviral response to virus infection (Ludwig et al., 2006).

1.4.3 The NF-κB pathway

Exposure of cells to any stress, proinflammatory cytokines, LPS, growth factors, and bacterial or viral antigens leads to the induction of specific signaling cascades that finally activate NF-κB (Hayden and Ghosh, 2012). NF-κB-mediated transcription regulates genes influencing a broad range of biological processes including innate and adaptive immunity, inflammation, stress responses, B-cell development, and lymphoid organogenesis. NF-κB is thus a central mediator of the immune response (Hiscott et al., 2001).

NF-κB can be activated by three different pathways: canonical or classical, non-canonical or alternate (Chen, 2005; Karin et al., 2004) and the atypical NF-κB activation pathway (Hayden and Ghosh, 2012). All three pathways have in common that they lead to the generation of DNA-binding dimers. In the unstimulated cell, DNA-binding dimers (p50/p65 for the canonical and non-canonical, p52/RelB for the atypical pathway) normally stay in the cytosol together with inhibitory IκB proteins.

Activation of the **canonical NF-κB pathway** depends on the IκB kinase (IKK) complex (Hinz and Scheidereit, 2014). Upstream signals lead to the interaction between the NF-κB essential modulator (NEMO) protein and further proteins containing ubiquitin-binding domains such as TGF-β activated kinase-binding protein 2 (TAB2). This allows the recruitment of TAB2 interacting kinase TGF-β activated kinase 1 (TAK1), which activates the IKKs (Wang et al., 2001). The catalytic IKKα and IKKβ subunits and the non-catalytic, regulatory NEMO (also known as IKKγ) subunit form the IKK complex (DiDonato et al., 1997; Karin et al., 2004). IKKα and IKKβ share an N-terminal kinase domain, and a C-terminal region containing a leucine zipper and helix-loop-helix motifs (Woronicz et al., 1997). Phosphorylation of two conserved serine residues within the activation loop of IKKα or IKKβ are important for IKK activation (Wang et al., 2001). Active IKKs phosphorylate IκBα. Then the IκB proteins are modified by ubiquitination, which then leads to proteolytic

degradation, thus releasing the DNA-binding NF-κB dimer from its inhibitor. While the importance of IKKβ for IκBα phosphorylation has been shown in knockout animals (Li et al., 1999), different other studies showed that the canonical IKKs can phosphorylate other cytoplasmic and nuclear substrates in addition to IκBα. Thus the IKKs are playing an important role in activating NF-κB and other signaling pathways such as insulin and Wnt signaling (Fig 7A) (Chariot, 2009; Scheidereit, 2006).

In B cells the **non-canonical NF-κB pathway** is induced mainly in response to stimulation of tumor necrosis factor (TNF) cytokine superfamily. This pathway involves proteolytic processing of the p100 precursor protein by the proteosome (Razani et al., 2011). The stabilization of NIK (NF-κB inducing kinase) and IKKα are important for this pathway. Phosphorylation of p100 at several serines in the C-terminus allows for ubiquitination of p100 at K855 and generates p52. The released p52 then dimerizes with the RelB subunit to form p52/RelB, which undergoes nuclear translocation to regulate gene expression, as schematically shown in Fig 7C (Chen, 2005; Karin et al., 2004).

In response to DNA damage, the **atypical NF-κB** activation pathway is activated via poly (ADP-ribose)-polymerase-1 (PARP-1). PARP-1 synthesizes poly ADP-ribose which allows the assembly of a protein complex containing NEMO, PIASy (protein inhibitor of activated STAT y) and the kinase ataxia-telangiectasia mutated (ATM). PIASy triggers the attachment of the small ubiquitin-related modifier (SUMO) to NEMO, followed by phosphorylation and ubiquitination of IκBα (Huang et al., 2003c). Then the IKKs are activated, which eventually generate DNA-binding NF-κB dimers (Fig 7B). These dimers are free to travel to the nucleus where they bind DNA and regulate gene expression (Kriete and Mayo, 2009).

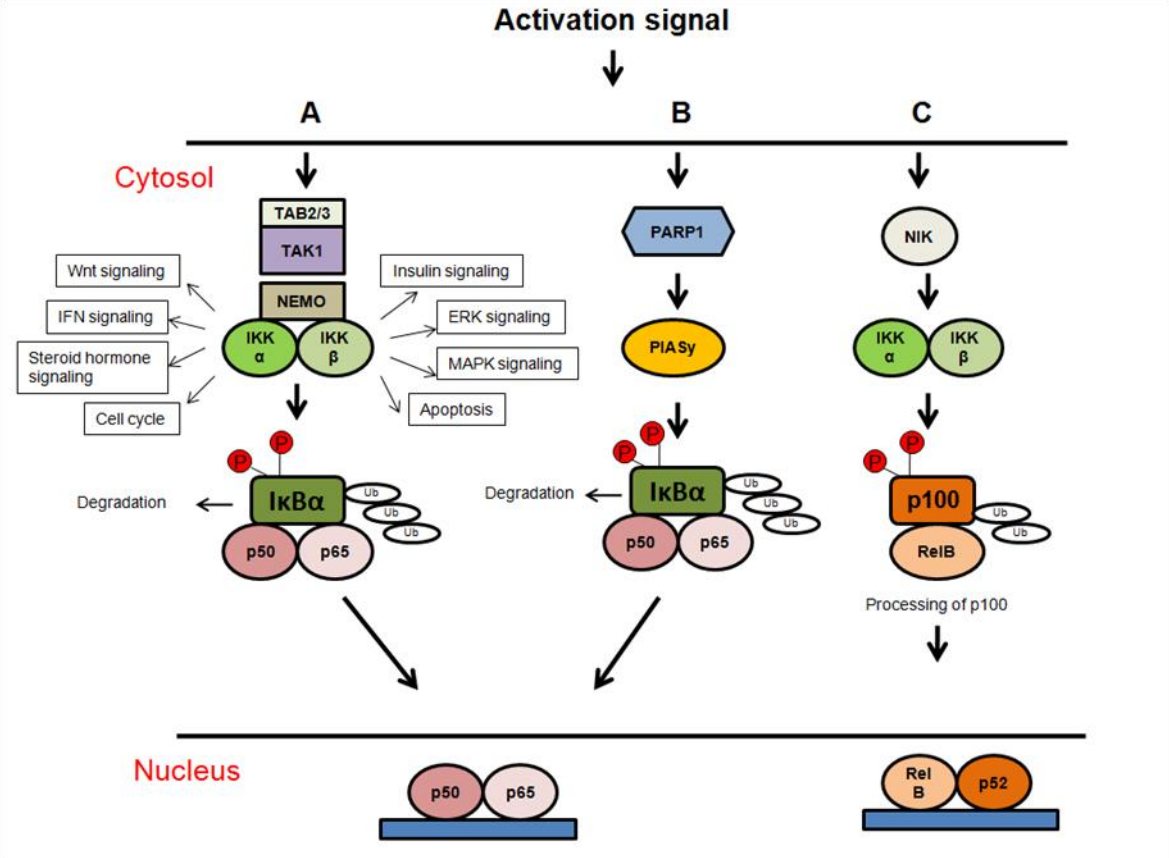

Figure 7: Schematic representation of three NF-κB pathways.(A) Schematic display of the canonical NF-κB pathway. This pathway can be activated by TNF-α, IL-1β, LPS or virus infection. IKKα and IKKβ are not only involved in NF-κB pathway but also in other signaling pathways Similarly, also IKKβ participates in the regulation of other pathways such as MAPK signaling, ERK signaling and many more. (**B**) Summary on the atypical NF-κB pathway, which is typically activated by DNA damage. **(C)** Summary of the non-canonical NF-κB pathway, which is activated by lymphotoxin β (LTβ) or B-cell activating factor (BAFF). Modified from (Schmitz et al., 2014).

1.4.3.1 Role of NF-κB for IAV infection

It is already known that IAVs activate the NF-κB signaling pathway (Ehrhardt et al., 2013; Flory et al., 2000; Mazur et al., 2007; Pahl and Baeuerle, 1995; Wang et al., 2000). The exact role of NF-κB for IAV transmission and replication is still not clear and there are different opinions on the function of NF-κB.

IAV supporting NF-κB functions: A number of studies showed that IAV induced NF-κB activation increases virus replication (Jin et al., 2014; Kumar et al., 2008; Pinto et al., 2011).

Several IKK inhibitors such as BAY11-7085, BAY11-7082 significantly decrease IAV infection of human lung carcinoma cell lines (Nimmerjahn et al., 2004). Also, the inhibition of NF-κB by expression of a non-degradable IκBα mutant or a dominant negative IKKβ mutant showed in decreased IAV propagation in lung A549 cells, again showing that NF-κB activity assists efficient IAV production (Wurzer et al., 2004).

IAV inhibiting NF-κB functions: Several reports noted an antiviral function of NF-κB *in vivo*. Mice lacking the A20 protein show exaggerated NF-κB activation after IAV infection, nevertheless these mice are protected against fatal IAV infection (Maelfait et al., 2012). This antiviral function of NF-κB most probably relies on its ability to induce the expression of inflammatory and antiviral mediators. In support of this notion, pre-treatment of mice with 5' triphosphate RNA (5' ppp RNA) to trigger the RIG-I-mediated induction of inflammatory and IFN-stimulated genes protects the animals from a subsequent infection with IAVs (Goulet et al., 2013).

1.5 Protein phosphorylation

Protein phosphorylation is a reversible posttranslational modification (PTM) occurring at Ser, Thr and less abundantly at Tyr residues. Phosphorylation is a typical starting point for modification cascades, while degradative ubiquitination is an irreversible end point (Sharma et al., 2014). By phosphorylation, a phosphate group is added to hydroxyl group by an enzyme called kinase. Kinases are typically activated by phosphorylation of specific residues in the activation loop of the kinase (Zhang et al., 2015). Kinases mostly have one or two tyrosines in the activation loop. For example, MAPK kinases have a TEY motif, which is phosphorylated on both Thr and Tyr, and most other kinases have a Thr within the loop. Just next to the activation loop, there is another loop which often binds the substrate residue just

C-terminal of the phosphorylated residues known as P+1 loop. The activation loop and the P+1 loop together form the activation segment, which is regulating the kinase activity (Scheeff et al., 2009). The counterpart of phosphorylation is dephosphorylation, which also regulates several cellular processes. Dephosphorylation is done by an enzyme named phosphatase. In eukaryotes, 1/3 to 2/3 of the proteome is getting phosphorylated (Cohen, 2002; Vlastaridis et al., 2017). One of the most important functions of phosphorylation is to activate or deactivate different enzymes and thereby regulating their functions (Oliveira and Sauer, 2012; Tripodi et al., 2015). P-Tyr account for less than 1% of the identified phosphorylation sites and these modifications have a short half-life owing to the high activity of phosphotyrosine phosphatases (Sharma et al., 2014).

1.6 Importance of phosphoproteomic studies

Phosphoproteomics is a branch of proteomics that focuses solely on the identification and characterization of phosphorylated proteins. By this process, dynamic changes in protein phosphorylation can be measured quantitatively on a global scale (Humphrey et al., 2015). Protein phosphorylation can be easily determined by mass spectrometry (MS). Proteomics can provide a wide range of view on complex and dynamic response to the host-pathogen interaction. Modern MS technology allows identification, quantification, and characterization of PTMs such as phosphorylation, ubiquitination of thousands of proteins in a single experiment. High-resolution MS with affinity-based phosphopeptide enrichment followed by organized bioinformatics analyses have opened a new way to evaluate phosphorylation-dependent signaling cascades in cells responding to different stimuli, such as virus infection. Recent proteomic studies allowed the identification of thousands of new phosphorylation sites (Humphrey et al., 2015).

1.6.1 Importance of phosphoproteomic analysis of virus infected cells

When a host cell is infected by virus or bacteria, they can hijack the host cell signaling networks to facilitate their replication process. On the other hand, when host cells sense the infection they may switch on signaling cascades to hinder pathogen replication and alert nearby cells to counteract occurring infections. Until lately phosphoproteomic analyses to explain infection-associated alterations in the protein phosphorylation status during viral infection were lacking, but several recent studies have shown the importance of phosphoproteomic analyses to investigate signaling pathways after infection with different viruses including HIV-1 (Wojcechowskyj et al., 2013), lytic gammaherpes virus (Stahl et al., 2013), porcine reproductive and respiratory syndrome virus (Luo et al., 2014), rift valley virus (Popova et al., 2010), Sendai virus (Ohman et al., 2015), and human cytomegalo virus (Oberstein et al., 2015). Several phosphorylation-dependent signaling events were identified based on the hypothesis that virus-induced signaling regulates viral replication and host responses to infection, but yet a large number of phosphorylations occurring on host cell proteins and viral proteins remain to be discovered.

Viruses have to utilize the host kinase machinery to phosphorylate viral proteins and to manipulate host cell signaling pathways (Jacob et al., 2011). Also, IAV infection triggers massive changes in gene expression, protein synthesis, vesicle trafficking and cytoskeleton organization of the infected cell (Hutchinson and Fodor, 2013). Many of the IAV-induced cell responses serve to facilitate or antagonize virus propagation. Virus-supportive cell functions include the translation, PTM, and maturation of viral proteins including the viral glycoprotein HA. Accordingly, various genome-wide RNAi screens have allowed the identification of host factors supporting IAV replication (Chou et al., 2015; Karlas et al., 2010), although with a surprisingly low incidence of overlap (Chou et al., 2015). These screens showed that the cellular proteins supporting IAV replication participate in all basic

cellular functions including signal transduction, nucleic acid metabolism and transport, vesicle trafficking and all steps of gene expression from transcription to translation (Watanabe et al., 2010). On the other hand, infected host cells initiate signaling pathways counteracting viral infection, as exemplified by the IFN system. The production and release of these antiviral cytokines is initiated by a signaling cascade triggered by the RNA-sensing RIG-I protein. The activated RIG-I can then bind to its downstream effectors to trigger the activation of protein kinases that ultimately lead to the activation of downstream transcription factors of the IRF and NF-κB families.

The relevance of phosphorylation of viral proteins has been seen in a number of studies. The IAV-encoded NS1 protein has several functions. It is also believed that the dsRNA binding capacity of NS1 is regulated through its phosphorylation at Thr215, Ser42, and Ser48 (Hale et al., 2008; Hsiang et al., 2012). In the NS1 protein, Thr215 is phosphorylated by ERK1/2 *in vitro*, however the biological function of this phosphorylation is not known yet. A recent study showed a functional interaction between the viral NS1 and Akt. The RNA-binding domain of NS1 interacted with Akt, resulting in increased Akt kinase activity, which in turn phosphorylated NS1 at the Thr215 residue (Hale et al., 2009). Mutation of NS1 Ser42 is eliminating the interaction of NS1 with dsRNA and decreases viral replication (Hale et al., 2009; Hsiang et al., 2012).

Another study investigated phosphorylation of the IAV-encoded M1 protein at Tyr132 (Wang et al., 2013). After viral entry, the M1 protein undergoes a pH-dependent conformational change, which helps in the release of the vRNP into the cytoplasm. The phosphorylation of Tyr132 is important for viral replication by controlling the nuclear import of M1 (Halder et al., 2013), but the kinase mediating this process is currently not known. Thus there is considerable interest to study IAV-triggered phosphorylation patterns in a

systematic fashion, as it has already done to study the dynamic changes of protein SUMOylation in IAV-infected cells (Domingues et al., 2015).

1.7 Aim of the study

(1) As the genetic variability of viruses is of great (patho)physiological relevance in IAV infections the first part of this study aimed to investigate the role of the NF-κB transcription factor for the replication ability of the avian-adapted SC35 and its mouse-adapted variant SC35Mas well as of reassortants of SC35 carrying segments of SC35M (generated by reverse genetics) in a wild type mouse cell line and cell lines generated by targeted genome engineering using CRISPR-Cas9 technology.

(2) In the second part of the study, the aim was to study the phosphoproteomic changes of IAV-infected mouse lung cells at early and late phases of infection with either SC35 or SC35M. This study identified novel phosphorylation sites in host cellular proteins as well as in viral proteins that serve to enhance or antagonize their function.

2 Materials and Methods

2.1 Materials

2.1.1 Chemicals and general materials

Name	Source
2-propanol (isopropanol)	Roth
4-(2-hydroxyethyl)-1-piperazineethanesulfonic acid (HEPES)	Sigma
ABsolute qPCR SYBR green ROX Mix	Thermo
Acetic acid	Roth
Acrylamide/bisacrylamide mix (37.5:1)	Roth
AEC (3-amino-9-ethylcarbazole)	Sigma
Agar	AppliChem
Agarose	AppliChem
Ammonium persulfate (APS)	Sigma
Aprotinin	Sigma
Avicel	FMC Biopolymer
Bovine serum albumin (BSA)	Sigma
Bromophenol blue	Merck
BSA (Solution, 30% (w/v))	Sigma
Calcium chloride ($CaCl_2$)	Merck
Cell culture plastics	Sarstedt
Chloroform	Sigma
Cryotubes	Sarstedt
Cuvette	Eppendorf

Name	**Source**
DEAE Dextran (MW: 500,000)	Pharmacia biotech
Deoxynucleotide triphosphates (dNTPs)	Thermo
Dimethylformamide (DMF)	Sigma
Dimethyl sulfoxide (DMSO)	Sigma
Disodium hydrogen phosphate (Na_2HPO_4)	Roth
DMEM, high glucose + GlutaMAX	Life Technologies
DNA sample buffer	Thermo
Eppendorf tube	Eppendorf
Ethanol	Sigma
Ethidium bromide	Roth
Ethylenediaminetetraacetic acid (EDTA)	Sigma
Falcon centrifuge tube	Falcon
Fetal calf serum (FCS)	Life Technologies
GeneRuler 100bp & 1kb DNA ladder	Thermo
Glycerol	Roth
Glycine	Roth
Hoechst 33342	Invitrogen
Hydrochloric acid (HCl)	Sigma
Hydrogen peroxide (H_2O_2)	Merck
Immersion oil for microscopy	Merck
Lipofectamine 2000	Invitrogen
Magnesium chloride ($MgCl_2$)	Sigma
Microtiter plate (96 wells)	Greiner

Name	**Source**
Minimum Essential Media (MEM) (10X)	Invitrogen
Methanol	Sigma
Mounting medium	Dianova
N,N,N',N'-tetramethylethylendiamin (TEMED)	Roth
Nonidet P-40 (NP-40)	Roche
Nuclease free water	Ambion
Oligo(dT)12-18 primer	Sigma
Opti-MEM®	Invitrogen
PageRuler Plus prestained protein ladder	Thermo
Paraformaldehyde (PFA)	Roth
Phenylmethanesulfonyl fluoride (PMSF)	Sigma
Potassium acetate	Roth
Potassium chloride (KCl)	Sigma
Potassium hydroxide (KOH)	Merck
Potassium dihydrogen phosphate (KH_2PO_4)	Sigma
Polyvinylidene difluoride (PVDF) membrane	Thermo
RiboLock RNase Inhibitor	Thermo
Roti-seal	Roth
Skimmed milk powder	Merck
Sodium azide (NaN_3)	Sigma
Sodium chloride (NaCl)	Sigma
Sodium dodecyl sulfate (SDS)	Bio-Rad
Sodium fluoride (NaF)	Roth

Name	Source
Sodium hydroxide (NaOH)	Roth
Sodium orthovanadate (Na_3VO_4)	Sigma
Sodium pyrophosphate	Sigma
Tris(hydroxymethyl)aminomethane (Tris)	Roth
Triton X-100	Sigma
Trizol	Invitrogen
Tissue culture dish	Greiner CELLSTAR
Tissue culture flask	Greiner CELLSTAR
Tryptone	Roth
Tween 20	Gerbu
Sequanol grade urea	Thermo
Whatman paper	MAGV
Western lightning ECL solutions	Perkin Elmer
Yeast extract	AppliChem
β-mercaptoethanol	Roth
β-glycerolphosphate	Calbiochem

2.1.2 Kits

Name	Source
Dual-Luciferase® reporter assay system	Promega
GeneJET plasmid maxiprep kit	Thermo
JETQUICK gel extraction spin kit	Genomed
JETQUICK PCR product purification spin kit	Genomed

Name	Source
Mini elute gel extraction kit	Qiagen
Mini elute PCR purification kit	Qiagen
NA-Fluor™ influenza neuraminidase assay kit	Applied Biosystem
QuikChange II XL kit	Agilent
RNeasy mini kit	Qiagen
Bicinchoninic acid (BCA) protein assay kit	Pierce

2.1.3 Enzymes

Name	Source
FastAP Thermo-sensitive alkaline Phosphatase	Thermo
P*fu* DNA Polymerase	Thermo
Restriction enzymes & buffers	Thermo
SuperScript II reverse transcriptase & buffer	Life Technologies
T4 DNA Ligase & buffer	Thermo
Trypsin/0.05 % (v/v) EDTA	Life Technologies
RNase A	Thermo
Shrimp Alkaline Phosphatase (SAP)	Roche
T4 polynucleotide Kinase (PNK)	Fermentas

2.1.4 Antibodies

Primary antibodies (clone)	Origin	Dilution	Source
Anti-p65 (C-20)	Rabbit, pAb	1:1000	Santa Cruz
Anti-phospho-IRF3, S396 (4D4G)	Rabbit, mAb	1:500	Cell Signaling

Primary antibodies (clone)	**Origin**	**Dilution**	**Source**
Anti-phospho-p38, T180/Y182	Rabbit, pAb	1:1000	Cell Signaling
Anti-phospho-p65, S536	Rabbit, pAb	1:1000	Cell Signaling
Anti-phosphotyrosine (4G10)	Mouse, mAb	1:500	Millipore
Anti-phospho-SAPK/JNK, T183/Y185	Rabbit, pAb	1:1000	Cell Signaling
Anti-phospho-c-Jun, S63 (54B3)	Rabbit, pAb	1:1000	Cell Signaling
Anti-NEMO (FL-419)	Rabbit, pAb	1:500	Santa Cruz
Anti-IRF3 (FL-425)	Rabbit, pAb	1:500	Santa Cruz
Anti-NP	Mouse, mAb	1:100	Kind gift from S. Ludwig
Anti-Flag (M2)	Mouse mAb	1:500	Sigma
Anti-phospho-Akt, T308	Rabbit, mAb	1:1000	Cell Signaling
Anti-phospho-Akt, S473 (D9E)	Rabbit, mAb	1:1000	Cell Signaling
Anti-Akt	Rabbit, pAb	1:500	Cell Signaling
Anti-NP (Immunofluorescence, PA5-32242)	Rabbit, pAb	1:250	Thermo
Anti-NS1 (IAV)	Mouse, mAb	1:500	Kind gift from S. Ludwig
Anti-phospho-NS1 (IAV)	Rabbit, pAb	1:100	Eurogentec
Anti-phospho-ERK1/2 (SC7976)	Rabbit, pAb	1:1000	Santa Cruz
Anti-phospho-IκBα (5A5)	Mouse, pAb	1:500	Cell Signaling
Anti-β-Tubulin (Tub2.1)	Mouse, mAb	1:1000	Sigma
Anti-actin	Rabbit, pAb	1:1000	Abcam

Primary antibodies (clone)	**Origin**	**Dilution**	**Source**
Anti-JNK (F-3)	Mouse, mAb	1:1000	Santa Cruz
Secondary Antibodies	**Conjugated to**	**Dilution**	**Source**
Goat-anti-mouse IgG	HRP	1:5000	Dianova
Goat-anti-rabbit IgG	HRP	1:5000	Dianova
Goat-anti-rabbit IgG	Cy3	1:5000	Dianova

2.1.5 Antibiotics

Name	**Working conc.**	**Selection**	**Source**
Ampicillin	100 µg/ml	Prokaryotes	Sigma
Puromycin	1 µg/ml	Eukaryotes/Prokaryotes	InvivoGen
Penicillin/Streptomycin	1000 U/ml	Prokaryotes	Life Technologies

2.1.6 Inhibitor

Name	**Working Conc.**	**Target**	**Source**
Defactinib	10 µM	Focal adhesion kinase	Selleckchem
Lapatinib	5 µM	ErbB2	Sigma
PHA-408	3 µM	IKK2	Axon Medchem
Aprotinin	10 µg/ml	Serine proteases	Sigma
Leupeptin	10 µg/ml	Proteases	Sigma
UNC-2025	5 µM	Protein tyrosine kinase	Selleckchem
PF 573228	10µM	Focal adhesion kinase	AdooQ

2.1.7 Oligonucleotides

All oligonucleotides were purchased from Sigma, Germany, dissolved in fresh MilliQ water and stored at -20°C.

Primer Name	Sequence (5' to 3')	Purpose
mNEMO-CRISPR-f	CACCGAGACCCTCCAGCGCTGCC	Cloning
mNEMO-CRISPR-r	AAACGGCAGCGCTGGAGGGTCTC	Cloning
mp65-CRISPR-f	CACCGCGATTCCGCTATAAATGCG	Cloning
mp65-CRISPR-r	AAACCGCATTTATAGCGGAATCGC	Cloning
mIL6-f	TGGATGCTACCAAACTGGAT	Real time PCR
mIL6-r	GGACTCTGGTTTGTCTTTC	Real time PCR
mIFN-beta-f	ATGAACGCTACACACTGCATC	Real time PCR
mIFN-beta-r	CCATCCTTTTGCCAGTTCCTC	Real time PCR
mTBP-f	GGGGAGCTGTGATGTGAAGT	Real time PCR
mTBP-r	CCAGGAAATAATTCTGGCTCAT	Real time PCR
mβ-Actin-f	GAGATTACTGCTCTGGCTCCTA	Real time PCR
mβ-Actin-r	TCATCGTACTCCTGCTTGCT	Real time PCR
PB1-SC35M-f	TCTAGGGCCCGAATTGATGC	Real time PCR
PB1-SC35M-r	CTGCCGTCTGAGCTCTTCAA	Real time PCR

2.1.8 Plasmids

cDNA/construct	Vector	Source
sgNEMO	pX459	This study
sgp65	pX459	This study

cDNA/construct	**Vector**	**Source**
SC35M-PB1 (A/Seal/Massachusetts/1/80 (H7N7)) mouse-adapted	pHW2000	Kind gift from H.-D. Klenk, Marburg
SC35M-PB2 (A/Seal/Massachusetts/1/80 (H7N7)) mouse-adapted	pHW2000	Kind gift from H.-D. Klenk,Marburg
SC35M-HA (A/Seal/Massachusetts/1/80 (H7N7)) mouse-adapted	pHW2000	Kind gift from H.-D. Klenk, Marburg
SC35M-NA (A/Seal/Massachusetts/1/80 (H7N7)) mouse-adapted	pHW2000	Kind gift from H.-D. Klenk,Marburg
SC35M-M (A/Seal/Massachusetts/1/80 (H7N7)) mouse-adapted	pHW2000	Kind gift from H.-D. Klenk,Marburg
SC35M-NS (A/Seal/Massachusetts/1/80 (H7N7)) mouse-adapted	pHW2000	Kind gift from H.-D. Klenk,Marburg
SC35-PB1 (A/Seal/Massachusetts/1/80 (H7N7))	pHW2000	Kind gift from H.-D. Klenk,Marburg
SC35-PB2 (A/Seal/Massachusetts/1/80 (H7N7))	pHW2000	Kind gift from H.-D. Klenk,Marburg
SC35-PA (A/Seal/Massachusetts/1/80 (H7N7))	pHW2000	Kind gift from H.-D. Klenk,Marburg
SC35-NP (A/Seal/Massachusetts/1/80 (H7N7))	pHW2000	Kind gift from H.-D. Klenk,Marburg
SC35-HA (A/Seal/Massachusetts/1/80 (H7N7))	pHW2000	Kind gift from H.-D. Klenk,Marburg
SC35-NA (A/Seal/Massachusetts/1/80 (H7N7))	pHW2000	Kind gift from H.-D. Klenk,Marburg

cDNA/construct	**Vector**	**Source**
SC35-M (A/Seal/Massachusetts/1/80 (H7N7))	pHW2000	Kind gift from H.-D. Klenk,Marburg
SC35-NS (A/Seal/Massachusetts/1/80 (H7N7))	pHW2000	Kind gift from H.-D. Klenk,Marburg
pHW72-Luci	pHW72	Kind gift from Henju Marjuki, Memphis, USA
pCI-neoRenilla-Luci	pCI-neo	Kind gift from E. Izaurralde, Tübingen

2.1.9 *E.coli*strains

Strain	**Source**
Top 10	Invitrogen
XL1-blue	Stratagene

2.1.10 Cell lines

Name	**Cell Type**
MLE-15	The immortalized mouse lung epithelial cells (MLE-15) is a cell line derived from transgenic mice harbouring SV40 TAg under the control of the human SP-C promoter.
293T	Human embryonic kidney cells stably expressing the large T antigen of SV40 virus.
A549	Human alveolar epithelial cells.
MLE-15 p65	MLE-15 cells with an Indel mutation in the p65 gene.

Name	Cell type
MLE-15 NEMO	MLE-15 cells with an Indel mutation in the NEMO gene.
MDCK-II	MDCK-II - Madin-Darby Canine Kidney II is a subclone derived from the heterogenous parent line MDCK.

2.1.11 Instruments

Name	Source
Abbocath-T (26Gx19mm)	Hospira
Cell culture incubator	Heraeus; Nuaire
Cell culture microscope	Hund
Chemidoc	Biorad
Confocal laser scanning microscope (TCS SP5)	Leica
Culture Hood (HB2448)	Heraeus
Western blot developing machine	Afga
Disposable razor med comfort	AMPri
Fine scale (Mettler PM460)	MettlerWaagen
Heat block	Jumotron A. Hartenstein
Luminometer	Berthold technologies
Magnetic stirrer	IKA Labortechnik
Megafuge 1.0 R	Heraeus
FLx800 Microplate fluorescence reader	Bio-tek Instruments
Microwave oven	Quelle/Technostar
Mini centrifuge	Biofuge 13, Heraeus

Name	Source
pH meter (Type 632)	Metrohm
Real time PCR machine 7300	Applied biosystem
Scale (P1200)	Mettler
Scanner Canonscan 9900F	Canon
SDS-PAGE gel system	Invitrogen
Semi-dry membrane transfer device	Biorad
Shaker (Type 3013)	New Braunswick
Sonicator	Branson
Spectrophotometer	Eppendorf
Thermo cycler	Biometra
Vortex (Vibrofix VF1)	IKA Labortechnik
Water bath (SW-20C)	Julabo

2.1.12 Buffers

NP40 lysis buffer
20 mMTris/HCl (pH 7.5)
1% (v/v) NP40
150 mMNaCl
10% (v/v) glycerol
25 mMNaF
1 mM Na_3VO_4
1 mM PMSF
10 µg/ml aprotinin
10 µg/ml leupeptin

5x SDS sample buffer
312.5 mMTris/HCl
25% (v/v) β-mercaptoethanol
50% (v/v) Glycerol
10% (w/v) SDS

0.01% (w/v) Bromophenol blue

10x SDS running buffer
250 mMTris
2 mM Glycine
1% (w/v) SDS

SDS stacking gel (5% (v/v))
125 mMTris/HCl (pH 6.8)
5% (v/v) Acrylamid/Bisacrylamide mix
0.1% (w/v) SDS
0.04% (v/v) APS
0.3% (v/v) TEMED

SDS separating gel
350 mMTris/HCl (pH 8.8)
8-15% (v/v) Acrylamid/Bisacrylamide mix
0.1% (w/v) SDS
0.04% (v/v) APS
0.075% (v/v) TEMED

TE buffer
10 mMTris/HCl (pH 8.0)
1 mM EDTA (pH 8.0)

Transfer buffer
50 mMTris/HCl
40 mM Glycine
20% (v/v) Methanol
0.038% (w/v) SDS

50x Tris-acetate-EDTA (TAE)
0.05 M EDTA
2 M Tris (pH 8.3)
1 M Acetic acid

10x Tris buffered saline (TBS-T)
250 mM Tris (pH 7.4)
1.37 mMNaCl
50 mMKCl
7 mM $CaCl_2$
1 mM $MgCl_2$
0.1% (v/v) Tween 20

DMEM/10% (v/v) FCS/antibiotics (complete DMEM 0.5L)
445 ml DMEM
50 ml FCS (heat inactivated)
5 ml 100x Penicillin/Streptomycin

DMEM/BSA/P/S (infection medium for MDCK-II, A549, MLE-15 and 293T)
492 ml DMEM
5 ml Penicillin/Streptomycin (P/S, 100x)
3 ml BSA (30% (v/v))

Freezing medium
90% (v/v) FCS
10% (v/v) DMSO

Phosphate-Buffered Saline (10x PBS)
0.137 M NaCl
0.27 mMKCl
8.1 mM Na_2HPO_4
1.47 mM KH_2PO_4
Total volume was adjusted to 1 L with $H_2O$and autoclaved.

Ca^{2+}/Mg^{2+} (100x)
1.32 g $CaCl_2$
1 g $MgCl_2$
These reagents were dissolved in 100 ml ddH_2O and then autoclaved and filtered through 0.2 µm membrane disc filters.

PBS/Ca^{2+}/Mg^{2+}/BSA/P/S (100 ml)
10 ml 10x PBS (see above)
87.4 ml ddH_2O (sterile)
1 ml Penicillin/Streptomycin (100x)
0.6 ml BSA (30% (v/v))
1 ml Ca^{2+}/Mg^{2+} (100x)

Avicel Stock (2.5% (w/v))
5 g Avicel-powder was dissolved in 200ml ddH_2O and then autoclaved.

Avicel Medium (100 ml) for focus assay
10 ml 10x MEM
33 ml ddH_2O
1 ml Penicillin/Streptomycin liquid (100x)
1 ml BSA (Solution, 30% (v/v))
50 ml avicel stock (2.5% (v/v))
1 ml 1% (v/v) DEAE-Dextran
4 ml $NaHCO_3$ (7.5% (v/v), pH=9.0-9.3)

Cell fixing buffer (100 ml)
95 ml PBS^{++}
4 ml Paraformaldehyde (PFA) 37% (v/v)
1 ml Triton X-100 (t-Octylphenoxypolyethoxyethanol)

Acetate buffer (1x)
7.708 g (50 mM) ammonium acetate powder
534 µl (8.8 mM) H_2O_2 (30% (v/v))
1950 ml dH_2O
pH was adjusted to 5.0

AEC staining solution (for one 96 well titration plate)
4.5 ml 1x acetate buffer
225 µl 20x AEC substrate (25 mg AEC in 2.5 ml Dimethylformamide)
10 µl H_2O_2 (30% (v/v))

Luria Bertani broth (LB)
1% (w/v) Bacto-trypton
0.5% (w/v) Yeast extract
1% (w/v) NaCl

P1 buffer
50 mMTris/HCl (pH 8.0)
10 mM EDTA
100 µg/ml RNase A

P2 buffer
200 mM NaOH
1% (w/v) SDS

P3 buffer
3 M Potassium acetate (pH 5.5)

Urea lysis buffer
5 ml (200 mM) HEPES (pH 8.0)
27 g sequanol grade urea
0.5 ml (100 mM) Sodium orthovanadate, activated
2 ml Sodium pyrophosphate
50 µl of β-glycerol phosphate
Add H_2O to 50 ml

2.2.13 Biosafety

All experiments involving infectious virus were performed in accordance with German regulations applicable to the propagation of influenza viruses. All experiments involving entire IAV were performed using enhanced biosafety level 2 and 3 laboratories (BSL2 and BSL3) approved for such use by the local authorities (RP, Giessen, Germany).

2.2 Methods

2.2.1 Methods in cell biology

2.2.1.1 Eukaryotic cell culture

Dulbecco's modified medium (DMEM) supplemented with 10% (v/v) fetal bovine serum (FCS), 1% (v/v) penicillin/streptomycin and 2 mM L-glutamine (complete DMEM) was used to grow the cell lines used in this study. Cells were incubated at 37˚C in a humidified atmosphere at 5% CO_2. Cells were cultured in 75 cm^2 or 175 cm^2 flasks and splitted every two days depending on the cell type by the use of trypsin or mechanical strength. For this the adherent cells were washed one time with pre-warmed 1x PBS and detached from the bottom surface of the flask by adding 3 ml trypsin/EDTA, followed by incubation for 2-20 min (depending on the cell type) at 37˚C. Trypsin activity was stopped by addition of 5 ml complete DMEM and cells were pelleted by centrifugation (300x g, 3 min), resuspended in the desired volume of complete DMEM and seeded in new sterile flasks, plates or dishes.

2.2.1.2 Storage of Cells

Freezing: Cells were first washed with 1x PBS and then 5 ml of 1x trypsin-EDTA was added. Cells were incubated at 37°C with 5% CO_2 and 95% humidity and left until cells were detached or loosely adhered, after which 5 ml complete medium was added. Cell suspensions were centrifuged (1200x g, 5 min at 4°C). The cell pellet was gently resuspended with 1 ml freezing medium and transferred into 2 ml cryotubes. The cryotubes were placed into a cooling device and left to freeze gradually in the -80°C freezer. After 24 h, cryotubes were transferred for long time storage at -150˚C.

Thawing: Cryotubes were removed from -150˚C and immediately transferred into a 37°C water bath until complete thawing. Cells were added to 10 ml of pre-warmed complete

DMEM, followed by centrifugation (300x g, 3 min at RT). After removal of the supernatant, the pellet was resuspended in complete DMEM and seeded into appropriate flasks. At the next day, the medium was changed to eliminate dead cells.

2.2.1.3 Transfection of eukaryotic cells

Eukaryotic cells were transfected using Lipofectamine® 2000 transfection reagent according to the manufacturer's protocol. To transfect the cells, the desired amount of plasmid DNA was mixed with 150 µL of OPTI-MEM reduced serum medium and mixed gently.The Lipofectamine® 2000 transfection reagent was also mixed with 150 µL of the OPTI-MEM reduced serum medium. 2 µl of Lipofectamine® 2000/µg of plasmid DNA was further added to this mixture, mixed gently by pipetting and incubated for 30 min at RT.Meanwhile, the cells to be transfected were washed one time with OPTI-MEM and add antibiotic-free OPTI-MEM. The transfection suspension was then added drop-wise to the cells, gently mixed and incubated for 8 hat 37ºC in a cell incubator. Afterwards, the medium was exchanged to fresh complete DMEM.

2.2.1.4 Infection of cells

The virus inoculum was prepared by adding the according amount of virus stock to a defined volume of PBS^{++}/BA depending on the desired multiplicity of infection (MOI) used for the experiment. Confluent cells in 6 well plates or 3.5 cm dishes were washed with 1x PBS^{++} and 500 µl of virus inoculum was laid on top of the cell surface. The plate was gently rolled to ensure that the virus inoculum is equally distributed over the cells. The cells were further incubated at RT for 1 h, after which the inoculum was removed by aspiration. Cells were washed one time with 1x PBS, and 2 ml of infection medium was added. Cells were then further incubated in 5% CO_2 at 37°C for the desired time points.

The calculation of MOI was done as follows:

$$\frac{1000\ \mu l}{\text{Virus titer (FFU)}} = \frac{X\ \mu l\ \text{virus}}{\text{MOIx cell amount in the culture}}$$

2.2.1.5 Generation and amplification of reassorted viruses

For the co-culture of 293T and MDCK-II (cells ratio 7:3) cells were seeded in 3.5 cm dishes 24 h before transfection and were grown to 70% confluence. Then they were transfected (2.2.1.3) with a combination of 8 plasmids encoding the different 8 viral RNA segments in the desired combination according to the genome composition of the required reassortant. 24 h after transfection, the transfection mixture was removed and the cells were incubated with 2 ml of fresh medium. To verify the successful de novo generation of influenza virus the transfected dishes were screened for appearance of a cytopathic effect (CPE) and the harvested medium was screened for infectious particle (2.2.1.9, Foci assay on MDCK-II cells). The progeny viruses were amplified on MDCK-II cells in 75 mm flasks by infection and titrated on MDCK-II cells by foci assays as described in section 2.2.1.9 and stored at -80°C. The generation of all viruses was carried out at biosafety level 3.

2.2.1.6 CRISPR (Clustered Regularly Interspaced Short Palindromic Repeats)-Cas9-mediated gene targeting

Oligonucleotides targeting the first exon of p65 and NEMO gene were cloned into pX459 (Addgene) to obtain the pX459-p65 and pX459-NEMO plasmids. MLE15 were transfected with either pX459 empty vector or pX459-p65 and pX459-NEMO, followed by three days of selection in DMEM containing puromycin (1µg/ml) to eliminate the untransfected cells. Single cell clones were isolated by serial dilution and tested for expression of the p65 and

NEMO protein and Cas9 by Western blotting (2.2.3.2). Cells expressing neither p65 or NEMO nor Cas9 were used for the subsequent experiments.

2.2.1.7 Lysate preparation

2.2.1.7.1 Cell lysis under native conditions

To prepare cell extracts under native conditions, the cells were washed once with cold 1x PBS, harvested by scraping and centrifuged (350x g, 5 min at 4ºC). The cell pellet was resuspended in an appropriate amount of NP-40 buffer freshly supplemented with protease and phosphatase inhibitors (2.1.12) and incubated on ice for 20 min. The lysate was cleared by centrifugation (13000x g, 10 min). The supernatant was collected and used in further experiments or mixed with 5x SDS sample buffer, boiled at 95°C for 5 min and analyzed by SDS-PAGE and Western blotting (2.2.3.1 and 2.2.3.2).

2.2.1.7.2 Cell lysis under denaturing conditions

The analysis of some post-translational modifications demanded protein extraction under denaturing conditions. Therefore, cells were harvested as described above and directly lysed in 100-250 µl of 1x SDS sample buffer. The lysate was boiled at 95°C for 5 min and sonicated two times for 20 sec with a Branson sonifier to shear the genomic DNA. Afterwards, the lysate was analyzed by Western blot analysis.

2.2.1.7.3 Cell Lysis for post transcriptional modification scan

MLE15 cells were grown in 145 mm dishes. After infection with SC35 or SC35M virus at a MOI of 1 for 1 h or 8 h cells were washed with 1x PBS (without Ca^{2+}/Mg^{2+}). 10 ml of urea lysis buffer was directly added to the cells and they were collected in 50 ml falcon tubes,

carefully resuspended and sonified 4 times for 30 sec with a Branson sonifier. After centrifugation (20000x g, 15 min at 4˚C) the supernatant was taken and used for BCA to measure the protein concentration. An aliquot of the supernatant was used for Western blot (2.2.3.2) while the remaining material was stored at -80^{o}C and then sent for mass spec analysis.

2.2.1.8 Immunofluorescence

Cells were grown in 12-well plates on glass cover slips and infected with SC35 or SC35M virus at a MOI of 3. 8-24 h post infection cells were washed twice with 1 ml of 1x PBS and fixed for 10 min with 0.5 ml of 4% (v/v) PFA at RT. The fixing solution was aspirated and cells were washed again with 2 ml of 1x PBS and permeabilized with 0.5 ml 0.5% (v/v) Triton X-100 for 7 min. The cells were then washed again with PBS and blocked for 60 min with 1 ml of 1x PBS containing 10% (v/v) BSA. Cells were incubated with 0.5 ml of the primary antibodies diluted in 1x PBS containing 1% (v/v) BSA overnight at 4°C. The next day cells were washed three times for 5 min with 1x PBS and incubated with 0.5 ml of the Cy3-conjugated secondary antibody diluted in PBS containing 1% (v/v) BSA for 2 h in the dark. The incubation was followed by three washing steps of 5 min each with 1x PBS. Nuclear DNA was stained by incubating the cells with Hoechst 33324 (1 µg/ml) for 7 min. Cells were again washed three times for 5 min with PBS and then mounted on microscope slides with IS mounting medium and sealed with roti-seal. The stained proteins were analyzed using a confocal laser scanning microscope (Leica TCS SP5). Only intact interphase cells were analyzed, dying or mitotic cells and cells expressing aberrantly high levels of the proteins were not analyzed.

2.2.1.9 Foci assay

Virus dilutions were made in the 96 well plates with U-form bottom. First 180 µl of PBS^{++} /P/S/BSA was pipetted into each well and 20 µl of the virus stock was added to the wells of the first row. The virus dilution (200 µl) was mixed by up and down pipetting and 20 µl of it was transferred into wells of the second row. The same steps were repeated up to the last row (A-H) to get 10^{-1} to 10^{-8} dilution series. For each row the pipette tips were changed. MDCK-II cells were seeded in 96-well plates and grown over night at 37°C with 5% CO_2 so that they were 90% confluent on the day of infection. The cells were washed once with 1x PBS^{++}, then infected by transferring 50 µl of the different virus dilutions and incubated at RT for 1 h. Virus inoculum was aspirated off and 150 µl Avicel medium was added to each well. The plate was placed at 37°C with 5% CO_2 for 30 h or 48 h depending on the virus strain. After the incubation, Avicel medium was removed by aspiration. Cells were washed twice with 1x PBS^{++} and fixed, as well as permeabilized, with 330 µl/well of 4% (v/v) PFA/1% (v/v) TritonX-100 in 1x PBS^{++} for 1 h at RT. Afterwards, cells were washed and three times with 1x PBS/0.05% (v/v) Tween20and incubated with 50 µl of primary antibody (anti NP-mAb), 1:6000 diluted in PBS^{++}/3% (w/v) BSA) for 1 h at RT. After aspirating the primary antibody dilution, cells were again washed three times with PBS/0.05% (v/v) Tween20, followed by secondary antibody incubation horse radish peroxidase (HRP)-conjugated anti mouse antibody, 1:1000 diluted in PBS^{++}/3% (w/v) BSA) for 45 min at RT. Cells were washed three times with PBS/0.05% (v/v) Tween20 and 40 µl of AEC staining solution was added into each well and placed at RT for 30-60 min. The AEC staining solution is used for staining peroxidase labeled compounds in immunohistochemistry or immunoblotting techniques. AEC produces an insoluble end-product which has a red color. Red stained foci were observed under the microscope, wells were washed with normal water to remove the rest of salts and air dried at RT. After drying, the plates were scanned at 1600 dpi and virus foci

were counted. A single focus was defined as more than 3 adjacent cells that were stained in one particular area, as opposed to single cell staining which is not indicative for the production of an infectious virus.

The viral titer was determined as follows:

FFU/ml = number of foci**x** volume factor**x** dilution factor

Volume factor: FFU (Foci forming unit) is related to 1 ml. If a dish was infected with 50 µl viral dilution solution, the factor is 20.

2.2.1.10 Hemagglutination (HA) assay

Red blood cells (RBCs) used in this test were obtained from specific pathogenfree (SPF) chickens or normal chickens that are shown to be clear from antibodies to influenza viruses. First of all, 20 ml fresh chicken blood was transferred to a 50 ml sterilized falcon tube containing 7.5 ml of 3.7% (w/v) sodium citrate. The RBCs were washed several times by filling the falcon tube to 50 ml with cooled 1x $PBS^{++}$and centrifuged (1500x g, 5 min at 4°C). The supernatant containing serum was separated from white blood cells and fat and the RBC pellet was then washed and centrifuged as described until clear supernatant was obtained. Finally, the washed RBC pellet was diluted with 1x PBS to a 10% (v/v) stock and from there into a 0.5% (v/v) working solution with cold 1x PBS^{++} for the HA assay. For this, 50 µl of1x PBS^{++} was dispensed into each well of a plastic U-bottomed 96 well plate, then 50 µl virus suspension/sample were applied to the first well in a row (rows A-H). The 1:1 diluted virus in well 1 was further 2 fold serially diluted by transferring 50 µl of the diluted virus into the next well of the row (wells from 1 to 12). At the last well the extra 50 µl were discarded.

Subsequently, 50 µl of 0.5% (v/v) chicken RBCs were dispensed to each well and then the RBCs were allowed to settle for about 30-60 min at 4°C.

The Hemagglutination units (HAU) are: 2^X, where X is the number of the last well without blood precipitated on the bottom.

2.2.2 Methods in molecular biology

2.2.2.1 Production of chemically competent *E.coli*

To produce chemically competent bacteria, 15 ml of antibiotic-free 1x LB medium was inoculated with the desired strain of *E.coli* from a glycerol stock and incubated overnight at 37°C with agitation. At next day 120 ml of pre-warmed 1x LB medium were added to the culture, followed by shaking at 37°C for approximately 1 h until the optical density (OD) at 600 nm reached a value between 0.5 and 0.7. All of the following steps were performed on ice or at 4°C. The bacteria were cooled down on the ice and thereafter centrifuged (4000x g, 4 min). The supernatant was discarded and the pellet was resuspended in 25 ml of a sterile, pre-cooled 0.1 M $CaCl_2$ solution. This suspension was incubated on ice for 30 min and the cells were collected again by centrifugation (4000x g, 4 min). In the next step, the cell pellet was resuspended in 3 ml of a sterile 0.1 M $CaCl_2$ solution containing 10% (v/v) glycerol. Aliquots of 100 µl competent *E.coli*were frozen in liquid nitrogen and stored at -80°C. Test transformations were performed in order to ensure high and efficient uptake of plasmid DNA.

2.2.2.2 Transformation of chemically competent E.coli by heat shock

To transform chemically competent *E.coli*strains, 100 µl of the competent cells were thawed on ice. Then up to 50 ng of plasmid DNA or 10 µl of a ligation reaction (section 2.2.2.12)

were added to the *E.coli*and mixed carefully. After 15 min incubation on ice, the mixture of chemically competent bacteria and DNA was placed at 42°C for 90 sec (heat shock) and then placed back on the ice for 2 min. 700 µl of LB medium was added and the transformed cells were incubated at 37°C for 45 min with agitation. Afterwards, the mixture was centrifuged, and the cell pellet was resuspended in the 100 µl LB medium and spread onto a pre-warmed LB plate containing antibiotics for the respective plasmid. The plates were incubated overnight at 37ºC. Next day, single colonies were picked and inoculated in LB medium with ampicillin and grown on a shaker overnight at 37°C. The next day, plasmid DNA was isolated from this bacterial culture. Glycerol stocks were prepared by mixing 850 µl bacterial culture with 150 µl autoclaved 100% (v/v) glycerol. Glycerol stocks were kept at -80°C for future use.

2.2.2.3 Purification of plasmid DNA from *E.coli*

For the extraction of plasmid DNA from *E. coli* in a small scale (Mini prep), an alkaline extraction protocol was used. 2 ml of transformed E. coli cells were grown overnight in selective LB medium. On the next morning, bacterial cells were harvested by centrifugation (4000x g, 3 min) and the pellet was resuspended by adding 200 µl buffer P1.The same volume of buffer P2 was added to lyse the *E.coli* cells. The tube was inverted multiple times and incubated at room temperature (RT) for 5 min. Thereafter the lysate was neutralized with 200 µl of chilled buffer P3 and mixed thoroughly. The tubes were then incubated for 20 min on ice and subsequently centrifuged (12000x g, 10 min) to pellet the genomic DNA and bacterial debris. The supernatant containing the plasmid DNA was precipitated by the addition of 0.7 volumes of isopropanol, pelleted by centrifugation (12000x g, 15 min) and

washed with 500 µl of 70% (v/v) ethanol. The ethanol was discarded, the DNA pellet was air-dried and dissolved in 30 µl H_2O or TE-buffer.

For large scale plasmid purifications (Maxi-Prep), the GeneJet Plasmid Maxiprep purification kit was used according to the manufacturer´s instructions. Pelleted bacterial cells were resuspended in resuspension buffer and subjected to SDS/alkaline lysis to liberate plasmid DNA. Cell debris and precipitated proteins were pelleted by centrifugation according to manufacturer´s instructions. The supernatant containing plasmid DNA was loaded onto the purification column. The high salt concentration of the lysate creates appropriate conditions for plasmid DNA binding to the silica membrane in the spin column. The adsorbed DNA was washed to remove contaminants and eluted with the elution buffer.

The concentration of the DNA was quantified by measuring the OD at 260 nm. An OD_{260} of 1.0 corresponds to 50 µg/ml of DNA. The ratio of the OD_{260}nm/OD_{280}nm was used to control the purity of the samples; DNA samples having a ratio between 1.8 and 2 were further used in experiments and also stored at -20°C.

2.2.2.4 RNA Isolation

Subconfluent cells in 6 well plates were infected in triplicates with different IAVs at different MOIs. The total RNA (viral and cellular) was extracted with the Trizol reagent at different time points post infection (p.i.). Briefly, the medium was aspirated from infected cells, washed with 1 ml of 1x PBS and 1 ml of Trizol was added to the cell monolayer in each well and incubated together for 5 min at RT. Trizol-treated cells were transferred into a microcentrifuge tube and incubated at RT for 10 min. 200 µl of chloroform was added to each reaction tube, mixed properly and incubated for 5 min at RT with intermittent shaking. The microcentrifuge tubes were then centrifuged (13000x g, 20 min at 4°C). This results in

separating the mixture into three phases. Subsequently, 500 µl of the upper phase was transferred into fresh microcentrifuge tubes. 500 µl isopropanol was added, mixed properly and incubated for 10 min at RT. Afterwards, the tubes were centrifuged (13000x g, 20 min at 4ºC). The supernatant was discarded carefully and 1 ml of 70% (v/v) ethanol was added to the pellet and centrifuged (13000x g, 5 min at 4°C). The supernatant from each tube was removed carefully, the pellet was air dried and dissolved in 30 µl of nuclease free water. The extracted RNA was used directly or kept at -80°C until use. RNA concentration and purity were quantified by OD_{260} nm and purity was measured by obtaining the ratio between OD_{260} nm and OD_{280} nm.

RNA concentration: 1 $OD_{260\ nm}$ = 40 µg/ml RNA

RNA purity: $OD_{260\ nm}/OD_{280\ nm} \approx 2.0$

2.2.2.5 Complementary DNA (cDNA) synthesis

The reverse transcription reaction, used to synthesize cDNA from the isolated mRNAs included the following components:

RNA	1 µg
Oligo(dT) primer	250 ng
dNTP mix (10 mM each)	1 µl
RNase-free H_2O	to 12 µl total volume

After heating to 65°C for 5 min and cooling on ice, the following reagents were added:

5x First-strand buffer	4 µl
0.1 M DTT	2 µl
RiboLock RNase Inhibitor	40 U
SuperScript II transcriptase	200 U

The samples were incubated in the thermocycler at 42°C for 55 min and thereafter the reaction was inactivated by heating at 70°C for 15 min. The cDNA was diluted with sterile water to a volume of 100 µl and used as a template for amplification in the quantitative real-time PCR.

2.2.2.6 Restriction digestion of DNA with endonucleases

For the sequence specific digestion of plasmid DNA, restriction endonucleases and buffers were used. Most restriction endonucleases recognize and cleave specific 4-7 bp long palindromic sequences, thereby creating 5' or 3' overhangs (sticky ends) or blunt ends of digested DNA.

For analytical digestion of plasmids or PCR products, the following reaction mix was incubated for 1 h at an enzyme-specific temperature (in general 30ºC or 37°C):

Restriction enzyme 1	1 - 2.5 U
Restriction enzyme 2	1 - 2.5 U
1x restriction buffer (or 2x Tango buffer)	2 µl
Plasmid DNA	1 µg
H_2O	to 10 µl total volume

Preparative digestion for subsequent ligation was performed by increasing the DNA amount and increasing the incubation time for the restriction to several hours. Restriction enzymes were heat-inactivated according to the manufacturer's instructions.

2.2.2.7 Agarose gel electrophoresis

Agarose gel electrophoresis of DNA samples was performed after restriction digestions or analysis of PCR reactions. To separate DNA fragments according to their size, 0.8-2.0% (w/v) agarose gels were prepared in TAE buffer and 0.2 µg/ml ethidium bromide was added.

Ethidium bromide intercalates into DNA and allows its visualization under UV light. Before the gel was loaded, DNA samples were mixed with 6x DNA loading dye. Gelswere run in TAE buffer at a constant voltage of 80 V.

2.2.2.8 DNA extraction from agarose gels

Gel electrophoresis the DNA fragment of interest was excised from an agarose gel using a clean scalpel. The DNA was extracted using the JET quick gel extraction spin kit according to the manufacturer´s instructions. After binding of the DNA to a silica membrane, the DNA was washed with an appropriate buffer and finally eluted with 30 µl sterile water.

2.2.2.9 Dephosphorylation of linearized plasmid DNA

To avoid self-ligation of vectors the 5'phosphates from both ends of the vector were removed using the shrimp alkaline phosphatase (SAP), thus the vector was not able to re-circularize without the insert.

The reaction mix for dephosphorylation with SAP was as follows:

Linearized plasmid DNA (1µg/µl)	1-3 µg
10x SAP buffer	2 µl
SAP (1 U/µl)	1 µl
H_2O	to 10 µl total volume

The mixture was then incubated for 30-60 min at 37°C. Afterwards the enzyme was inactivated by incubation at 65°C for 15 min or removed by separating the sample in an agarose gel.

2.2.2.10 Phosphorylation of insert

The transfer of the γ-phosphate of adenosine triphosphate (ATP) to the 5′-OH group of DNA is catalyzed by T4 polynucleotide kinase (T4 PNK). The mixture for PNK reaction is as follows,

Primer Forward	2 µl
Primer Reverse	2 µl
10x reaction buffer	10 µl
10 mM ATP	1 µl
H_2O	84 µl
PNK (10 U/µl)	1 µl

The reaction was performed at 37 °C for 1 h and PNK was inactivated by heat (75°C for 10 min).

2.2.2.11 Ligation of DNA fragments

Insertion of DNA fragments into vector plasmids was performed by enzymatic ligation. Dephosphorylated vector DNA was mixed with insert DNA in a molecular ratio of 1:1 or 1:3. Ligation was performed in the following reaction mix for at least 2 h at RT or with a decreasing temperature gradient for 16 h at 4ºC:

10x T4 DNA ligase buffer	2 µl
T4 DNA ligase (1U/µl)	1 µl
Linear vector DNA (20-100 ng)	1-3 µl
Insert DNA (1:1 or 1:3)	2-10 µl
H_2O	to 20 µl total volume

A sample of the reaction mix was directly used for transformation of competent *E.coli*and the remaining DNA was stored at -20°C.

2.2.2.12 Quantitative real-time PCR

To quantify changes in expression levels of specific genes, mRNA changes in different samples were determined by isolation of total RNA, conversion into cDNA and amplification with gene specific primers by quantitative real-time PCR. The fluorescent dye SYBR Green used inthe real-time PCR intercalates non-specifically between the bases of dsDNA after every round of amplification, thereby allowing the amplification and at the same time the accurate quantification of the target sequence. The reaction was performed in 96 well plates and included the following components:

cDNA (2.2.2.5)	2 µl
Forward primer	50-100 nM
Reverse primer	50-100 nM
1x SYBR Green ROX mix	5 µl
H_2O	to 10 µl total volume

The PCR reactions were carried out using an Applied Biosystems 7300 Real-time PCR system with the following parameters:

Initial denaturing step	15 min	95°C
Denaturing	15 sec	95°C
Annealing of the primers	30 sec	60°C
Elongation	1 min	72°C
Number of cycles	40	step 2-4

Following the amplification, a melting curve analysis was performed to evaluate the specificity of the amplification products. Ct-values were normalized to the housekeeping gene and the relative abundance of transcripts was calculated by the comparative ΔΔ Ct method.

2.2.2.13 Site-directed point mutagenesis

To introduce point mutations into DNA sequences, the StratageneQuikchange II site-directed mutagenesis kit was used according to manufacturer's protocol. The procedure required the

plasmid with the insert of interest as a template and two synthetic oligonucleotide primers carrying the desired point mutation. The PCR reaction was prepared with the following reagents:

dsDNA template	20 ng
dNTP mix (10 mM each)	1 µl
Forward primer	125 ng
Reverse primer	125 ng
10x reaction buffer	5 µl
Quik solution reagent	3 µl
Pfu Ultra DNA polymerase	2.5 U
H_2O	to 50 µl total volume

The amplification of the mutated plasmids was carried out under the following cycling conditions:

Initial activation step	1 min	95°C
Denaturation	50 sec	95°C
Annealing of the primers	50 sec	60°C
Elongation	1 min per kb	68°C
Number of cycles	18	step 2-4
Final elongation step	7 min	68°C

Following the amplification, the PCR products were treated with the restriction endonuclease DpnI. This enzyme specifically recognizes the sequence GATC with a methylated Adenin and therefore cleaves only the methylated non-mutated template DNA but not the newly synthesized, unmethylated PCR product containing the mutation. The DpnI-treated PCR-product was then transformed into competent *E.coli*and the entire transformation reaction was plated on LB agar plates. The resticted strand will be replaced according to the non-restricted, mutated strand by bacterial enzymes. Plasmid DNA was isolated from the bacteria and further characterized by restriction cutting and sequencing.

2.2.3 Methods in biochemistry

2.2.3.1 SDS polyacrylamide gel electrophoresis (SDS-PAGE)

SDS-PAGE was performed to separate proteins by their molecular size and for further analysis by Western blotting (2.2.3.2). SDS gels were freshly prepared consisting of stacking and separation gels. SDS and potent reducing agent β-mercaptoethanol were used to denature and negatively charge the polypeptide chains and to disrupt disulfide bonds which mediate inter- and intra-molecular protein interactions. Discontinuous gel electrophoresis allowed gathering of proteins in the upper stacking gel and subsequent separation by size during migration through the lower separating gel.

Samples were denatured by addition of SDS sample buffer and incubation at 95°C for 5 min. The appropriate volume of samples was loaded in each lane of the gel together with a molecular-weight marker in a separate lane. Gels were prepared as 8 - 15 % (v/v) acrylamide depending on the expected protein size. Gels were run in SDS running buffer at a constant voltage of 80 V for 2-3 h.

2.2.3.2 Western blot

Proteins separated by SDS-PAGE were transferred to and immobilized on a polyvinylidene fluoride (PVDF) membrane by the Western blot method, which allows the detection of proteins by specific antibodies. For the transferring step, the methanol-activated PVDF and three Whatman papers were soaked in transfer buffer; then two layers of Whatman paper, the PVDF membrane, the gel and another layer of Whatman paper were stacked and the transfer was performed using a semi-dry transfer device at a constant voltage of 24 V for 2-3 h. After the proteins were transferred to the PVDF membrane, the membrane was blocked in 5% (w/v) non-fat dried skimmed milk powder or BSA in 1x TBS-T buffer for 30 min at RT in

order to reduce unspecific binding from antibodies. Primary antibodies were diluted in TBS-T containing 1% (w/v) non-fat dried skimmed milk powder or TBS-T containing 1% (w/v) BSA and the PVDF membranes were incubated with 10 ml of the respectively primary antibody overnight at 4°C. Next day the membranes were washed five times for 5 min in TBS-T, afterwards incubated with the corresponding horseradish peroxidase-coupled secondary antibody in 10 ml of skimmed milk for 2 h at RT. Unbound antibodies were removed by washing the membrane five times for 5 min with TBS-T and proteins were detected using the Western Lightning ECL solutions and developed either using an autoradiography or the Chemidoc touch imaging system.

2.2.3.3 Luciferase assay

To test which mutation in the PB1 subunit affects viral polymerase activity, the Dual-Luciferase reporter assay system kit was used according to manufacturer's protocol. Briefly, 293T cells were seeded in 6-well plates ($2x10^5$ 293T cells/well) and co-transfected with 1µg of either pHW2000-PB1 or various mutations thereof or empty pHW2000 plasmid (polI/ploII responsive) mixed with 2 µg of pol I-driven plasmid to generate a vRNA-like polI-transcript encoding the firefly luciferase gene (pHW72-Luci), 1 µg pCI-neoRenilla-Luci (transfection control) and 2 µg each of pHW2000-NP-SC35M, pHW2000-PB2-SC35M, pHW2000-PA-SC35M to reconstitute in vitro the respective RNP complexes. Transfection was performed using Lipofectamine for 8 h. After 24 h post-transfection, the cells were harvested, washed, lysed with 1x passive lysis buffer. 10 µl LARII substrate was mixed with 2 µl of cell lysate in a luminometer tube and firefly luciferase activity was measured. After addition of 10 µl of stop and glow buffer, the bioluminescence of Renilla luciferase was determined using a

luminometer. The relative activities were calculated after the normalization of the Renilla luciferase activities to the activities of the firefly luciferase.

2.2.3.4 Neuraminidase assay

The NA activity of viruses was measured by fluorescence-based assay according to the manufacture's protocol. Briefly, wild-type and mutated viruses were titrated by HA assay and the amount corresponding to 60 HA units for each virus was used. Viruses were inactivated by using 0.2% (v/v) Triton X-100 at 37ºC for 2 h. Equal titers of the IAVs were serially diluted in a black, 96 well, flat bottom plates with assay buffer and NA-Fluor™ Substrate working solution was added to each well. The reaction was incubated for 1 h in 37°C and terminated by adding NA-Fluor™ Stop solution to each well. Relative fluorescence unit (RLU) was measured by using FLx800 microplate fluorescence reader with an excitation wavelength of 360 nm and an emission wavelength 460 nm.

2.2.4 Statistical analysis

Statistical tests and graphical data presentations were carried out using GraphPadPrism 5.0 software (GraphPad Software, USA). The statistical significance of differences between the indicated groups was tested by using the unpaired Student's t-test. All data were presented as Standard Error of the Mean (SEM). The degree of significance is presented byasterisks (*), while (ns) represents non-significant difference.

2.2.5 Bioinformatic analysis

All statistical analyses were performed by Dr. Axel Weber (Institute of Pharmacology, University of Giessen) with whom I interacted closely to coordinate the analyses of the phosphoproteomic screen. Statistical analyses were realized by self-created scripts in R statistical language (R Core Team, 2017) including packages for R or for R/Bioconductor. Tables containing color coded columns and heatmaps were created with Microsoft Excel 2010. Sets of regulated phosphoproteins in the kinetic analyses were analyzed by STRING database version 10.5. The phosphosite motif analysis was done by using motif-x version 1.2 10.05.06. Enrichment analyses for Gene ontology (GO) terms and Kyoto Encyclopedia of Genes and Genomes (KEGG) pathways were done by the use ofcompare Cluster function of the R package ClusterProfiler version 3.4.4. The joint overrepresentation analysis of KEGG and GO biological process terms was done in Cytoscape version 3.5.0 using the app ClueGO version 2.3.4.

3 Results

3.1 The role of IAV genotype on NF-κB function

3.1.1 Generation of NF-κB defective MLE-15 cells

It has been already known for long time that NF-κB has an important role in IAV propagation and replication. Some studies showed IAV supporting functions of NF-κB, while some displayed an antiviral role of NF-κB (Maelfait et al., 2012; Nimmerjahn et al., 2004). To identify the precise role of NF-κB in IAV propagation and adaptation to new species, two critical components of canonical NF-κB activation pathway were eliminated by using the CRISPR-Cas9 system in MLE-15 cells.

The NEMO protein was targeted as it is an essential component of the IKK complex and required for the canonical NF-κB activation pathway (Yamaoka et al., 1998). IKKs also display NF-κB-independent functions upon phosphorylation of different additional cytoplasmic and nuclear substrate proteins (Chariot, 2009). Also the important DNA-binding subunit p65 was targeted by CRISPR-Cas9.

MLE-15 cells were transfected with a vector directing the expression of Cas9 and an appropriate sgRNA targeting the first exon of either the gene encoding NEMO (pX459-NEMO), the gene encoding p65 (pX459-p65) or an empty control, followed by puromycin selection for two days in order to establish stable cell lines. Single cell clones were isolated and tested for expression of the NEMO or p65 protein and Cas9 by Western blotting. Cells expressing neither NEMO or p65 nor Cas9 were selected for further use (Fig 8A,B). These cells were then characterized by DNA sequencing. The NEMO mutation inserted a frameshift after amino acid 53, thus ensuring that all functionally relevant domains of te protein are not

expressed (data not shown). The p65 mutation destroyed the start codon, leading to the complete absence of the p65 protein (data not shown).

In a first set of experiments it was important to ensure that IAV induced NF-κB activation was defective after deletion of p65 or NEMO. Control MLE-15 cells or p65 deficient ($p65^-$) or NEMO deficient ($NEMO^-$) cells were infected with SC35 or SC35M at a MOI of 1 for 24 h, followed by analysis of expression of the IL-6 gene. IL-6 is a prototypical NF-κB target gene and its promoter contains a functional p65 binding site (Handschick et al., 2014; Libermann and Baltimore, 1990). The analysis of relative mRNA levels by qPCR showed that knockout of p65 or NEMO can significantly prevent inducible IL-6 expression (Fig 8C).

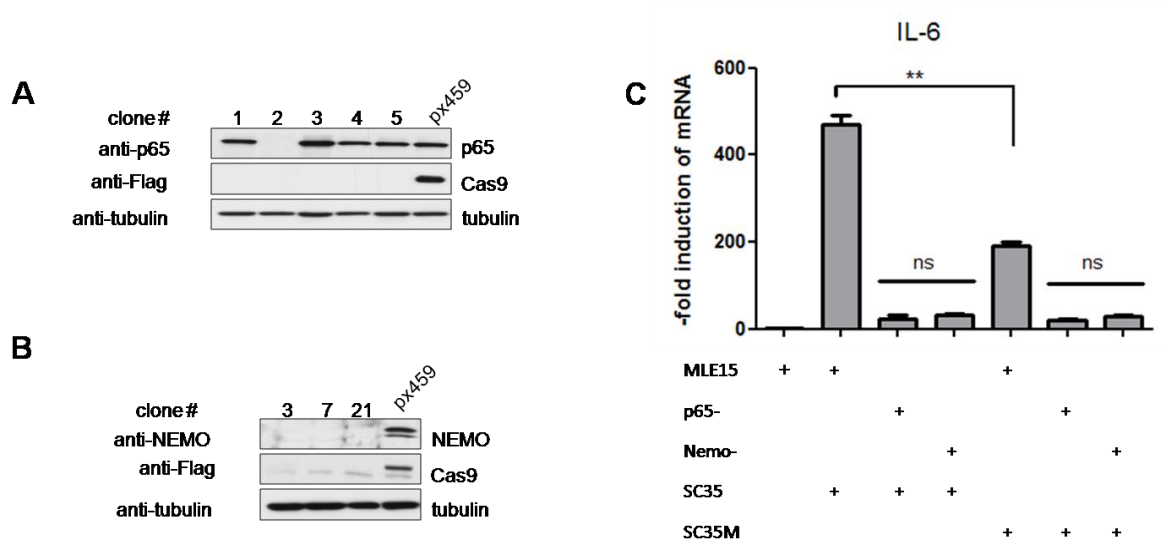

Figure 8: Generation and characterization of NF-κB-defective MLE-15 cells.(A) Cells were transfected with the vector px459 or px459-p65. Transfected cells were selected by puromycin treatment, and surviving clones were grown to colonies. A fraction of the cells were lysed, and equal amounts of protein were tested by immunoblotting for expression levels of p65, Cas9, and tubulin with specific antibodies. **(B)** The experiment was performed similarly as in panel A, with the difference that cells were transfected with px459-NEMO and extracts from cell clones were tested for the expression of NEMO. **(C)** The indicated cells were infected with SC35 or SC35M (MOI of 1), and IL-6 gene expression was quantified by qPCR 24 h p.i. Error bars display standard errors of the means (SEM) derived from two independent experiments performed in triplicate. Student's t test was used for statistical analysis. **, $p<0.01$. ns, not significant.

3.1.2 NF-κB inactivation improves propagation of the avian, non-adapted SC35 virus in murine MLE-15 cells

MLE-15 control cells or MLE-15 p65$^-$ or MLE-15 NEMO$^-$ cells were infected with SC35 or SC35M virus at a MOI of 0.001. Supernatants were harvested 24 hour post infection (h p.i.) to measure the replication of the respective virus. The mouse-adapted SC35M viruses grew to a higher titer in the murine MLE-15 cell line irrespective of the functionality of the NF-κB system. In contrast, the poor propagation of bird-adapted SC35 virus was significantly improved upon deletion of either p65 or NEMO (Fig 9A).

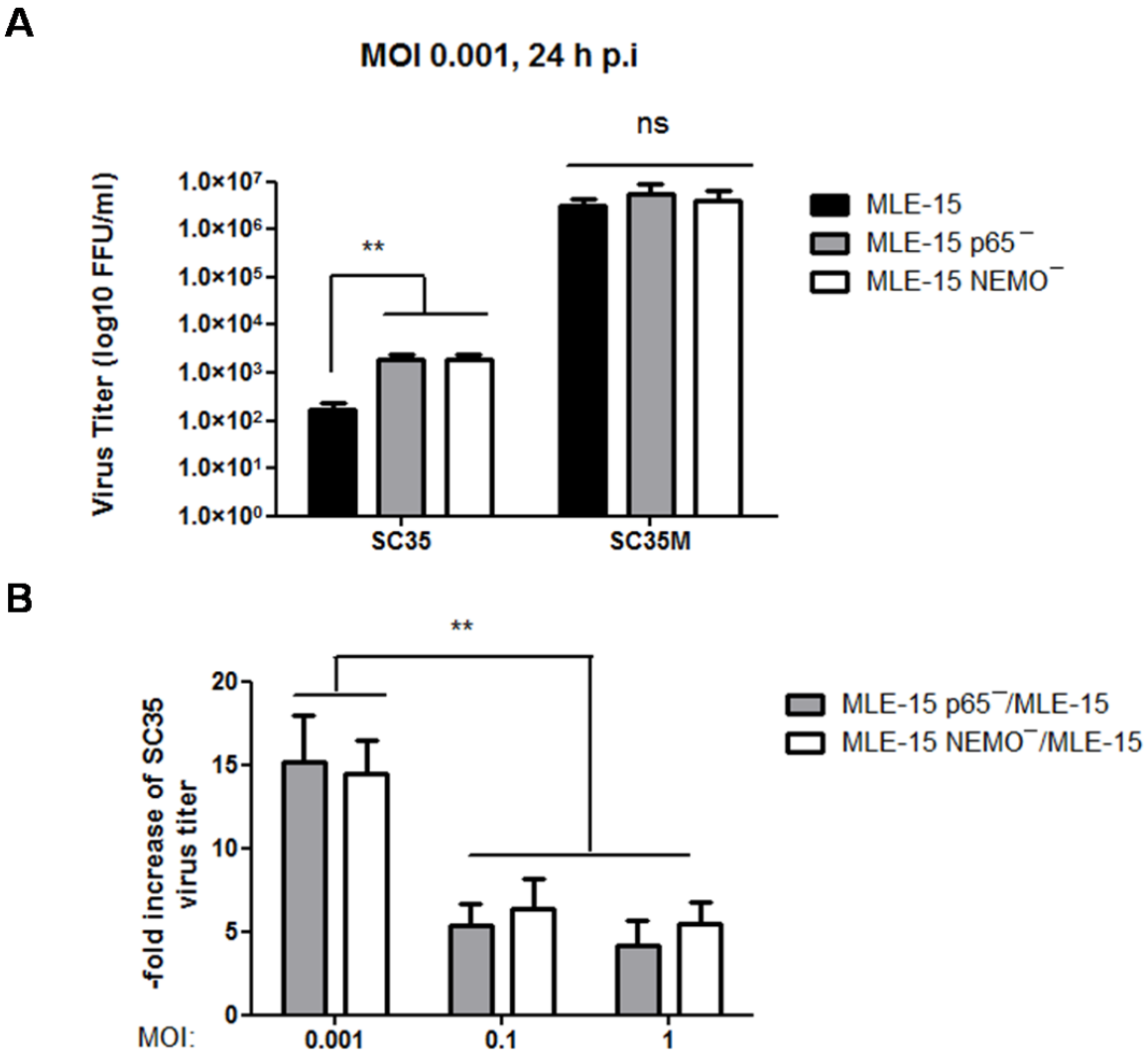

Figure 9: Inhibition of NF-κB allows increased production of SC35.(A) The indicated MLE-15 cells were infected with SC35 or SC35M (MOI of 0.001). The plaque titers were determined 24 h p.i. on MDCK-II cells. The virus titer is indicated; error bars show SEM obtained from three independent experiments performed in triplicate. **(B)** MLE-15 cells and their NEMO- and p65-deficient derivatives were infected with SC35 at different MOI. The plaque titers were determined 24 h p.i. and the ratio between virus numbers in knockout cells and those in control cells is displayed on the y axis. Error bars show SEMs obtained from five independent experiments performed in triplicate. **, p<0.01.ns, not significant.

To further investigate whether the contribution of NF-κB to SC35 propagation is dependent on the virus load, control or $p65^-$ or $NEMO^-$ cells were infected at different MOIs (0.001, 0.1, 1) and virus titers were determined 24 h p.i. The antiviral role of NF-κB was most prominent at a low MOI of 0.001, but this effect was significantly reduced at higher virus concentrations, which showed only minor differences lacking biological and statistical significance (Fig 9B).

3.1.3 NF-κB deficiency affects expression and localization of IAV-encoded proteins

As the NS1 protein is an important viral factor counteracting cellular immune responses it was interesting to investigate whether the improved replication of SC35 virus in p65 and NEMO knockout cells would also be reflected at the level of viral NS1 protein expression. Control or $p65^-$ or $NEMO^-$ cells were infected with SC35 or SC35M at a MOI of 1. Cells were lysed after 0, 3, 6 and 8 h p.i. Infection of cells with SC35M allowed NS1 detection 6 h p.i. in cells with or without functional NF-κB (Fig 10A). Infection of control cells with SC35 showed poor NS1 expression after 6 h of infection, while $p65^-$ and $NEMO^-$ cells displayed earlier and stronger expression of the NS1 of SC35 (Fig 10A).

To investigate the impact of NF-κB signaling on IAV encoded proteins by a different experimental approach, the intracellular localization of the NP protein was analyzed by indirect immunofluorescence. The intracellular localization of NP is a convenient marker for the early stage (0 to 4 h p.i.) of the viral replication cycle where the NP accumulates in the

nucleus to help the virus replication as part of the RNP complex. At a later stage (4 to 8 h p.i.) the RNPs (containing the NP) are exported in the cytoplasm to be transported to the cell membrane where they are packaged into progeny virions and budding from the cell surface (Whittaker et al., 1996).

In order to find out whether NF-κB activity can influence the intracellular localization of NP, control cells, p65 and NEMO knockout cells were infected with SC35 for 6 h. Indirect immunofluorescence revealed that some NP is still found in the nucleus of most SC35 infected control cells, while in $p65^-$ or $NEMO^-$ cells, the NP protein mostly localized in the cytoplasm (Fig 10B). The immunofluorescence experiment also showed an increased amount of NP in p65 and NEMO deficient cells, supporting the idea that infection is already more efficient in NF-κB deficient cells. No changes in NP localization were observed in SC35M infected cells (data not shown). All together these data showed that effect of NF-κB on IAV replication is already seen at the earlier stages of virus replication prior to their release from the host cell.

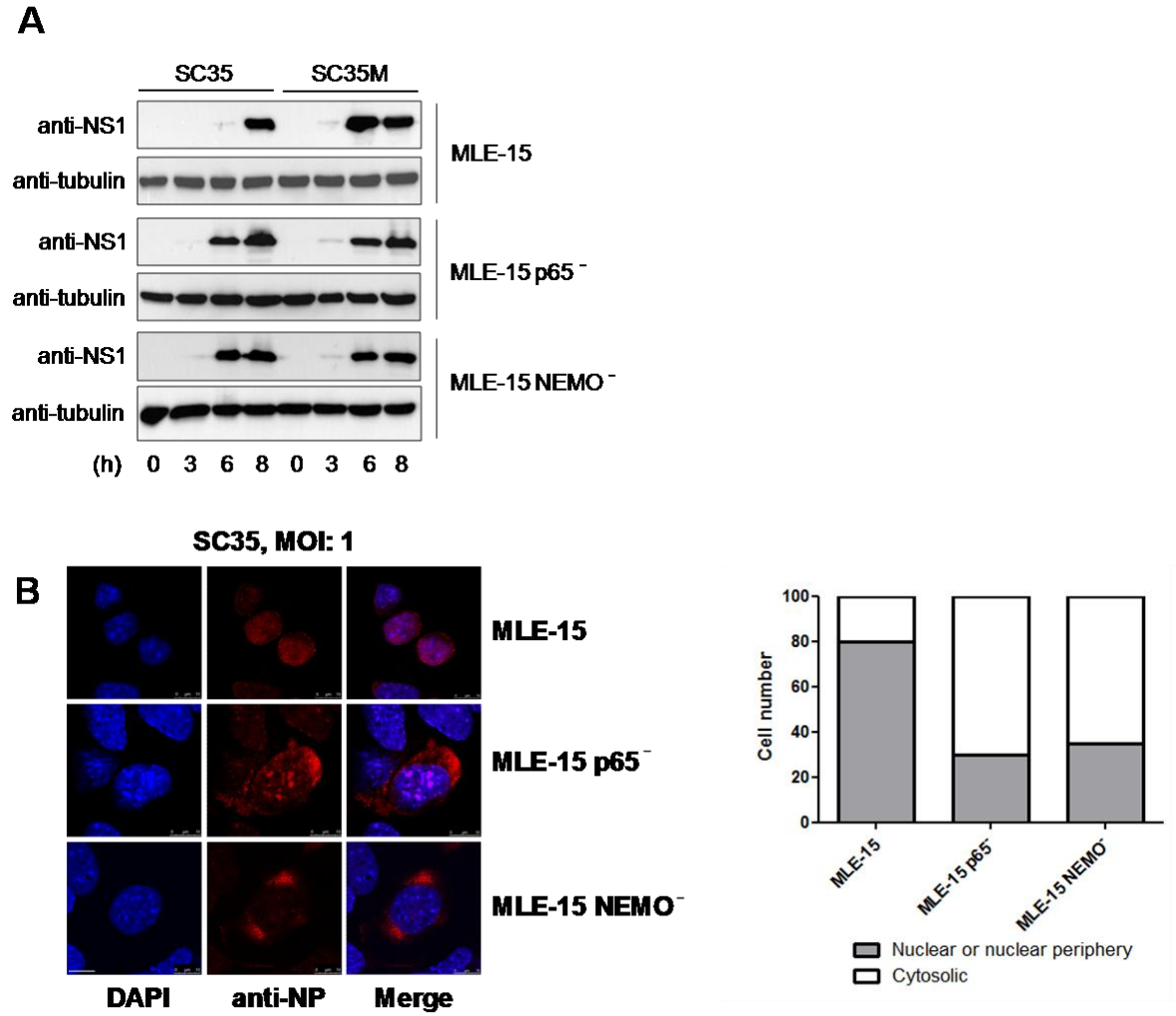

Figure 10: NF-κB deficiency increases expression of SC35 NS1 and earlier nuclear export of SC35 NP.(A) The indicated cells were infected with SC35 or SC35M (MOI of 3) for the indicated periods. Cells were harvested, and cell extracts were analyzed by immunoblotting for the occurrence of the viral NS1 protein and the loading control tubulin with specific antibodies. **(B)** MLE-15, MLE-15 NEMO$^-$, and MLE-15 p65$^-$ cells were infected with SC35 (MOI of 1). Cells were fixed 6 h p.i., and the amount and localization of NP were determined by indirect immunofluorescence. The left part shows pictures from cells representing typical localization s of NP. Nuclear DNA was stained by Hoechst. The right part shows a quantitative analysis of NP localization in 100 cells.

3.1.4 IKKβ inhibition results in increased SC35 replication in MLE-15 cells

While in this study NF-κB showed an antiviral role with genetically modified cells, previous studies using IKK inhibitors found proviral IKK functions (Ehrhardt et al., 2013; Haasbach et al., 2013; Mazur et al., 2007). Thus it was interesting to find out whether the antiviral function of NF-κB could also be seen by an independent experimental approach using an IKK

inhibitor with a high degree of specificity, such as the second generation selective IKKβ inhibitor PHA-408 (Mbalaviele et al., 2009).

To determine the lowest inhibitor concentration effectively blocking NF-κB activation in MLE15 cells, cells were pretreated with increasing amounts of PHA-408 and subsequently stimulated with the NF-κB activating cytokine TNFα. A concentration of 3 µM PHA-408 almost completely inhibited inducible phosphorylation of IκBα (Fig 11A) and IL-6 expression (Fig 11B). Inhibition of IKK activity by PHA-408 increased production of SC35 (Fig 11C), but only slightly interfered with the propagation of SC35M (Fig 11D).

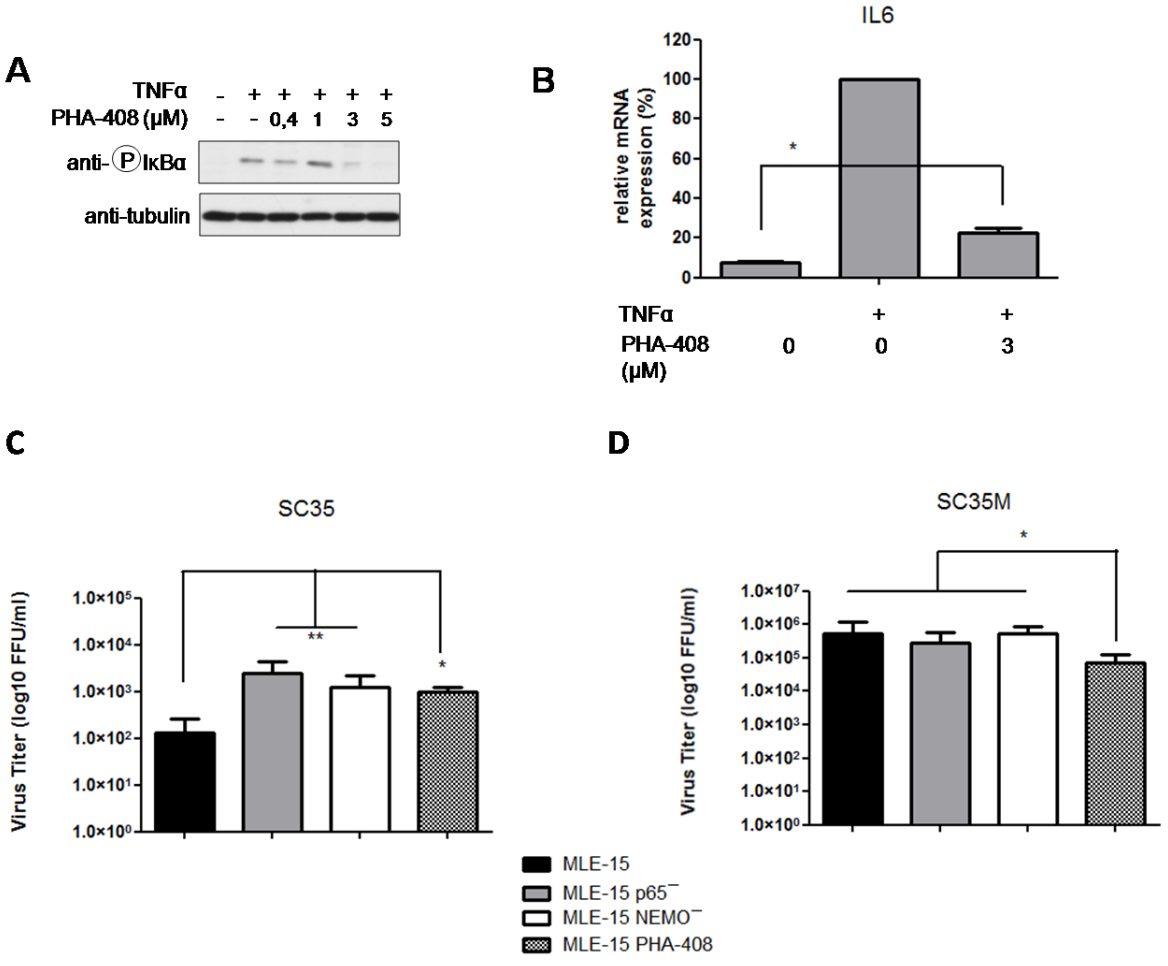

Figure 11: Effect of PHA-408 on replication of SC35 and SC35M viruses.(A) MLE-15 cells were preincubated for 1 h with the indicated concentrations of PHA-408 or vehicle. Cells were then stimulated for 20

min with TNFα and analyzed by immunoblotting for IκBα phosphorylation. **(B)** MLE-15 cells were preincubated for 1 h with PHA-408 and stimulated for 6 h with TNFα. The expression of IL-6 mRNA was quantified by qPCR. Error bars show SEM obtained from two independent experiments performed in triplicate. *, p <0.05. **(C,D)** MLE-15 cells were treated with 3 µM PHA-408 or vehicle. These cells and MLE-15 NEMO$^-$ and MLE-15 p65$^-$ cells were infected with SC35 and SC35M (MOI of 0.001). Virus titers were determined 24 h p.i. Error bars show SEM from two independent experiments performed in triplicate. The p values are indicated by asterisks: *, p< 0.05; **, p <0.01.

Human A549 cells were also used to test the effect of the inhibitor on IAV replication. A549 cells were pre-treated with PHA-408 and then infected with SC35 or SC35M with a MOI of 0.001 or 1. The results showed slightly increased replication of SC35 and SC35M, which were statistically and biologically not significant (Fig 12A,B).

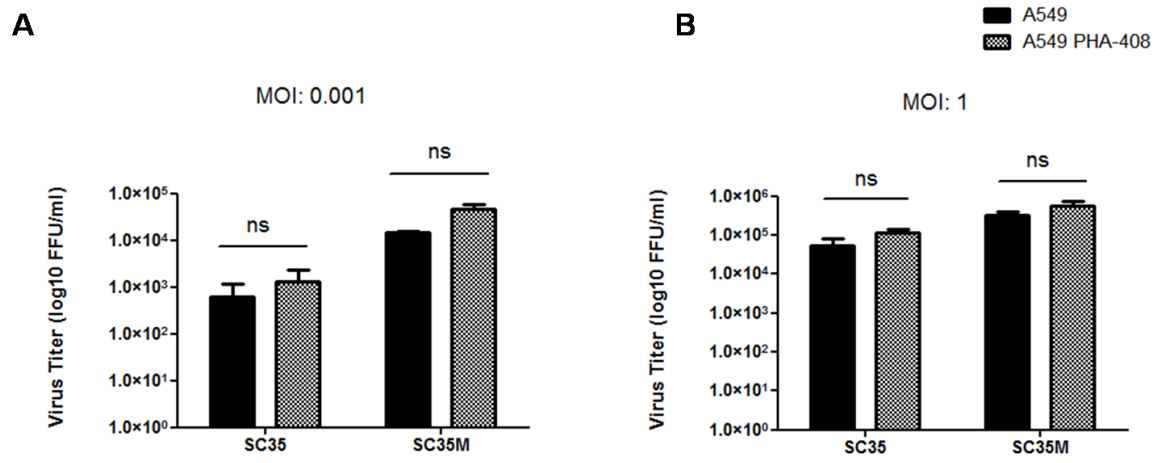

Figure 12: Effect of PHA-408 on A549 cells. **(A,B)** A549 cells were treated with 3 µM PHA-408 or vehicle. These cells were infected with SC35 and SC35M (MOI of 0.001 or 1). Virus titers were determined after 24 h. Error bars show SEM from three independent experiments performed in triplicate. ns, not significant.

In summary, inhibition of NF-kB either by genetic knockout or by pharmacological IKK inhibitors revealed different results. These differences might be due to differences in the strength of inhibition and possible off-target effects as all the commonly used inhibitors affect more than one target (Bain et al., 2007). This raises the necessity to reveal the importance of NF-κB in further species via CRISPR-Cas9 perturbation rather than by small molecule inhibitors.

3.1.5 NF-κB-dependent IRF3 phosphorylation and IFNβ expression contribute to its antiviral function

The antiviral function of NF-κB may depend on its ability to affect intracellular functions, for example the differential regulation of caspase 3 activation or vRNA synthesis (Kumar et al., 2008; Wurzer et al., 2003). Alternatively NF-κB may contribute to the synthesis of virus-regulating cytokines such as IFNβ.To test the impact of NF-κB on IFNβ gene expression, control cells or NF-κB deficient cell lines were infected with SC35 or SC35M at a MOI of 1 for 8 h. The mRNA expression levels of virus-induced IFNβ was analyzed by qPCR. Infection with SC35 resulted in elevated IFNβ expression compared to SC35M infection (Fig 13A),which is consistent to previous concept of a weakened cytokine response in SC35M infected cells (Gabriel et al., 2009).

When control or NF-κB-deficient cell lines were infected with SC35M, the expression of IFNβ was partially impaired in the absence of functional NF-κB, suggesting the existence of a compensatory mechanism. On the other hand, SC35 infection showed a very low level of IFNβ expression in the $NEMO^-$ or $p65^-$ cell lines, suggesting their dependency on NF-κB signaling. As NF-κB and IRF pathway show mutual cross-regulation (Grumont and Gerondakis, 2000; Iwanaszko and Kimmel, 2015), it was interesting to check whether the inactivation of NF-κB function can affect the phosphorylation and activation of IRF3. MLE-15 control cells and their p65 and NEMO deficient derivatives were infected with SC35 at a MOI of 3. Cell lysates were collected at different time points. IRF3 phosphorylation was measured using a phospho-IRF3 antibody. These experiments showed that the IRF3 phosphorylation is partially diminished in $NEMO^-$ cells and strongly impaired in $p65^-$ cells (Fig 13B) upon SC35 infection. The diminished IRF3 phosphorylation is consistent with reduced IFNβ gene expression in NF-κB defected cells and might be explained by lack of NF-κB derived signals required for complete activation of the IRF3 kinases IKKε and TBK1

(Bulek et al., 2011). To investigate whether the increased virus titer from infected NF-κB defective cells can be attributed to reduced expression of IFNβ, MLE-15 wild-type, p65^{-} and NEMO^{-} cells were preincubted with recombinant IFNβ and the impact on virus replication was measured. Pre-incubation with IFNβ only allowed to measure SC35 virus replication in control cells at a MOI>0.001 and reduced the difference in virus replication between NF-κB defective cells and MLE-15 control cells with an increased amount of IFNβ (Fig 13C). From these results it can be concluded that a significant part of the antiviral effect of NF-κB is due to its contribution of IFNβ expression.

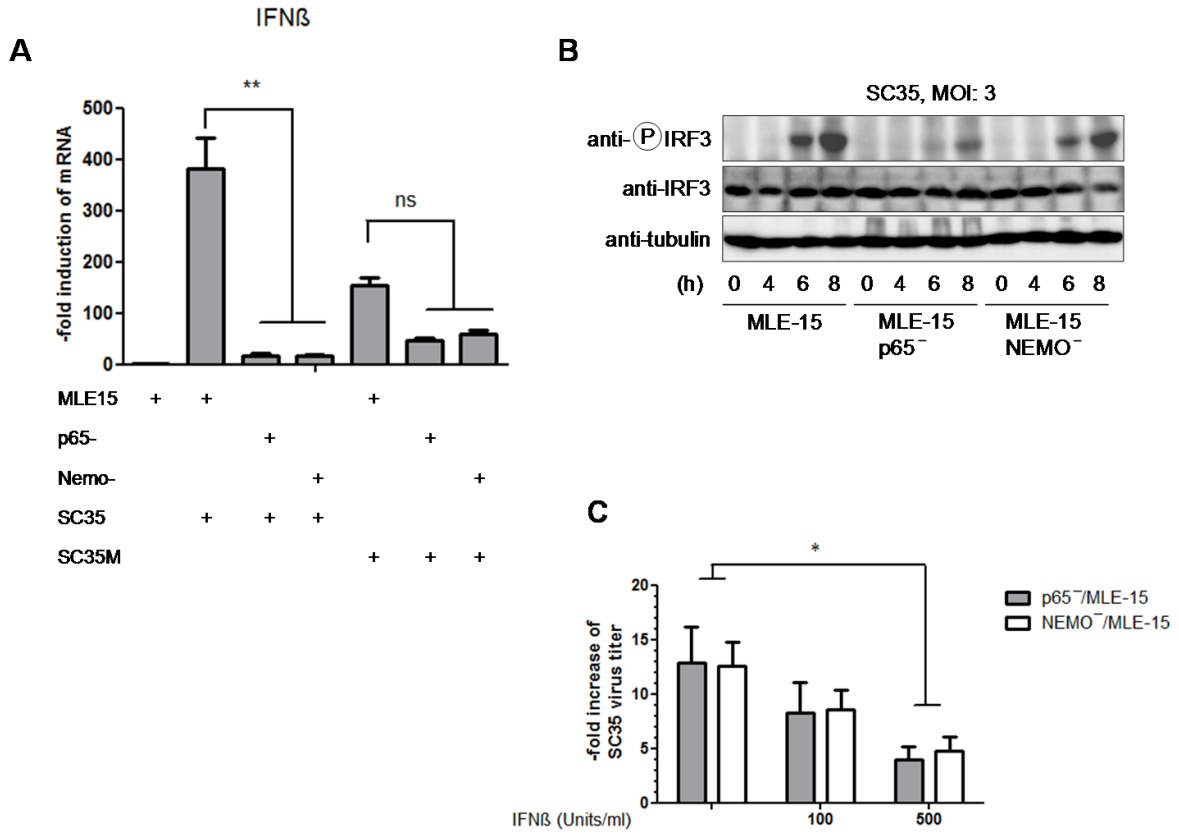

Figure 13: The antiviral effect of NF-κB partially depends on its ability to trigger IFN expression (A) The indicated MLE-15 cell lines were infected with SC35 or SC35M (MOI of 0.001) for 8 h. Cells were harvested and expression of the IFNβ gene was quantified by qPCR. Error bars show SEM from three independent experiments performed in triplicate. **(B)** The indicated cells were infected with SC35 or SC35M (MOI of 3) for the indicated periods. Cells were harvested, and cell extracts were analyzed by immunoblotting for the occurrence and phosphorylation of IRF3 with specific antibodies. Error bars show SEM (n=3). **(C)** Control cells, p65^{-} and NEMO^{-}cells were preincubated for 14 h with recombinant IFNβ at the indicated concentrations. Subsequently cells were infected with SC35 (MOI of 0.05), and virus titers were determined

after 24 h p.i. The ratio between virus numbers in knockout cells and those in control cells is displayed on the y axis. Error bars show SEM (n=3). The P values are indicated by asterisks: *, P<0.05; **, P<0.01. ns, not significant.

3.1.6 The IAV genotype is decisive for the antiviral function of NF-κB

In total SC35 and SC35M have nine amino acid difference, which occur in the segments of PB2 (3 amino acids), PB1 (2 amino acids), PA (1 amino acid), NP (1 amino acid), HA (1 amino acid) and NA (1 amino acid) (Gabriel et al., 2005). To identify the virus encoded proteins mediating NF-κB sensitivity, distinct segments of SC35M were used to replace the respective segments of SC35 using reverse genetics.

Various plasmid combinations were transfected into 293T and MDCK-II cocultured cells and the resulting reassorted viruses were used to infect MLE-15 control cells and their $p65^-$ and $NEMO^-$ derivatives. As expected, a recombinant SC35 virus expressing all six genes (PB2, PB1, PA, NP, NA, HA) from SC35M lost its sensitivity to NF-κB activity (Fig 14), as no further increase in virus titer was observed in infected $NEMO^-$ or $p65^-$ cell lines. A SC35 virus containing the NP segment from SC35M (named as SC35-NP^{SC35M}) was still sensitive to NF-κB inhibition (Fig 14). In the same way, the individual exchange of PB2, PB1, PA and HA did not lose the sensitivity to NF-κB function. Interestingly, the expression of NA from SC35M (named as SC35-NA^{SC35M}) was fully sufficient to render the resulting SC35-NA^{SC35M} virus completely inert to any NF-κB effect. A SC35 virus expressing the HA segment from SC35M or the combined exchange of several segments resulted in viruses showing a strongly increased sensitivity to the antiviral activity of NF-κB. These data showed that various combinations of viral proteins differentially affect the sensitivity to the antiviral function of NF-κB.

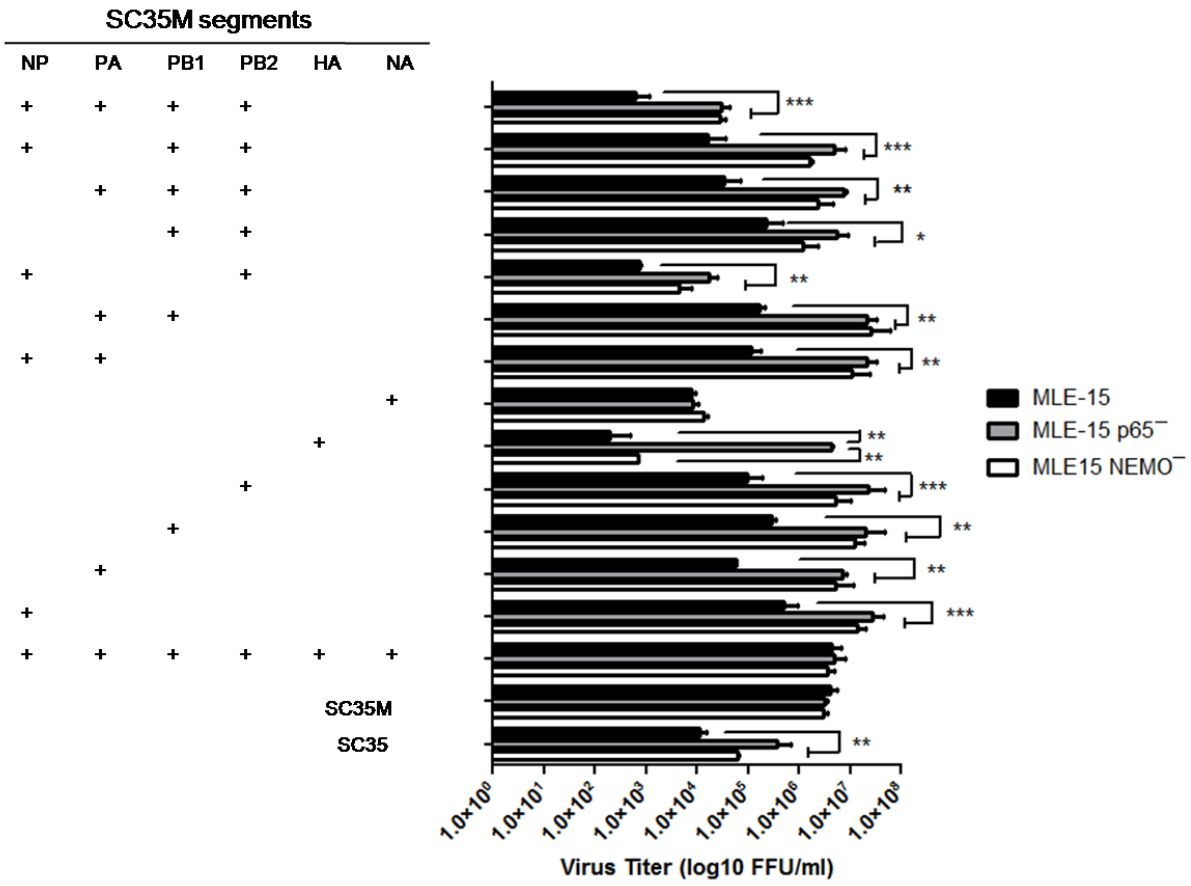

Figure 14: Impact of viral proteins on the antiviral function of NF-κB. Plasmids encoding the indicated SC35M segments were combined with plasmids encoding the other SC35 segments to produce reassortant viruses. These chimeric viruses and the SC35 and SC35M controls were then used to infect control MLE-15 cells, MLE-15 NEMO^{-}cells, or MLE-15 p65^{-}cells (MOI of 0.001), and virus titers were determined 24 h p.i. Mean values from three independent experiments are shown. Error bars indicate SEM. The *P* values are indicated by asterisks: *, P < 0.05; **, P < 0.01; ***, P < 0.001.

3.2 Phosphoproteome analysis of IAV-infected mouse lung epithelial cells

3.2.1 Identification of IAV-regulated phosphorylations

To identify IAV-regulated phosphorylation events the cellular phosphorylation responses were investigated at early (1 h) and late (8 h) time points of IAV infection. In this experiment the aim was to compare the responses elicited in widely used MLE-15 cells by mouse-adapted SC35M virus and the non-adapted avian SC35. MLE 15 cells were infected with SC35 or SC35M with a MOI of 1 for 1 h or 8 h. Post infection cell extracts were prepared in a denaturing urea buffer to preserve all phosphorylations and to inhibit all enzymes (kinases or phosphatases) that could affect the results post lysis. Samples from these lysates obtained from control and virus-infected cells were validated via Western blot experiments by testing the occurrence of several already established phosphorylations in the activation loops of JNK, ERK and Akt kinases (Nacken et al., 2014) (Fig 15A). These extracts were then further processed as schematically shown in Fig 15B by Cell Signaling, the company actually performing the mass spectrometry experiment. Proteins were digested with trypsin and phosphorylated peptides were enriched by two different methods: The first method used IMAC columns to enrich peptides phosphorylated at Ser, Thr or Tyr. As Tyr phosphorylations are less abundant (Reddy et al., 2017), Tyr-phosphorylated peptides were enriched with specific antibodies in a parallel approach. The label-free based PTMScan® method (Stokes et al., 2012) allowed the identification of 15,473 non-redundant peptides with phosphorylations at Ser/Thr and 2,442 non-redundant peptides harboring phospho-Tyr (Fig 15C, Table 2). Most peptides purified by IMAC columns contained phosphorylated Ser either alone or together with phosphorylated Thr or Tyr. The vast majority of peptides enriched by the phospho-Tyr antibody contained at least one phosphorylated Tyr, indicating that the purifications worked properly. The number of IAV-regulated phosphorylation sites within a given protein was quite variable (Fig 15D). IMAC-enriched phosphorylations typically

occurred more than once and almost thousand proteins were phosphorylated at more than 6 different residues. In contrast, around 450 proteins were found with a Tyr phosphorylation only once and multiple Tyr phosphorylations were rare (Fig 15D).

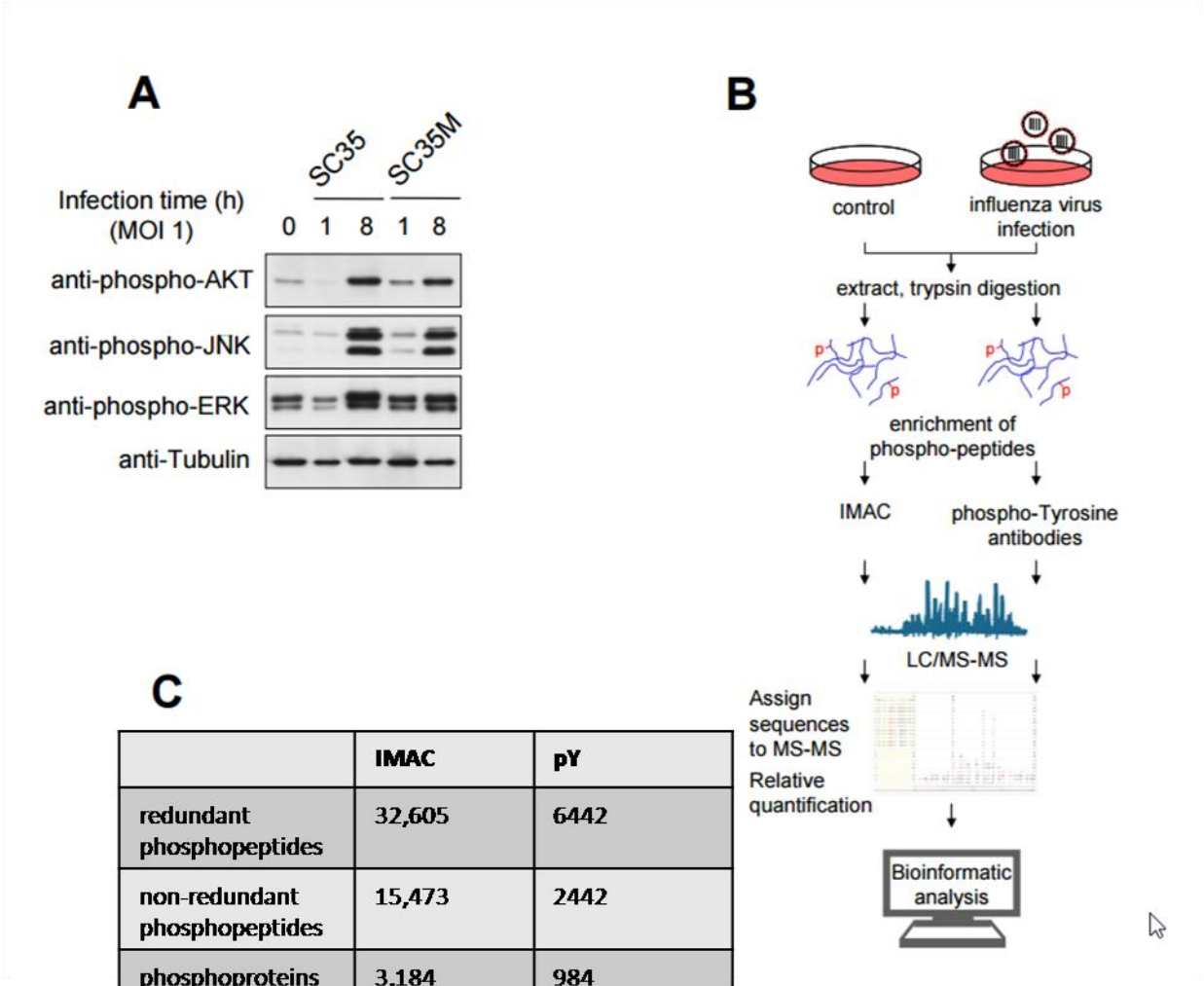

C

	IMAC	pY
redundant phosphopeptides	32,605	6442
non-redundant phosphopeptides	15,473	2442
phosphoproteins	3,184	984

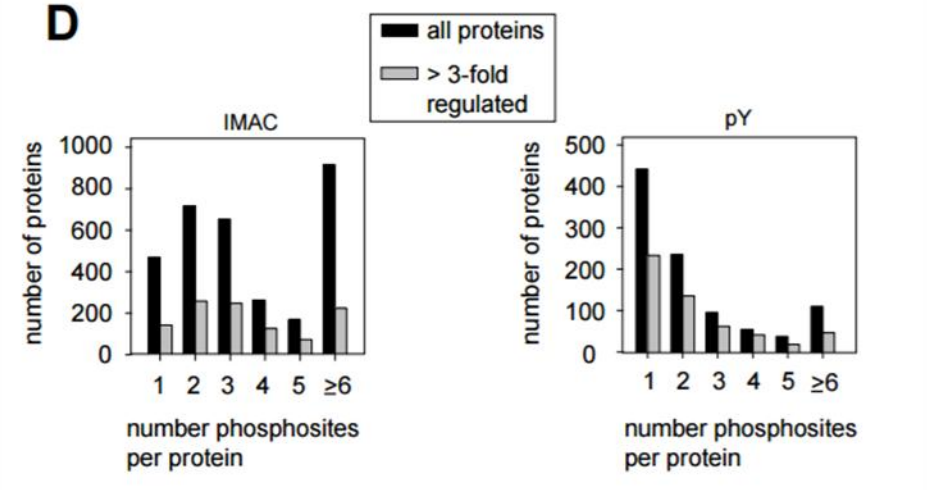

Figure 15: Phosphoproteomeanalysis of IAV-infected MLE-15 mouse lung cells.(A) Cells were infected with SC35M or SC35 for 1 h or 8 h as shown. Cells were lysed with denaturing buffer and equal amounts of protein from the lysates were analyzed by immunoblotting for the occurrence and phosphorylation of the indicated proteins with specific antibodies. **(B)** Schematic display of the workflow employed for the phospho-proteome screening. The extracts were analyzed using the quantitative label-free PTMscan® approach (Cell Signaling Technology). Extracted proteins were digested with trypsin and separated from non-peptide material by solid-phase extraction with Sep-Pak C18 cartridges. One fraction of the extract was used to enrich peptides phosphorylated at Ser/Thr or Tyr by IMAC. Another fraction was taken to enrich Tyr-phosphorylated peptides with a specific antibody. Enriched phospho-peptides were analyzed via LC-MS/MS and spectra are assigned with SORCERER 2 v.4.0. Relative quantitation was based on the chromatographic peak apex intensity or integrated peak area in the MS1 channel. Validated target lists were then assembled by score filtering, search for intended targets, search for peptides homologous to intended targets, a minimum MS1 peak intensity filter, and PTMScan. After relative quantitation validated target lists were assembled by score filtering and subjected to bioinformatic analysis. **(C)** Table summarizing the number of identified phosphopeptides and phosphoproteins. **(D)** Statistical analysis of the number of phosphorylation sites per protein. The bioinformatic analysis of data was performed in collaboration with Dr. Axel Weber (Institute for Pharmacology).

Time point (h)	0		1				8			
Influenza A virus	none		SC35		SC35M		SC35		SC35M	
type of phospho scan	pY	IMAC	pY	IMAC	pY	IMAC	pY	IMAC	pY	IMAC
3-fold up			180	514	113	533	83	757	440	886
3-fold down			284	320	66	159	145	466	262	554
2-fold up			389	1218	262	1220	190	1716	655	1879
2-fold down			447	944	230	503	321	1460	519	1526
1.5-fold up			656	2638	537	2579	486	3259	823	3323
1.5-fold down			654	2275	539	1609	599	2943	782	3021
number of phosphorylated S sites	524	22379	521	22385	524	22381	526	22383	527	22363
number of phosphorylated T sites	323	5949	323	5948	324	5952	325	5954	326	5946
number of phosphorylated Y sites	2069	1009	2072	1011	2066	1010	2077	1011	2079	1008
total number of phosphorylated sites	2916	29337	2916	29344	2914	29343	2928	29348	2932	29317
total number of detected peptides	2402	15466	2400	15470	2399	15470	2409	15471	2413	15461
number of detected genes	975	3181	981	3183	978	3182	979	3184	982	3182

Table 2: Statistical analysis of the phosphoproteome screen. Cells were infected with SC35M or SC35 influenza viruses for 1 or 8 h. Cells were lysed and the trypsin-digested peptides were enriched for phosphorylated peptides either by IMAC or with phospho-Tyr specific antibodies (pY). Data were filtered using the R-software package for non-redundant phosphorylation sites occurring on Ser, Thr or Tyr residues. These modification sites were assigned to their corresponding genes. In this table it shows the genes which (due to differential splicing or protein processing) often encode more than one protein variant(s). The bioinformatic analysis of data was performed in collaboration with Dr. Axel Weber (Institute for Pharmacology).

The number of proteins undergoing regulated IMAC-enriched phosphorylation (>1.5-fold regulation) in MLE-15 cells infected with SC35 or SC35M was roughly similar at 1 h or 8 h time points of infection. Similarly, the number of upregulated phosphoproteins was comparable with the number of diminished phosphorylations (Fig 16A,B). A further increase

in the threshold to >2-fold and >3-fold regulated proteins decreased the number of phosphorylated proteins (Fig 16A,B). Similarly, also the number of SC35 or SC35M-induced Tyr phosphorylation sites at 1 h or 8 h p.i. decreased from >1.5-fold when increasing the threshold to >3-fold regulation (Fig 16C,D). Nearly half of the IMAC-enriched phosphorylations were affected by both viruses (Fig. 14A,B). In contrast, both viruses showed more differences in the regulation of Tyr phosphorylation (Fig. 14C,D).

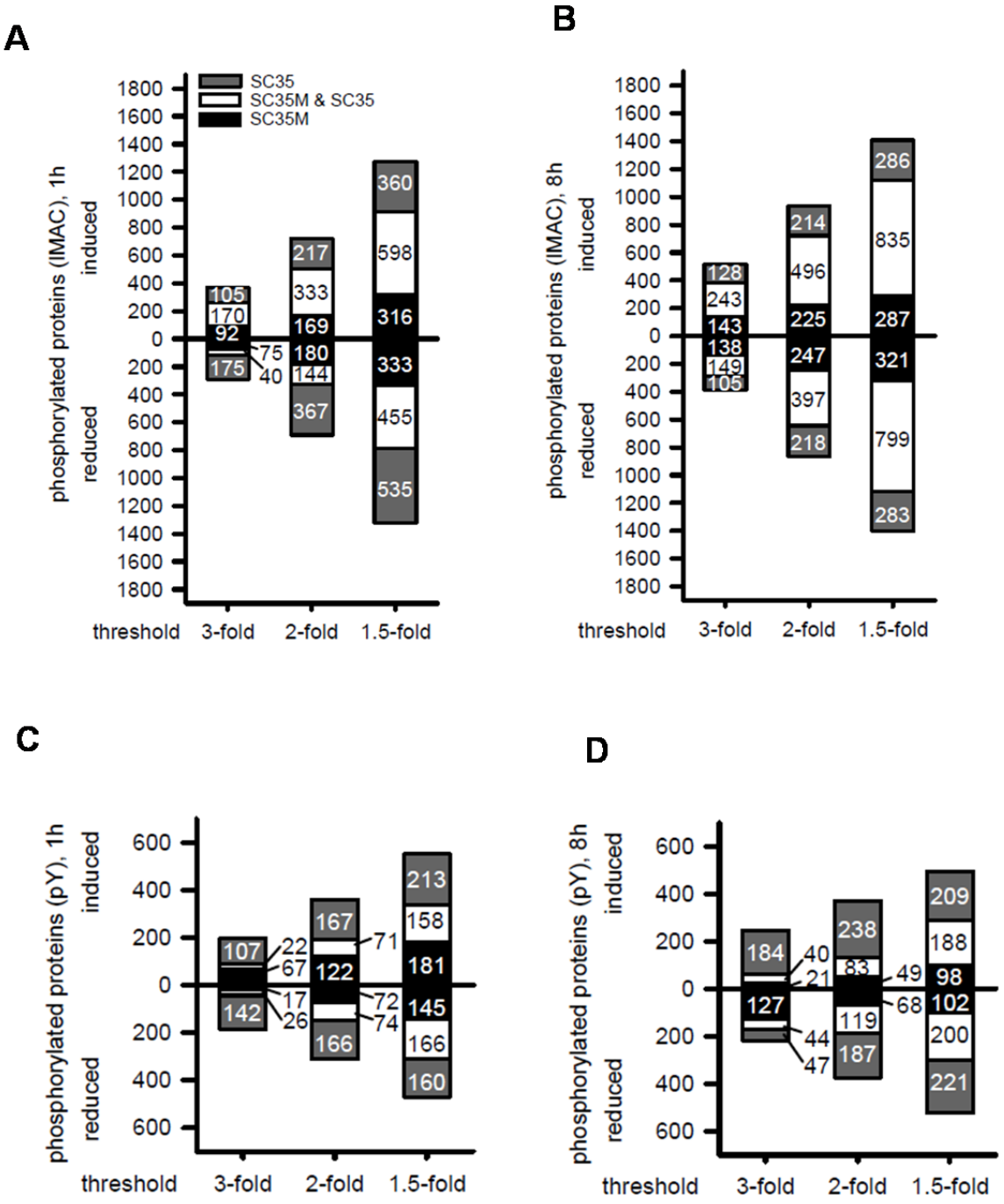

Figure 16: Statistical analysis of regulated protein phosphorylation.(A) The IMAC-purified phospho-peptides were mapped to proteins. The proteins experiencing elevated or reduced phosphorylation 1 h after infection with SC35M or SC35 were grouped according to the threshold of -fold regulation. **(B)** The analysis was done as in (A) with the difference that only regulated phosphorylations occurring after 8 h of infection are shown. **(C)** Proteins harboring tyrosine phosphorylation sites identified by enrichment with the tyrosine phosphorylation-specific antibody were grouped according to the threshold of -fold regulation. The amount of up- and down-regulated events after 1 h of infection with SC35 or SC35M were shown. **(D)** The analysis was done as in (C) with the difference that only regulated phosphorylations occurring after 8 h of infection were

shown. The bioinformatic analysis of data was performed in collaboration with Dr. Axel Weber (Institute for Pharmacology).

The bioinformatic analysis of the obtained data also showed that not all phosphorylation sites within a given protein were uniformly up- or down-regulated and revealed the occurrence of oppositely regulated phosphorylations. Stronger changes in phosphorylation do not only show a more dynamic regulation, but may also indicate a biologically more important modification. The analysis of phosphorylations regulated > 3-fold showed that the number of virus-induced Ser/Thr phosphorylations exceeded the number of diminished modifications (Fig 17A,B). Interestingly, infection with the non-adapted SC35 virus resulted in a general decrease of Tyr phosphorylation. As the two viruses only differ at nine positions, it was interesting to study the impact of these changes on changes of the phosphoproteomes. To address this question it was important to analyze all modifications that were regulated >3-fold during at least 1 time point. This analysis showed that the majority of induced IMAC phosphorylations were elicited by both viruses, while the down-regulated phosphorylations showed a smaller overlap between SC35 and SC35M infections (Fig 17C). In addition, the analysis of regulated Tyr phosphorylations showed that 49% of the proteins with up-regulated and 20% of proteins with down-regulated phosphorylations were affected by both viruses (Fig 17D). In summary, these results indicate that the percentage of shared phosphorylations is much higher for inducible phosphorylations. The differential phosphorylations indicate virus genotype-specific signaling, but it has to be considered as well that a certain fraction of phosphorylations could have little or no functional importance (Levy et al., 2012). For further analysis the investigation was mainly focused on phosphorylation sites co-regulated by both viruses in order to identify virus genotype-independent common principles in host cell signaling.

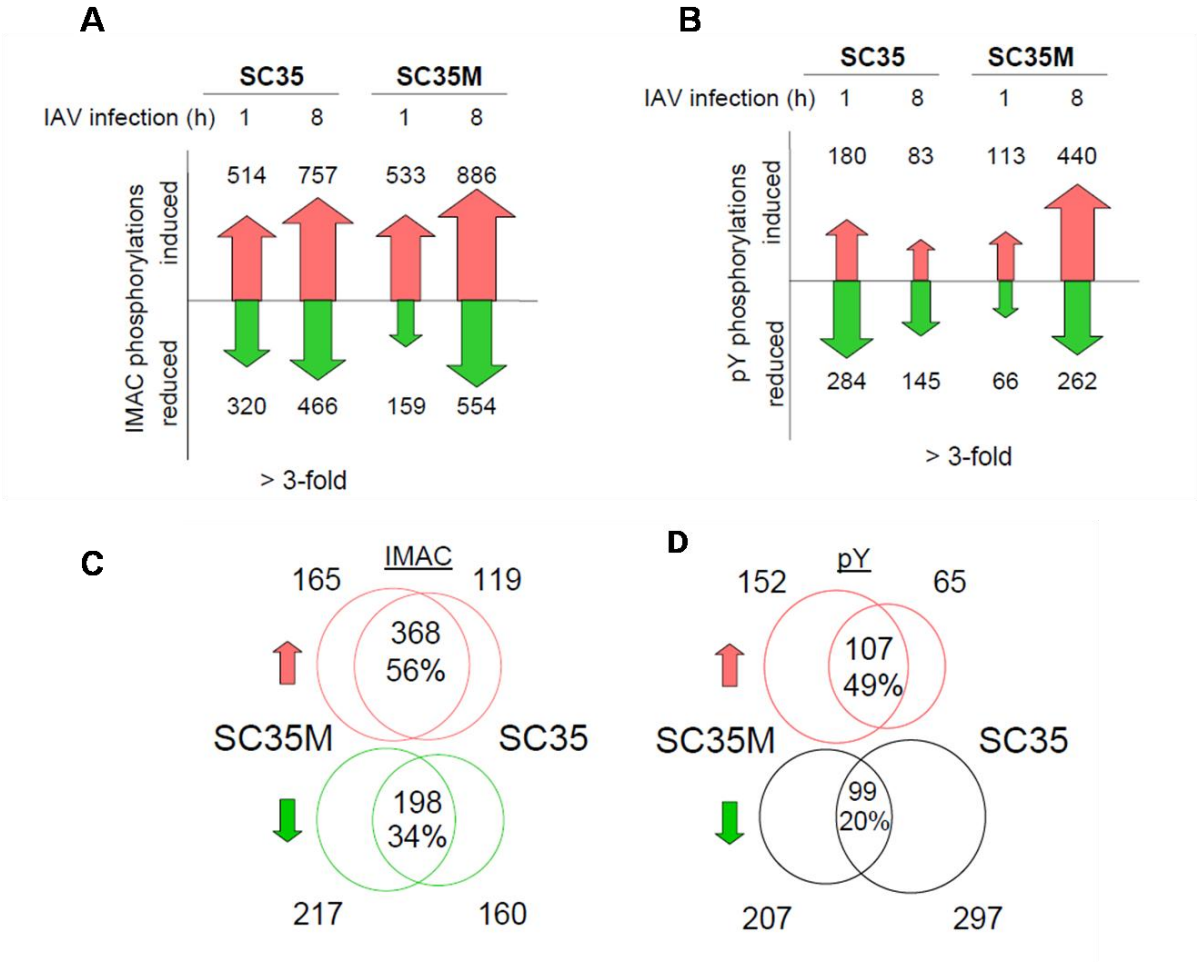

Figure 17: Comparison of virus regulated phosphorylation.(A) IMAC-purified phospho-peptides were mapped to proteins, polypeptides experiencing a >3-fold up- or downregulation of phosphorylation are displayed. **(B)** The evaluation was done as in (A) the only difference was that the data based on the enrichment of Tyr phosphorylated peptides were used for the analysis. **(C)** Venn diagrams comparing proteins showing a >3-fold regulation of phosphorylation during at least 1 time point triggered by SC35, SC35M or both viruses. **(D)** The evaluation was done as in (C) with the difference that only data based on the enrichment of tyr phosphorylated peptides experiencing > 2-fold regulation were considered. The bioinformatic analysis of data was performed in collaboration with Dr. Axel Weber (Institute for Pharmacology).

3.2.2 Identification of IAV-regulated kinases

The involvement of kinases can be deduced from the identification and analysis of common substrate phosphorylation motifs using the motif-x tool (Schwartz and Gygi, 2005). After 1 h and 8 h of IAV infection, frequent phosphorylations in peptides containing the RXXpS motif were found. This analysis also identified frequent modification of Ser directly flanked by prolines (Pro) or in the vicinity of acidic amino acids (Fig 18A). These sequences correspond

to preferred substrates of different kinases including AKT, Calmodulin-dependent protein kinase II, and PKA, as displayed in Fig 18A. The analysis of substrate motifs for phosphorylation of Tyr showed the prevalence of very short motifs where the phosphorylated amino acid is directly flanked by Ser, Gly or Ala or harboring a Pro in the +3 position (Fig 18B). However, the absence of typical substrate phosphorylation motifs for Tyr kinases precluded the identification of candidate kinases. The IAV-mediated regulation of protein kinases can also be deduced from the phosphorylation state of key amino acids contained in the activation loop, which is contained in most kinase domains (Cargnello and Roux, 2011). Phosphorylation of these activation loop residues are typically required for full kinase activity (Nolen et al., 2004) and thus the phosphorylation state of the kinase activation loop is often used as proxy to analyze the activation state of the respective kinase (McSkimming et al., 2017). The analysis of regulated activation loop phosphorylation confirmed phosphorylation and thus activation of JNK and ERK kinase. It also showed regulated phosphorylation of several kinases that have not been implicated in IAV replication thus far (Fig. 16C). The regulated kinases comprise the Ser/Thr kinases HIPK2 and HIPK3 and Tyr kinases such as MERTK, MET and FAK.

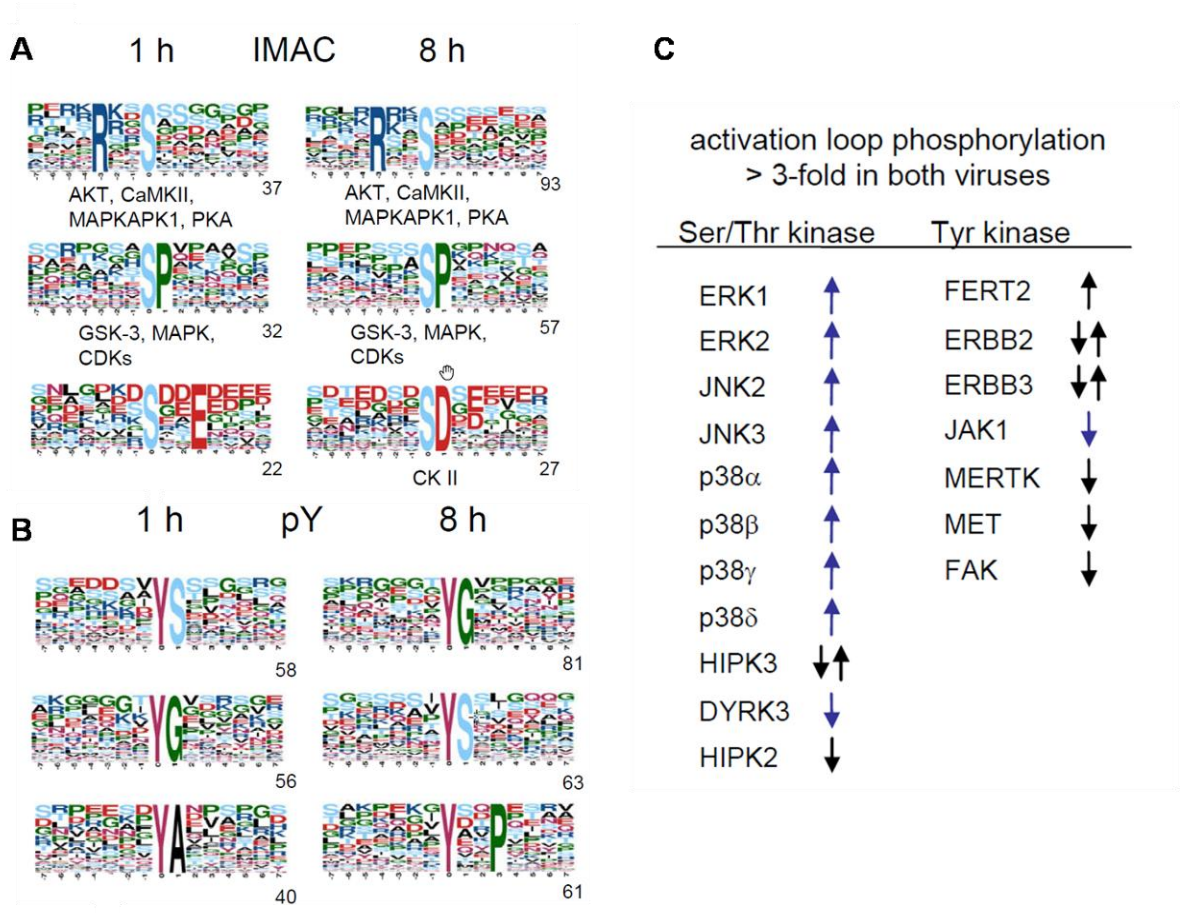

Figure 18: Identification of phosphosite motifs and IAV-regulated kinases. (**A**) Sequence logo graphs of significantly enriched phospho-site motifs for modified Ser/Thr are shown, the number of different peptides used for the generation of the logos are indicated at the right. Candidate kinases modifying these sites were identified using the PhosphoMotif Finder tool. (**B**) The sequence logo analysis was performed as in (A) with the exception that Tyr phosphorylation motifs were identified. (**C**) Regulation of key residues in the activation loop of kinases regulated by both viruses. Only kinases where SC35 and SC35M caused > 3-fold changes in the activation loop are displayed. Arrows pointing up or down indicate increased or decreasedphosphorylations, respectively; the blue color indicated a known and black color indicated unknown implication in IAV replication. The bioinformatic analysis of data was performed in collaboration with Dr. Axel Weber (Institute for Pharmacology).

3.2.3 Identification of IAV-regulated host cell pathways

After extraction of protein lists, bioinformatics analysis was also done with tools which were initially developed for the analysis of microarray data such as gene ontology (GO) and Kyoto Encyclopedia of Genes and Genomes (KEGG) enrichment. These analyses were done for all proteins where at least one phosphorylation was regulated >3-fold in either direction. The GO analysis for cellular components showed enrichment for annotations related to many different

subcellular structures including cell anchoring and adherens junctions and vesicle trafficking (Fig 19A), consistent of a viral life cycle involving many intracellular compartments. Consistently, in addition GO analysis for molecular function showed the involvement of diverse functions including signaling events, transcription factors and their regulators as well as mRNA metabolism (Fig 19B). Also the GO analysis for molecular processes showed the involvement of phosphorylated proteins in several processes including adhesion, locomotion, as well as organization of actin and the cytoskeleton (Fig 19C). The results from the combined KEGG and GO pathway analysis emphasize the notion of the overrepresentation of pathways engaged in cell adhesion, motility and cytoskeletal organization. The strong overrepresentation of phosphorylated proteins is also evident upon direct visualization of the modified proteins in the KEGG pathways, as seen for the focal adhesion pathway (Fig 20A).

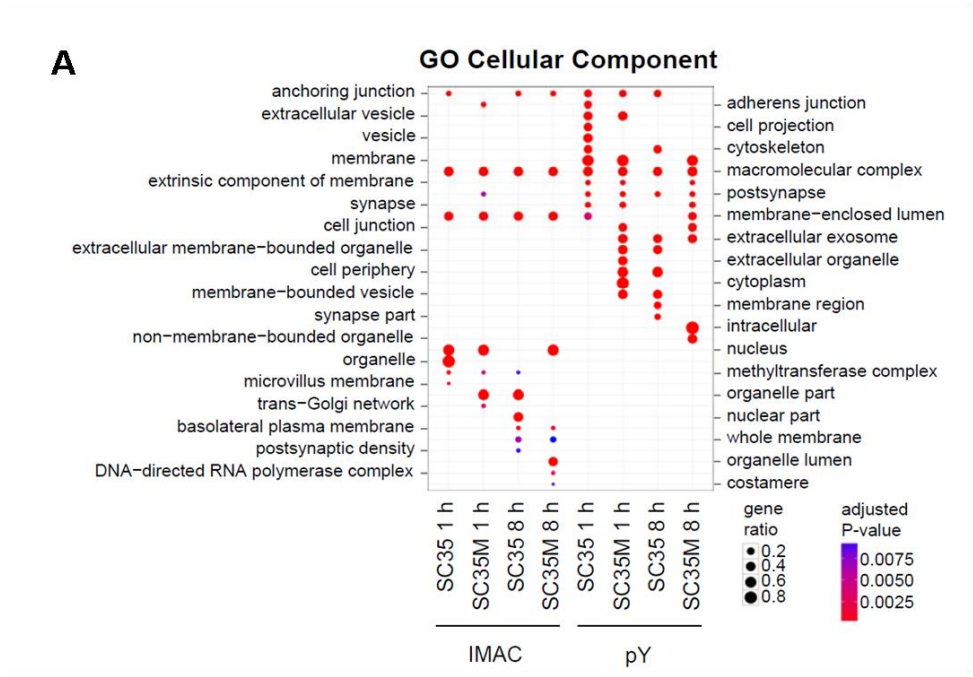
A
GO Cellular Component
anchoring junction
extracellular vesicle
vesicle
membrane
extrinsic component of membrane
synapse
cell junction
extracellular membrane−bounded organelle
cell periphery
membrane−bounded vesicle
synapse part
non−membrane−bounded organelle
organelle
microvillus membrane
trans−Golgi network
basolateral plasma membrane
postsynaptic density
DNA−directed RNA polymerase complex
adherens junction
cell projection
cytoskeleton
macromolecular complex
postsynapse
membrane−enclosed lumen
extracellular exosome
extracellular organelle
cytoplasm
membrane region
intracellular
nucleus
methyltransferase complex
organelle part
nuclear part
whole membrane
organelle lumen
costamere
SC35 1 h
SC35M 1 h
SC35 8 h
SC35M 8 h
SC35 1 h
SC35M 1 h
SC35 8 h
SC35M 8 h
IMAC
pY
gene ratio
0.2
0.4
0.6
0.8
adjusted P-value
0.0075
0.0050
0.0025

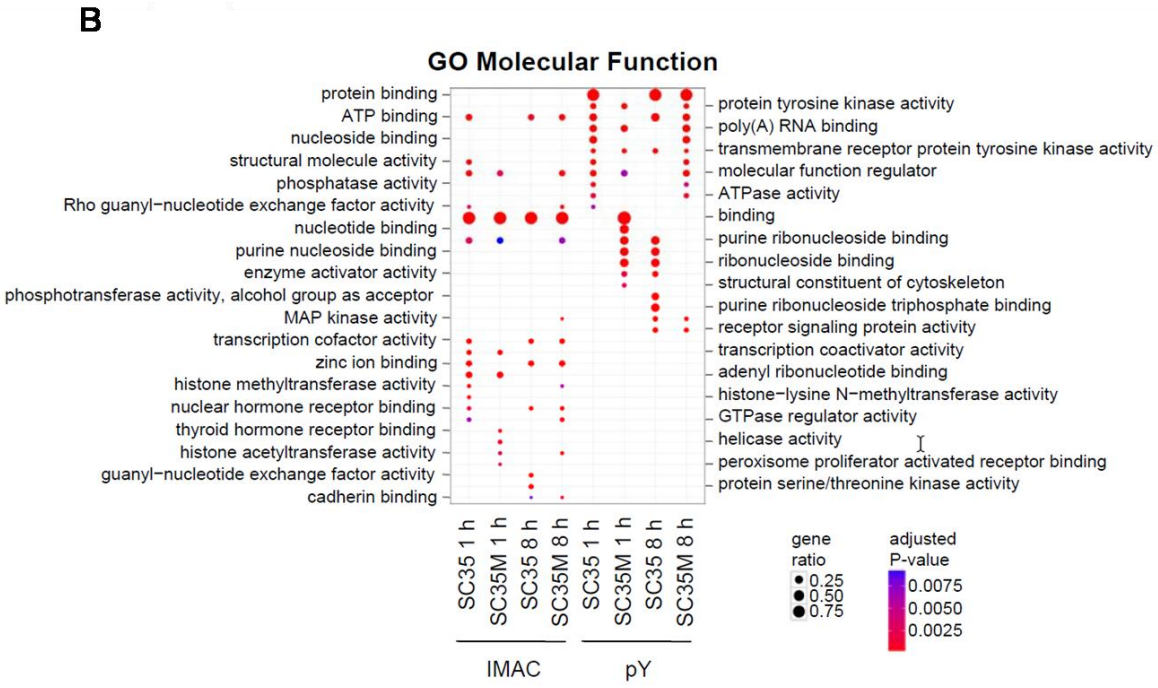
B
GO Molecular Function
protein binding
ATP binding
nucleoside binding
structural molecule activity
phosphatase activity
Rho guanyl−nucleotide exchange factor activity
nucleotide binding
purine nucleoside binding
enzyme activator activity
phosphotransferase activity, alcohol group as acceptor
MAP kinase activity
transcription cofactor activity
zinc ion binding
histone methyltransferase activity
nuclear hormone receptor binding
thyroid hormone receptor binding
histone acetyltransferase activity
guanyl−nucleotide exchange factor activity
cadherin binding
protein tyrosine kinase activity
poly(A) RNA binding
transmembrane receptor protein tyrosine kinase activity
molecular function regulator
ATPase activity
binding
purine ribonucleoside binding
ribonucleoside binding
structural constituent of cytoskeleton
purine ribonucleoside triphosphate binding
receptor signaling protein activity
transcription coactivator activity
adenyl ribonucleotide binding
histone−lysine N−methyltransferase activity
GTPase regulator activity
helicase activity
peroxisome proliferator activated receptor binding
protein serine/threonine kinase activity
SC35 1 h
SC35M 1 h
SC35 8 h
SC35M 8 h
SC35 1 h
SC35M 1 h
SC35 8 h
SC35M 8 h
IMAC
pY
gene ratio
0.25
0.50
0.75
adjusted P-value
0.0075
0.0050
0.0025

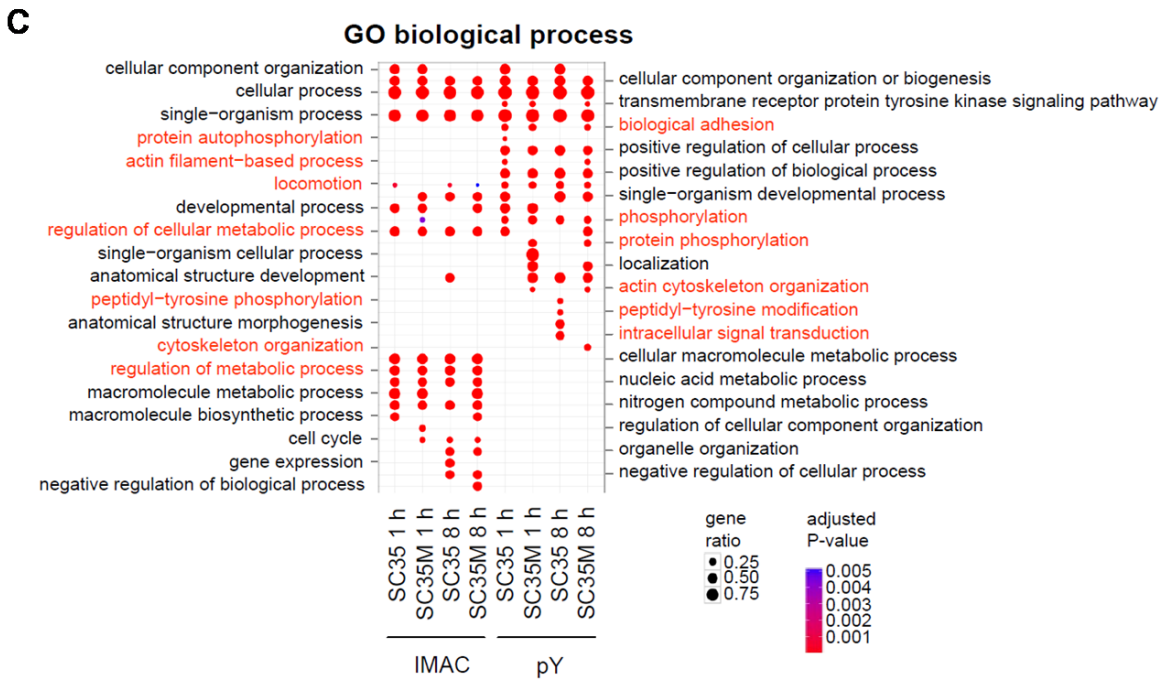

Figure 19: GO analysis of proteins displaying IAV-regulated phosphorylation changes. (**A**) All proteins showing >3-fold regulated phosphorylation were analyzed for the overrepresentation of cellular components in the GO pathway database, the p values are indicated. (**B**) The regulated proteins were also analysed for enrichment of molecular functions. (**C**) The biological processes overrepresented in the group of dynamically phosphorylated proteins are displayed. A similar analysis was done using the KEGG database, processes identified by KEGG and also by GO databases are given in red. The bioinformatic analysis of data was performed in collaboration with Dr. Axel Weber (Institute for Pharmacology).

3.2.4 FAK-dependent signaling contributes to efficient IAV replication

The focal adhesion pathway and actin reorganization are regulated by the cytoplasmic tyrosine kinase FAK, which is also regulated upon IAV infection (Fig 18C). As this kinase can be specifically inhibited by Defactinib, a small molecule inhibitor already used in several clinical studies for the treatment of cancer (Gabriel et al., 2008; Zhirnov et al., 2008), MLE-15 cells were treated with Defactinib either 1 h pre infection or 1.5 h post infection with SC35M virus and measured the impact on virus propagation. Defactinib treatment indeed interfered with virus propagation, but consistent with a role of FAK for the entry process of IAVs the inhibition of virus propagation was less prominent when the inhibitor was administered 1.5 h post infection (Fig 20B). As FAK controls several downstream pathways

including PI3K and MAPK signaling (Sulzmaier et al., 2014), the effects of Defactinib on IAV-triggered signaling cascades were measured. Pre-incubation of cells with Defactinib inhibited IAV-induced activation of TBK1 and also interfered with the activation of NF-κB signaling, as judged by absent IκBα phosphorylation in the presence of the inhibitor (Fig 20C). Absent FAK activity resulted in slightly increased virus-induced c-Jun phosphorylation despite diminished JNK activity and had no impact on the phosphorylation of AKT or p38. The same experiment also revealed that FAK inhibition also caused delayed and diminished synthesis of the viral NS1 protein (Fig 20C), in line with the inhibitory activity of Defactinib on IAV replication (Fig 20B). The administration of Defactinib to cells 1.5 h p.i. did not affect the major signaling pathways (Fig 20D), suggesting that FAK is important for the entry steps of IAV early during infection.

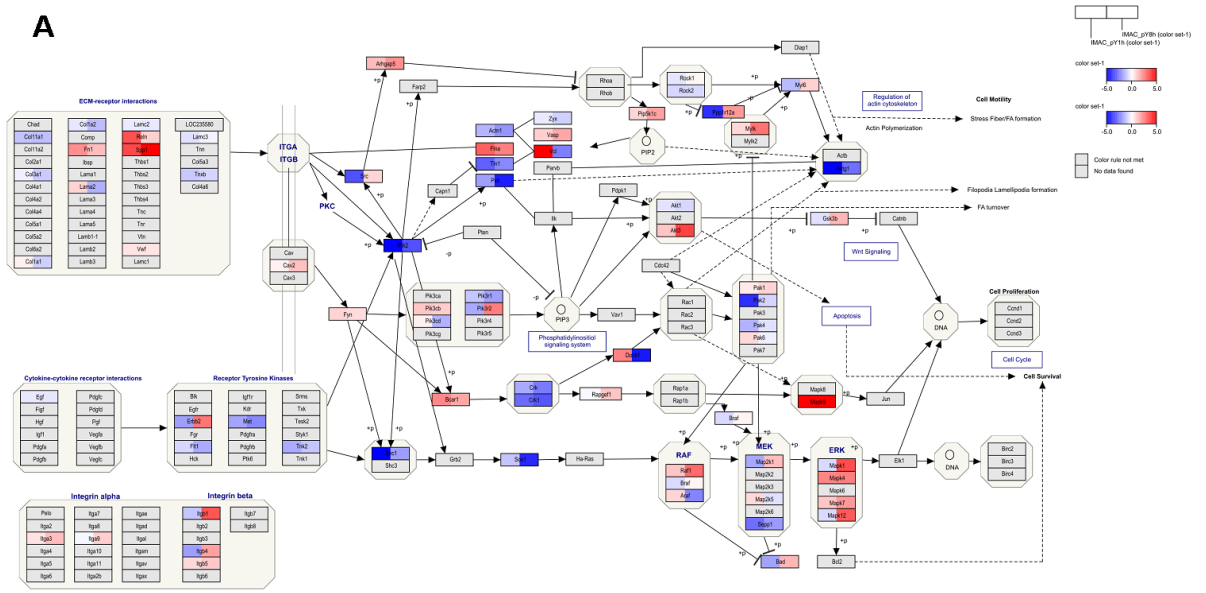

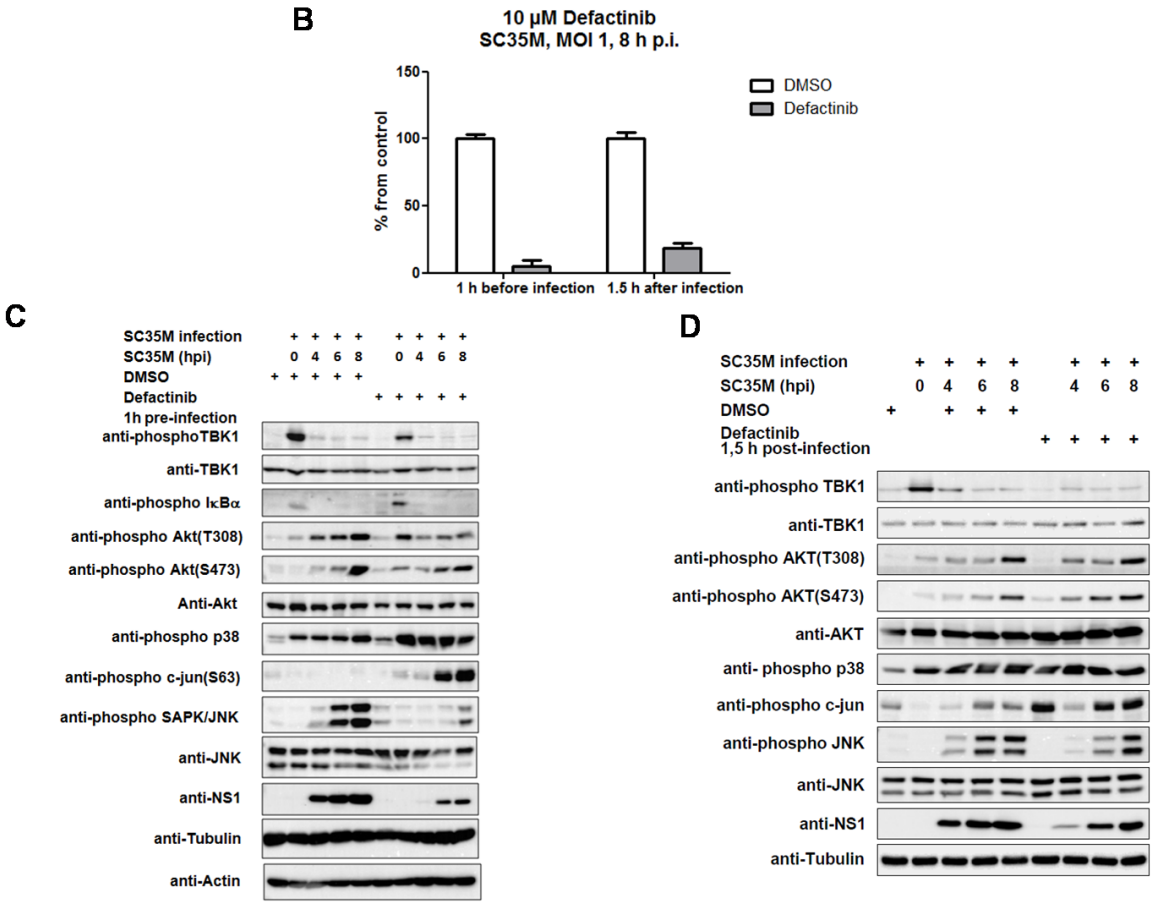

Figure 20: Visualization of dynamically phosphorylated members of the focal adhesion pathway and functional characterization of FAK.(A) Network diagram displaying the phosphorylation changes in the focal adhesion KEGG pathway. Proteins are indicated by rectangles, phosphorylations measured either after IMAC or pY enrichment at 1 h or 8 h after infection are displayed. The -fold change in phosphorylation are displayed by colors using Pathvisio 3.2.1. The bioinformatic analysis of data was performed in collaboration with Dr. Axel Weber (Institute for Pharmacology). **(B)** MLE-15 cells were incubated with 10 µM of Defactinib or DMSO either 1 h pre-infection or 1.5 h post infection with SC35M (MOI = 1). The plaque titers were determined 24 h p.i. on MDCK-II cells. The virus titer (FFU/ml) is indicated, error bars show SEMs obtained from three independent experiments performed in triplicates. The experiment was done by Irina Kuznetsova. **(C,D)** MLE-15 cells were incubated with 10 µM of Defactinib. Decfactinib was added either 1 h before infection or 1.5 h after infection, followed by infection with SC35M (MOI = 1) for various time periods as shown. Equal amounts of protein were analyzed by Western blotting for the occurrence and phosphorylation of the indicated proteins. Comparable data were obtained from three different experiments. Western blots were performed by Dr. Vera V. Saul.

3.2.5 Phosphorylation of IAV proteins supports or antagonizes their function

The phosphoproteome screen also allowed the detection of phosphorylated residues in viral proteins. Eight of the previously known phosphorylation sites (Kathum et al., 2016; Turrell et al., 2015) were confirmed and 12 new modified amino acids in several viral proteins (Fig

21A) were identified. All modifications were detected for SC35 and SC35M-encoded proteins. Some of the identified phosphorylation sites occur in evolutionary conserved sites with a potential functional relevance. For example, modification of NS1 at Thr49 was identified, which is directly next to the previously identified phosphorylation site at Ser48 in a region that is directly involved in RNA binding and functionally relevant (Barnwal et al., 2015; Carrillo et al., 2014; Marc et al., 2013). In order to obtain insight into the structural consequences of Ser48/Thr49 phosphorylation, published NS1 structures (Cheng et al., 2009; Jureka et al., 2015) were used as templates in order to calculate the structure of SC35M NS1 using the Swiss-Model server (Fig 21B). Both phosphorylation sites are at the end of an α-helix which interacts with dsRNA. The *in silico* model also suggests a direct contact between phosphorylated Thr49 and the RNA ribose. These NS1 phosphorylations can also be detected by an independent experimental approach using phospho-specific antibodies that were raised against this epitope. Western blotting confirmed the occurrence of NS1 phosphorylation and the specificity of the phospho-specific antibodies (Fig 21C).

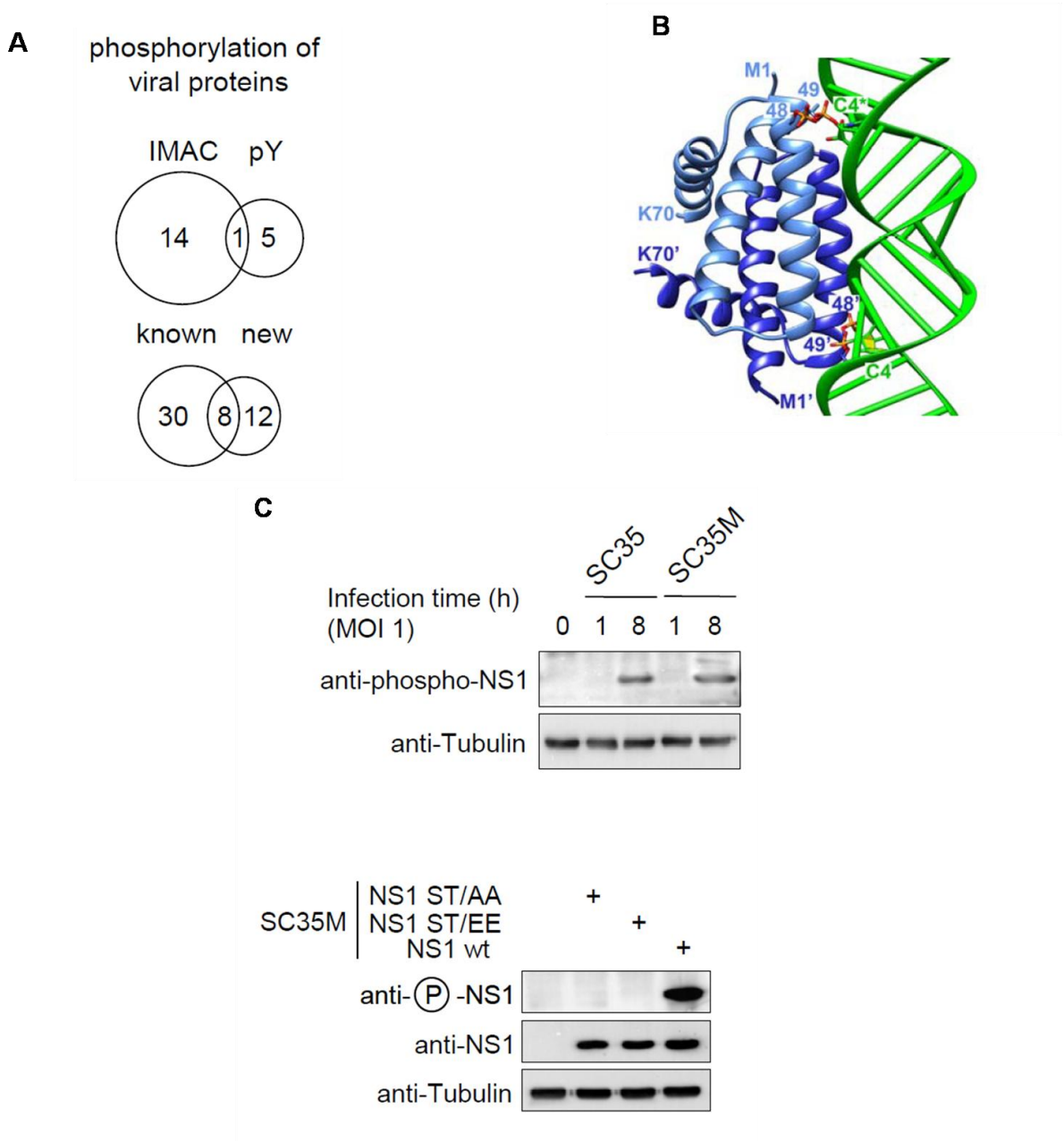

Figure 21: Phosphorylation of viral proteins. (**A**) Venn diagrams displaying the number of identified phosphorylation sites on viral proteins as detected after enrichment of peptides via IMAC columns or P-Tyr antibodies. (**B**) The published NS1 structures (PDB: 2ZKO, 2N74, 3M8A, 2Z0A) were used as templates in order to calculate the structure of SC35M NS1 using the Swiss-Model server. The phosphorylations at Ser48 and Thr49 are shown in red and the possible contact to dsRNA bases is visualized. The model was calculated by Dr. Karin Fritz-Wolf (University of Giessen). (**C**) Upper panel: MLE-15 cells were infected with SC35 or SC35M for the indicated periods. Cells were harvested and cell extracts were analyzed by immunoblotting for NS1 phosphorylation using phospho-specific antibodies. Lower panel: Plasmids containing the segment encoding the SC35M NS1 gene or derivatives thereof where Ser48 and Thr49 were changed to Glu or Ala were combined with plasmids encoding the other SC35M segments to produce reassortant viruses. These different viruses were used to infect MLE-15 cells (MOI = 1), followed by cell lysis after 8 h and immunoblotting to detect the occurrence and phosphorylation of NS1 as shown.

To investigate the functional relevance of some phosphorylations, the reverse genetics approach was used to create mutated SC35M viruses, as visualized in the a schematic diagram (Fig 22A). This system allowed to generate recombinant viruses upon transfection of 8 plasmids encoding the viral RNAs into a co-culture of 293T/MDCK-II cells, followed by a first titration (Titration 1, Fig 22B) to determine whether the viruses could be rescued. During the next step (Schematic representation in Fig 22C), MLE-15 cells were infected and virus replication in the lung cells was measured by a second titration (Titration 2, Fig 22D). For NS1, the two phophorylation sites Ser48 and Thr49 were mutated either to Alanine (Ala) or to its phosphomimicking form to Glutamic acid (Glu). In both cases infectious virus particles were generated (Fig 22B). SC35M (NS1-wt, NS1 ST 48,49 AA and NS1 ST 48,49 EE) viruses were then used to infect MLE-15 cells for 24 h with a MOI of 0.001 and to determine the replication efficiency of the viruses. No significant differences in the virus replication were observed (Fig 22D).

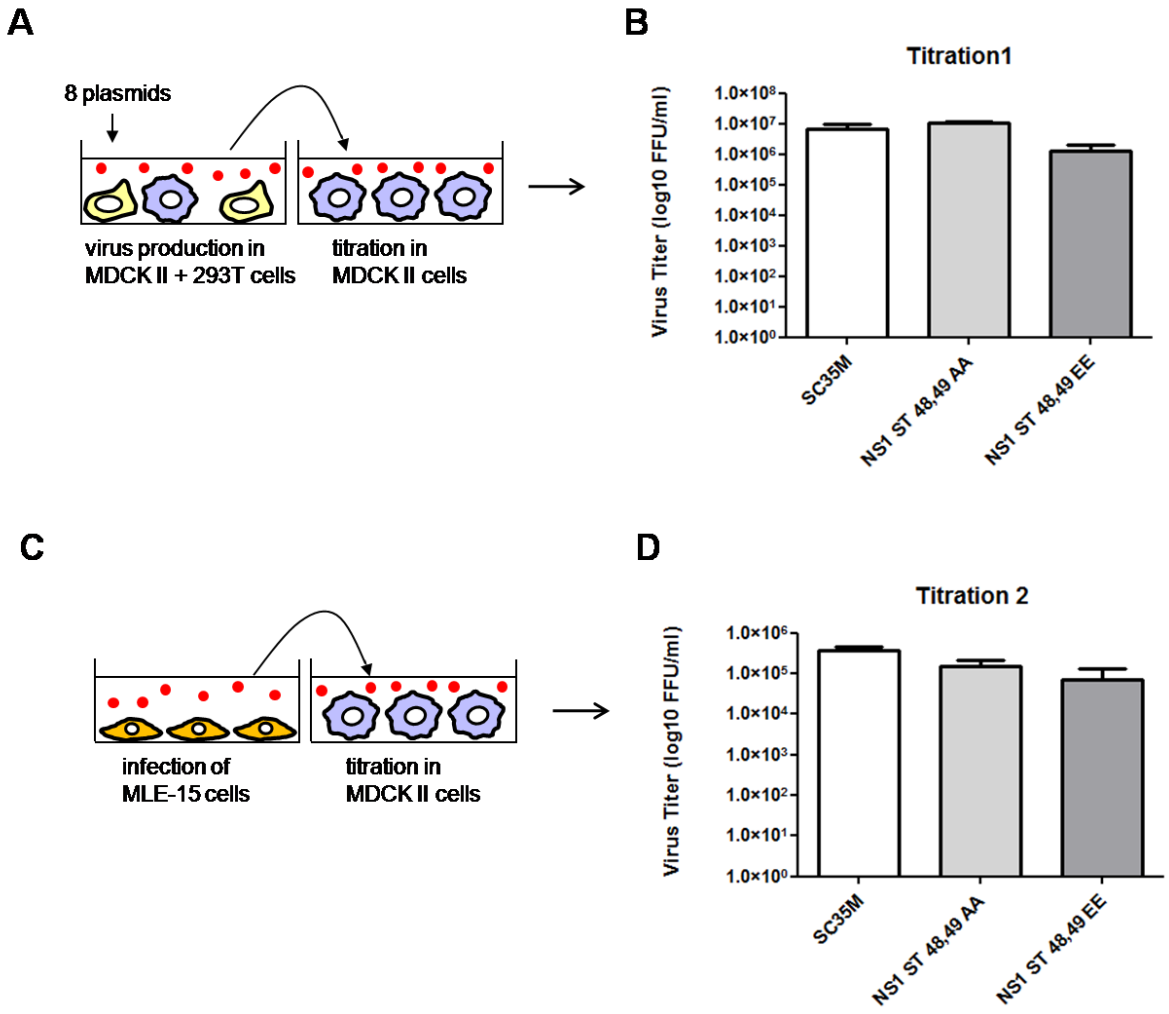

Figure 22: NS1 mutated SC35M virus production and replication. (**A**) Schematic display of the workflow for the production of recombinant IAV viruses encoding mutated viral proteins. **(B)** Plasmids encoding the wild-type or mutated forms of SC35M IAV proteins were transfected into 293T/MDCK-II cells. Two days later the cell culture supernatant was harvested and used to determine the number of functional viruses by titration in MDCK-II cells. Mean values from these titrations are shown, error bars display SEMs obtained from three independent experiments performed in triplicate. **(C)** Schematic display of the workflow for the replication of recombinant IAV viruses encoding mutated viral proteins. **(D)** 293T/MDCK-II cells were transfected with plasmids encoding the wild-type or mutated forms of the indicated proteins to produce reassortant viruses. These viruses were used to infect MLE-15 cells (MOI = 0.001) and virus titers were determined 24 h p.i..Mean values from three independent experiments performed in triplicate are shown, error bars display SEMs.

While I could not detect the functional relevance of NS1 phosphorylations, it was then interesting to investigate the impact of further phosphorylations occurring on viral proteins. A further example for a phosphorylated residue with potential functional relevance is found on the viral RNA polymerase subunit PB1 at Thr223. *In silico* modeling suggested that

phosphorylation of Thr223 in the fingertips might affect template binding and NTP channeling (Fig 23A). Phosphorylation-defective and phospho-mimicking mutations were produced not only for the PB1 and NS1 proteins, but also for neuraminidase (NA), which can be modified at Ser178 close to the catalytic center (Fig 23B) (Yen et al., 2006).

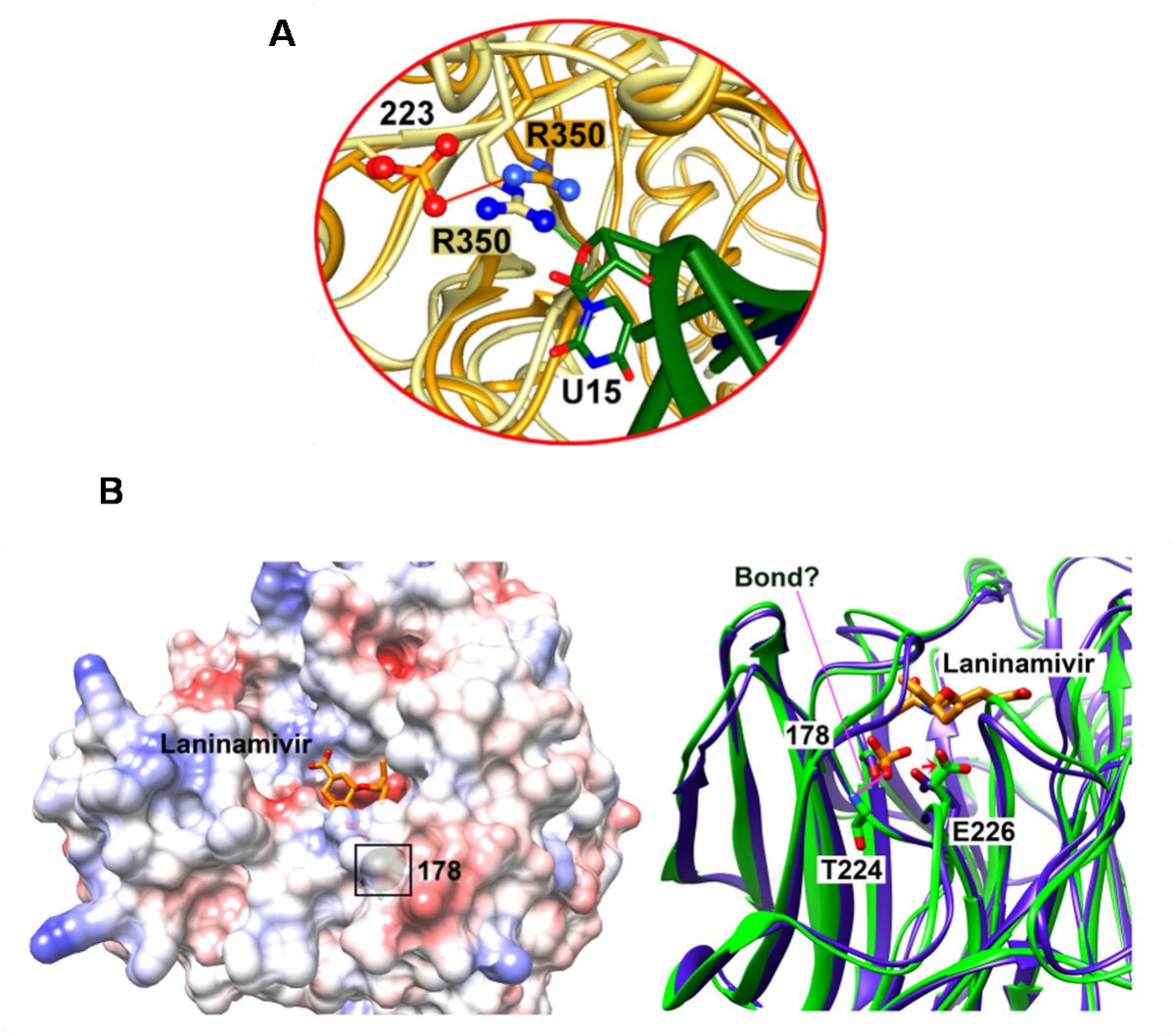

Figure 23: Functional analysis of IAV protein phosphorylation.(A) The published PB1 structure (PDB: 2ZKO) was used to model the impact of PB1 Thr223 phsphorylation on template binding. The impact of Thr223 phosphorylation on the contact to Uracil 15 in the RNA is shown in the enlarged section. **(B)** The left part shows a molecular model of NA from SC35M based on the high homology to the structure (PDB: 4QN7). The electrostatic potential of the molecular surfaces of NA are color coded, the position of the catalytic center is visualized by the binding of Laninamivir and the position of Ser178 at the surface is shown. The right part shows ribbon models for NA from SC35M in the unphosphorylated (blue) and phosphorylated (green) state. The models were calculated by Dr. Karin Fritz-Wolf (University of Giessen).

The schematic representation displayed in Fig 24A shows the production of SC35M viruses encoding the mutated PB1 proteins. The infection experiment showed that mutation of PB1 Thr223 to Glu did not yield infectious virus particles (Fig 24B). This suggests that PB1 Thr223 phosphorylation might serve to antagonize viral polymerase function. It was then interesting to analyze the effects of PB1 phosphorylation on viral polymerase activity using a plasmid-based mini-replicon system (Pleschka et al., 1996). A Pol I-driven plasmid encoding the luciferase reporter gene was cotransfected into HEK293T cells with plasmids encoding the viral PB2, PA, NP and PB1 proteins and its mutated derivatives. The analysis of luciferase activity showed completely absent polymerase activity when PB1 Thr223 was mutated to Glu (Fig 24E), which clearly indicates why rescue of the virus with this mutation was unsuccessful (Fig 24B). Mutation in the Thr223 phosphosite of PB1 to Glu abolishes the entire polymerase activity.

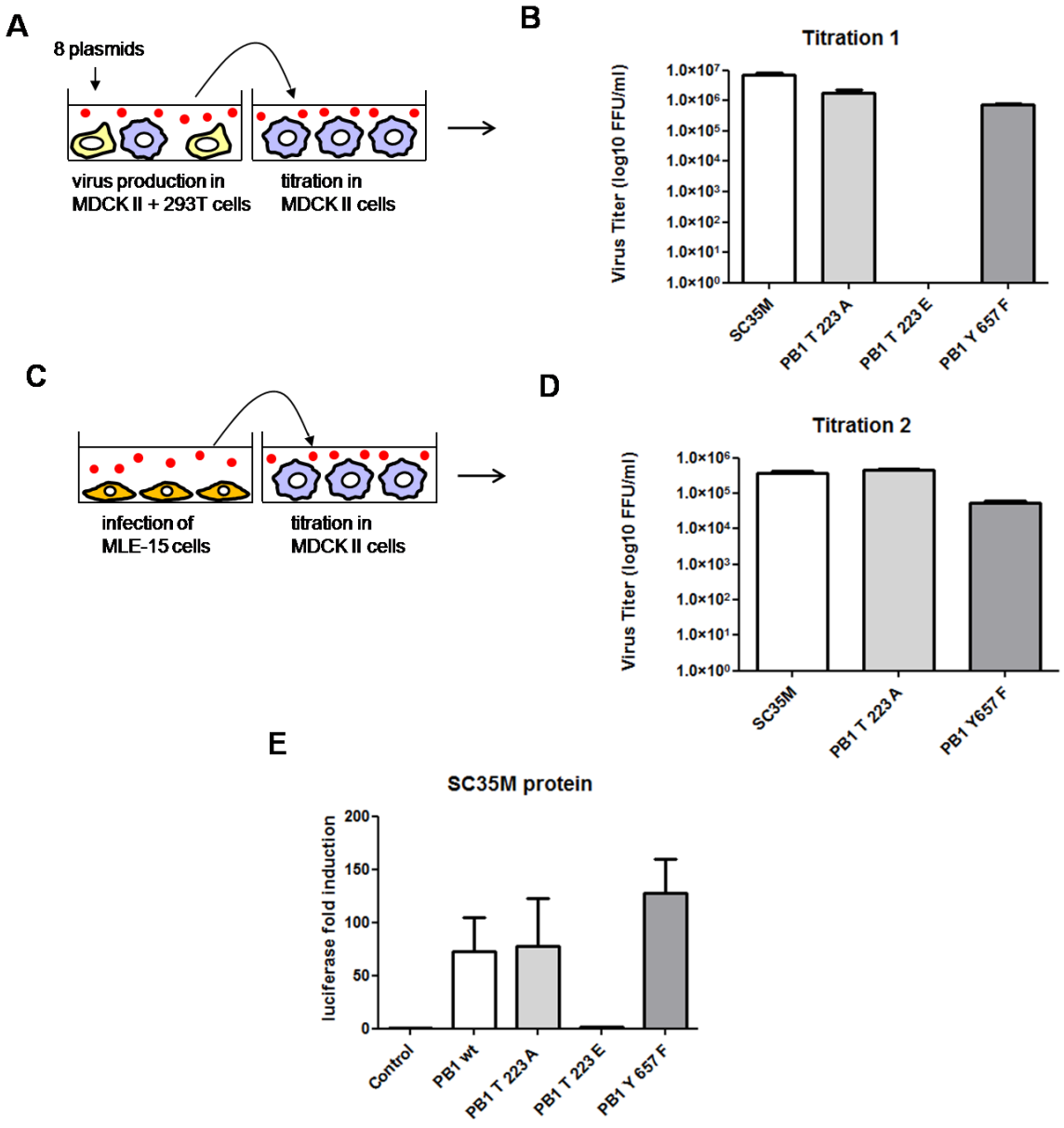

Figure 24: PB1 mutated SC35M virus production, replication and functional testing. (**A**) Schematic display of the workflow for the production of recombinant IAV viruses encoding mutated viral proteins. **(B)** Plasmids encoding the wild-type or mutated forms of SC35M IAV PB1 proteins were transfected into 293T/MDCK-II cells. Two days later the cell culture supernatant was harvested and used to determine the number of functional viruses by titration in MDCK-II cells. Mean values from these titrations are shown, error bars display SEMs obtained from three independent experiments performed in triplicate. **(C)** Schematic display of the workflow for the replication of recombinant IAV viruses encoding mutated viral proteins. **(D)** 293T/MDCK-II cells were transfected with plasmids encoding the wild-type or mutated forms of the indicated proteins to produce reassortant viruses. These viruses were used to infect MLE-15 cells (MOI = 0.001) and virus titers were determined 24 h p.i..Mean values from three independent experiments performed in triplicate are shown, error bars display SEMs. (**E**) HEK 293T cells were transfected with a viral UTR-driven firefly luciferase reporter gene, a plasmid leading to expression of Renilla luciferase and plasmids encoding PB2, PB1, PA, and NP proteins. After one day cells were lysed and Renilla and Firefly luciferase activities were determined. The graph shows firefly luciferase activity normalized to the Renilla luciferase control, error bars display SEMs obtained from three independent experiments performed in triplicate.

While these data showed that the essentiality of some phosphorylation sites precluded the generation and release of recombinant viruses, the effects of other modifications could be tested on MLE-15 cells for replication. Molecular modeling showed that Ser178 is close to and points towards the active center of the neuraminidase of NA, which was visualized by displaying the location of the competitive inhibitor Laninamivir (Fig. 23B left). A molecular model predicting the structural changes triggered by NA Ser178 phosphorylation showed that the phosphate group will result in the movement of the Glu226 side chain and might make a possible contact to Thr224. The phosphorylation-induced structural changes might facilitate substrate docking while leaving the enzymatic center intact (Fig. 23B right). Therefore, SC35M NA was mutated at Ser178 position with Ala or Glu. The experiment showed that inhibition of NA Ser178 phosphorylation resulted in strongly reduced virus production (Fig 25B) as well as virus replication (Fig 25D). These results raise the possibility that inhibition of NA Ser178 phosphorylation interferes with its enzymatic activity. To test this hypothesis NA activity of the SC35M virus and derivatives thereof expressing NA phosphorylation-deficient and phospho-mimicking versions were determined. Various dilutions of IAVs were used to determine neuraminidase activity using an *in vitro* assay. The phosphorylation-deficient NA Ser178Ala mutant consistently showed impaired NA activity (Fig 25E), suggesting that NA Ser178 phosphorylation assists in its enzymatic activity.

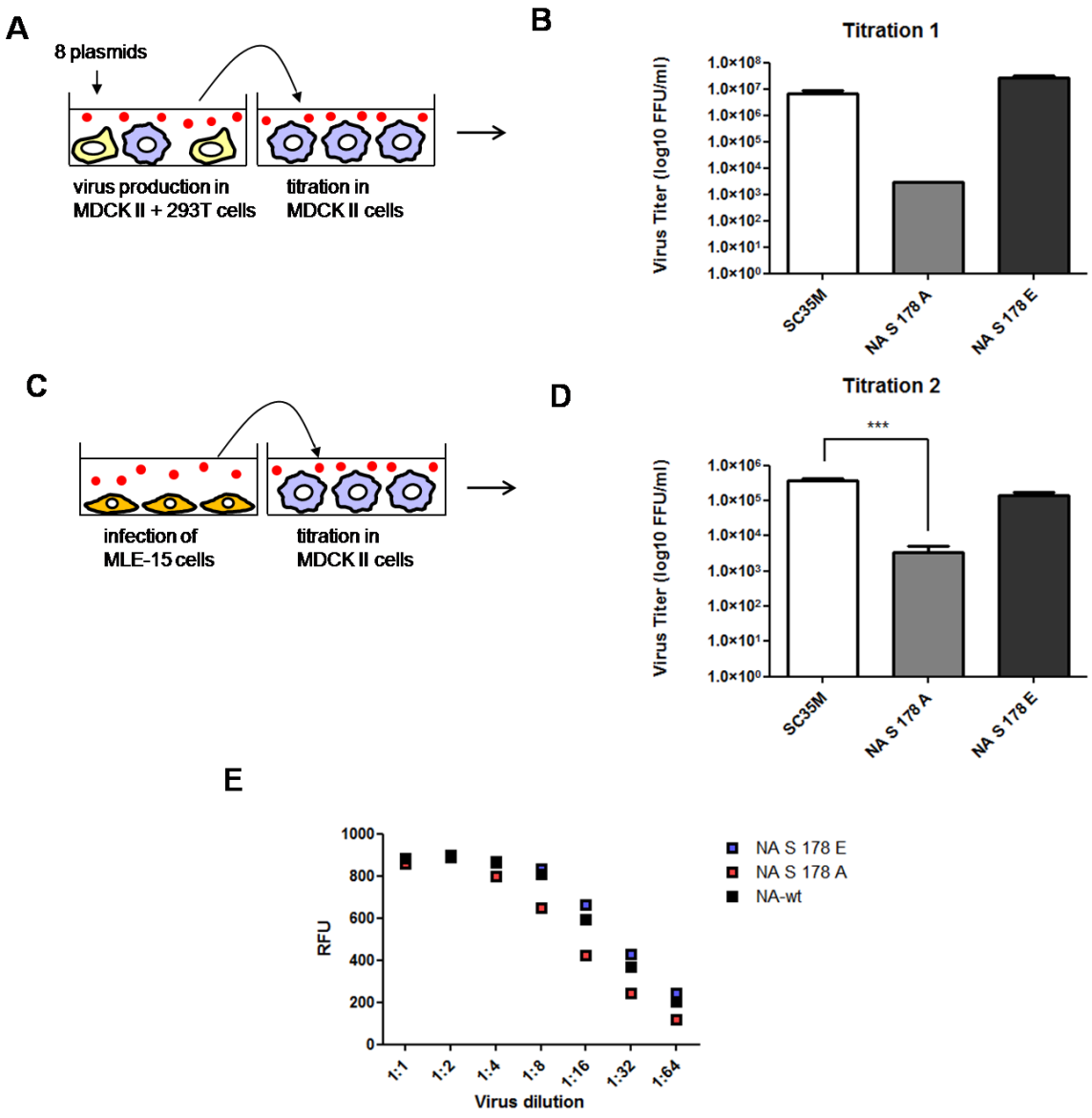

Figure 25: NA mutated SC35M virus production, replication and functional testing. (**A**) Schematic display of the workflow for the production of recombinant IAV viruses encoding mutated viral proteins. **(B)** Plasmids encoding the wild- or mutated forms of SC35M IAV NA proteins were transfected into 293T/MDCK-II cells. Two days later the cell culture supernatant was harvested and used to determine the number of functional viruses by titration in MDCK-II cells. Mean values from these titrations are shown, error bars display SEMs obtained from three independent experiments performed in triplicate. **(C)** Schematic display of the workflow for the replication of recombinant IAV viruses encoding mutated viral proteins. **(D)** 293T/MDCK-II cells were transfected with plasmids encoding the wild-type or mutated forms of the indicated proteins to produce reassortant viruses. These viruses were used to infect MLE-15 cells (MOI = 0.001) and virus titers were determined 24 h p.i..Mean values from three independent experiments performed in triplicate are shown, error bars display SEMs. The *P* values are indicated by asterisks: ***, $P < 0.001$. **(E)** NA enzymatic activity of SC35M and SC35M NA mutated viruses (S178A, S178E) (HAU=60) were determined by using a microplate fluorescence reader at excitation and emission wavelength of 360 nm and 460 nm, respectively. All results represent the mean of six independent experiment.

The functional analysis of some of these phosphosites showed that some phosphorylations such as the PB1 modification serve to interfere with their polymerase function, thus providing an example for a novel anti-viral signaling mechanisms. Other phosphorylations such as NA modification close to the catalytic center support their enzymatic function, opening new avenues for the therapeutic interference with IAV replication.

4. Discussion

4.1 The impact of the influenza virus genotype on NF-κB function

4.1.1 IAV genotype influences the impact ofNF-κB on viral replication

In the first part of this study I used the CRISPR-Cas9 system and MLE-15 cells to investigate the function of NF-κB for IAV replication.NF-κB knockout cells were generated by CRISPR-Cas9 technology, a new tool based on a bacterial Cas9 nuclease from *Streptococcus pyogenes* (Cong et al., 2013). The genetic inhibition of the NF-κB activation by two independent approaches made the MLE-15 cells more susceptible to IAV infection by the avian-adapted SC35 virus. In contrast, the mouse-adapted SC35M virus replication was not affected by the NF-κB status of the MLE-15 cells. Both strains differ by 9 amino acids in 6 different viral genome segments (Gabriel et al., 2005).The observed difference in NF-κB dependency of the SC35 and SC35M viruses comprised the background of my study to investigate the impact of NF-κB on the replication of various SC35 reassortants carrying SC35M segments. Reassortants were generated using the reverse genetics technology(Nicolson et al., 2005; Ozaki et al., 2004).

I found that the recombinant SC35 virus expressing the NA protein from SC35M was not affected by the anti-viral function of NF-κB. Whereas, the replication of a reassortant SC35 expressing the HA protein from SC35M was enhanced 10,000-fold upon deletion of the p65 gene. This result highlights that the role of the NF-κB transcription factor in IAV replication is depending on the viral genotype. This may in part explain the contradictory results showing either pro- or anti-viral functions of NF-κB, as discussed in detail in a review (Schmitz et al., 2014).

Therefore, it would be beneficial to investigate whether the observed anti-viral function of NF-κBis restricted to specific host cells (cell type, species) or to specific IAVs. For further

studies, the genetics of the virus should be considered when investigating the effect of the NF-κB system on IAV replication in a given host. In this study I used MLE-15 cells to investigate the anti-viral function of NF-κB. In the future, the impact of genetic NF-κB inhibition by the CRISPR-Cas9 system could be tested in human cells and cells from further species important for IAV transmission. It is also not clear which of the different steps in the IAV life cycle are affected by NF-κB. It would be interesting to analyze viral genome transcription/replication, e.g. by a strand-specific qPCR-based procedure to distinguish between IAV vRNA, cRNA, and mRNA (Kawakami et al., 2011). This method would be suitable to determine critical NF-κB-regulated steps in the IAV RNA replication and transcription activity. The effects of NF-κB on later steps of the IAV life cycle could be further monitored by determining the accumulation and intra-cellular localization of viral proteins, such as NS1 and NP. Previously, it was shown that the NF-κB subunit p50 binds to RNA (Huang et al., 2003). Therefore, it would also be interesting to know whether p65 subunit of NF-κB has also the ability to bind to RNA.

4.1.2 The impact of NF-κB-dependent IFN expressionon viral infection

One of the most important findings in this study is that the role of the NF-κB pathway is most noticeable after infection of MLE-15 cells with the SC35 virus at a low MOI. It is known that NF-κB acts antiviral during the initial phase of viral infection through activating anti-viral IFNs and further chemokines which eventually attract neutrophils and monocytes *in vivo*(Muramoto et al., 2014; Xiao et al., 2013). This allows uninfected cells to detect IAV with higher sensitivity and to produce even larger amounts of anti-viral IFNs (Stetson and Medzhitov, 2006). IFNs are induced in a cell-type specific manner through TLRs or RIG-I-dependent pathways, both pathways are capable of activating IRF and NF-κB which are necessary to activate the IFN promoter (Nan et al., 2014). In my results I found that SC35

virus-induced IFNβ expression was fully and SC35M virus-induced IFNβ expression was partially dependent on functional NF-κB signaling. However, the role of NF-κB and its interplay with IFN in antiviral immunity does not show a coherent picture. There are some studies where the authors showed that NF-κB is not crucial for IFN gene expression. For example, Wang and co-workers showed that in case of MEF cells infection with RNA viruses (Sendai virus (SeV) and Newcastle disease virus (NDV)), NF-κB was not important for IFNβ gene expression(Wang et al., 2007).

In my work I foundan important contribution of NF-κB p65 for the IAV-stimulated IRF3 phosphorylation, thus identifying a different angle of cross-regulation between NF-κB and IRF pathways (Grumont and Gerondakis, 2000; Iwanaszko and Kimmel, 2015). Impaired IRF3 phosphorylation might be attributable to defective expression or activation of the IRF kinase IKKε, which is induced in response to inflammatory insults (Bulek et al., 2011). Another possibility could be a defective activation of TBK1 in p65 knockout MLE-15 cells which results in lower amounts of activated IRF3 in response to virus infection (Matsui et al., 2006; Perry et al., 2004).

4.1.3 The impact of NF-κB on virus replication independent from the IFN system

In my results I showed that inhibition of IKKβ activity by the specific inhibitor PHA-408 led to increased replication of the chicken-adapted SC35 virus in murine MLE-15 cells. In contrast, different cell lines displaying reduced NF-kB activity (due to expression of dominant negative mutants for IKKβ (IKK KD) or IκBα) or increased NF-kB activity (due to overexpression of a constitutive active IKKβ variant) showed a virus-supportive function of NF-κB (Wurzer et al., 2004). One of the cell lines in this study were Vero cells, which do not express type-I IFN (Wurzer et al., 2004). Thus the observed virus-supporting effects of NF-

kB are independent from the IFN system. The authors state that the pro-viral effect of NF-κBis related to the virus-induced and NF-κB-dependent expression of pro-apoptotic factors (TRAIL and FasL), which enhance virus propagation in an autocrine and paracrine way, by supporting apoptosis related activation of caspases which is needed for efficient IAV replication (Muhlbauer et al., 2015; Wurzer et al., 2004). Furthermore, Nimmerjahn and co-workers also showed that an active NF-κB signaling pathway is a general prerequisite for a productive IAV infection. A cell line, which has low levels of NF-κB activity (Burkitt's lymphoma cell line), is resistant to IAV infection, but upon the activation of NF-κB signaling, the cells become susceptible to IAV infection (Nimmerjahn et al., 2004). Based on my results the antiviral effect of NF-κB in an IAV infection seems to be relevant for non-adapted IAV and during an early state of the infection (e.g. low MOI).

4.1.4 The effect of IAV-induced cytokine production on viral infection

At later stages of an established infection, the massively released virus progeny might cause an exaggerated NF-κB activation that further supports IAV replication (Muhlbauer et al., 2015; Wurzer et al., 2004). However, this overshooting of NF-κB response also underlies the excessive pro-inflammatory response during influenza virus pneumonia (Juozapaitis and Antoniukas, 2007; Ozawa and Kawaoka, 2011; Palese and Young, 1982). IAVs cause pneumonia in humans, with progression to lung failure and fatal outcome. Deregulated release of cytokines triggers cell death of alveolar epithelial cells (Ito, 2000). IAV-infected patients suffering from acute respiratory distress syndrome (ARDS) are characterized by local and systemic increases in cytokines (IL-6, IL-10, IL-15, and TNF) and reactive oxygen intermediates (Ozawa and Kawaoka, 2011). The causative effect of increased cytokines on lung injury suggests that interference with exaggerated innate immunity responses could be of therapeutic use (Ma, 2009). Interference of drugs with the exaggerated production of

inflammatory cytokines will protect from tissue damage and is an important goal to control mortality by IAV infection. On the other hand, it must be considered that early inflammation during the infection phase has anti-viral and beneficial effects. Thus, it is important to have drugs that selectively interfere with signaling pathways contributing to the exacerbated production of inflammatory mediators causing lung injury, while maintaining the ability of host cells to mount an anti-viral response.

The NF-κB pathway is not only compromised in patients taking anti-inflammatory drugs such as steroids (Ma et al., 2010a), but also in individuals where mutations or epigenetic events affect key components of the core NF-κB module. These germ line or somatic mutations include point mutations and deletions (NEMO, c-REL, NFKB2, IKBA, and SCYLD), chromosomal translocations (p65 and BCL-3), and also gene amplifications (e.g., c-REL) (Ma et al., 2009; Ma et al., 2010b; Tuna et al., 2012; Vincent et al., 2009). NF-κB mutations typically result in the early onset of cancer and inflammatory diseases but may also increase the susceptibility to IAV infection. Talon and co-workers showed that one naturally occurring mutation in the NEMO gene leads to an in-frame splicing event and the exclusive production of a shortened NEMO protein. A patient carrying this mutation showed strongly diminished RNA-induced induction of the IFNβ response and an increased susceptibility to viral infections (Talon et al., 2000b). Another report described a synonymous mutation in the gene encoding NEMO that enhances alternative splicing and leads to the production of a shorter protein (Δ-NEMO). Cultivated cells from these individuals showed an impaired association of Δ-NEMO with TBK1 and an incomplete RNA-induced nuclear translocation of NF-κB. Concomitantly cells expressing Δ-NEMO displayed impaired RNA-induced IFNβ production and permitted increased virus propagation (Talon et al., 2000a). Wang and co-workers showed that silencing of NEMO by small interfering RNA led to increased replication of IAVs in A549 cells (Wang et al., 2012). Since NEMO can indirectly start the

transcription of IFNs via activating NF-κB (Bernasconi et al., 2005), overexpression of NEMO resulted in increased expression of IFNα/β (Wang et al., 2012). Therefore, it is assumed that IAVs must have evolved some mechanism to inhibit IFNα/β production through direct or indirectNEMO regulation. Indeed, Kochs and co-workers and Min and co-workers revealed that the viral protein NS1 plays a vital role in suppressing IFNα/β production via inhibiting NF-κB activation through physically binding to the target molecules such as dsRNA and PKR (Kochs et al., 2007; Min et al., 2007). A schematic model of the possible role NF-κB on SC35 infection is depicted in Fig. 26.

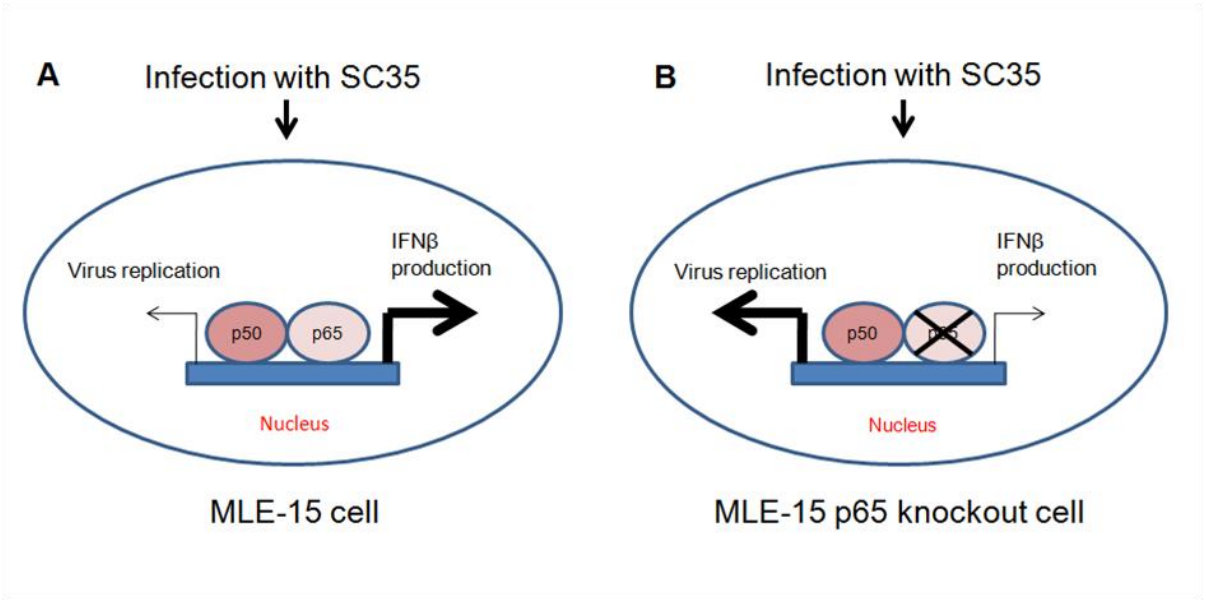

Figure 26: Schematic model to represent the effects of inactive NF-κB on SC35 infection. MLE-15 control cells **(A)** and MLE-15 p65 knockout cell **(B)** show differential IFNβ expression levels and virus replication rates, for details see text.

4.1.5 Viral mechanisms counteracting the host defense

While one part of the antiviral NF-κB response was mediated by IFNs, I found further antiviral functions of this transcription factor at earlier stages of virus replication. My results showed that NF-κB has an effect on the synthesis rateof NS1 and the intracellular localization of NP.To counteract the anti-viral function of NF-κB, IAVs employ several mechanisms to

dampen NF-κB activity. Ayllon and Gracia showed that the NS1 protein antagonizes IAV-induced activation of the canonical NF-κB activation pathway by constitutive association with IKKα and IKKβ to inhibit their catalytic activities. Furthermore, NS1 inhibits the non-canonical NF-κB activation pathway (Ayllon and Garcia-Sastre, 2015; Gao et al., 2012a). Probably, the evolution of IAVs will not only be directed at inhibiting the NF-κBsignaling steps leading to IFN production, but also at adapting the virus to avoid excessive early stage activation of NF-κB. Therefore, not only replication of the mouse-adapted SC35M is unaffected by NF-κB in the murine MLE-15 cells, but the virus may also have evolved to restrict NF-κB activity to reduce expression of pro-inflammatory cytokines such as IL-6, which seems to play an important role in providing a defense against IAV infection (give citation). Increased mortality due to IAV infection could occur if IL-6 production or signaling would be disturbed by genetic or environmental factors (Dienz et al., 2012).

4.2 Influenza virus-dependent phosphoproteome changes

In the phosphoproteomic screen I have identified phosphorylations of cellular and viral proteins. I investigated the functional relevance of phosphorylation of cellular substrates and kinases and of viral proteins.

4.2.1 Effect of IAV infection on the phosphorylation of cellular proteins in MLE-15 cells

This study identified thousands of IAV-regulated phosphorylationsevents of cellular proteins in MLE-15 cells. These regulated phosphorylation events are either a direct consequence of the virus infection or are due to secondary cell (stress) events, especially during the late times of infection. Inducible phosphorylation can result in either activation or inactivation events (Roux and Thibault, 2013). Interestingly, in my work the comparative analysis of SC35M and SC35-mediated phosphorylations showed a stronger overlap between the two viruses for inducible phosphorylations, suggesting that in this setting the inducible phosphorylations are

of broader relevance. While approximately half of the regulated Ser/Thrphosphorylations were common to SC35 and SC35M, this overlap was significantly lower for Tyr phosphorylations. This finding supports the previous notion of a distinct regulatory nature of Tyr and Ser/Thr-based signaling(Sharma et al., 2014).

While some of the phosphorylations will be of critical importance for IAV infection, others will not have a direct physiological consequence. It is assumed that a substantial part of phosphorylation events are non-functional phosphorylations, which may result from random encounters between protein kinases and degenerated substrate recognition motifs of substrates in the crowded environment of the cell (Landry et al., 2009; Lienhard, 2008). It will thus be very important to identify the key phosphorylation sites with a functional role in virus replication. Candidates for functionally relevant phosphorylations may be found in some of the co-phosphorylated protein complexes identified in this study. It will also be interesting to study the possible role of host cell phosphorylations in proteins with a known importance in the IAV life cycle. Such candidate proteins were previously revealed in a number of different whole-genome shRNA screens (Brass et al., 2009; Hao et al., 2008; Karlas et al., 2010; Konig et al., 2010; Shapira et al., 2009; Sui et al., 2009). At least in two screens, it was shown that 128 human genes are affecting influenza virus replication (Watanabe et al., 2010). Out of these 128 effected human genes, 126 also occur in mouse cells. One-third of the proteins with a putative role in the IAV life cycle were dynamically regulated by IAV-dependent phosphorylations (data not shown), showing a strong overrepresentation of phosphorylation events for these proteins. As IAVs infect many different species ranging from birds to horses, pigs, and aquatic mammals, further phosphoproteomic studies are needed to allow identification of protein residues that are frequently phosphorylated also in other host species in response to IAV infection.

It will be very relevant to study the function of IAV-regulated kinases, as they act as upstream regulators affecting the modification of many downstream phosphorylation events rather than only one single phosphorylation site. This screen did not only confirm the involvement of known kinases such as ERK1/2 and JNK signaling in IAV infection (Gao et al., 2012b) but also revealed new candidate kinases as identified by regulated activation loop phosphorylation and substrate motif analysis (Fig. 28, upper part). In the phosphoproteome data analysis, IAV-dependent regulation of a number of Tyr kinases including FAK, which are potentially interesting group of drug targets,were found. My work shows that inhibition of virus replication with the pre-clinically FAK inhibitor Defactinibwas more efficient upon pre-incubation when compared to Defactinibtreatment after infection. This is consistent with a proposed role of FAK for the early steps of virus infection (Elbahesh et al., 2014). FAK controls multiple downstream pathways and its inhibition will not only affect JNK activity as shown in this study, but most probably also further effector pathways. FAK and its downstream targets cooperate to mediate the massive cytoskeletal reorganizations that facilitate virus entry and budding (Banerjee et al., 2014; Kumakura et al., 2015), but probably also intercellular spreading of the virus (Roberts et al., 2015).

4.2.2 Phosphorylation of viral proteins in IAV-infected MLE-15 cells

This study also identifies a number of new phosphorylation sites in IAV proteins. But the published and new phosphorylations are not equally distributed between the viral proteins, as quantified in Fig 27. For example, no phosphorylations events have been found for the PB1-F2 and PA-X proteins, whereas the matrix protein M1 is heavily phosphorylated at multiple residues.

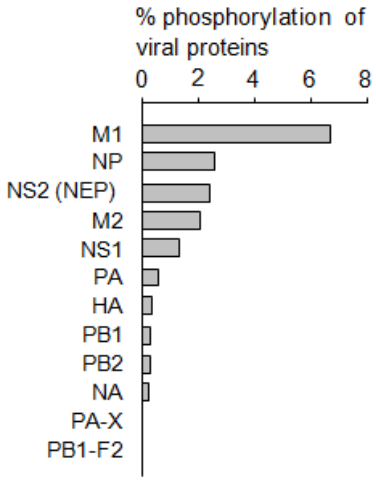

Fig 27: Number of phosphorylation sites in each viral proteins. The known and novel phosphorylation sites identified in this study were combined and the percentage of phosphorylated residues was calculated on the basis of SC35M proteins.

It will now be important to reveal the functions for the phosphorylations occurring at residues that are conserved between different IAV strains. Systematic studies are needed to identify residues supporting or antagonizing the functions of viral proteins. This classification will be of potential practical relevance, as the identification of virus supportive phosphorylations and the responsible kinases could open new avenues for the therapeutic interference with IAV replication. I identified phosphorylations inhibiting the function of viral proteins such as the modification of PB1 at Thr223. This provides an interesting example for a new and IFN-independent anti-viral signaling mechanism. To study the function of key phosphorylations in more detail, it will be important to continue to generate phospho-specific antibodies against key residues with functional relevance. These will allow to measure these modifications *in vivo* and to identify the responsible kinases in the future.

Also, IAV-mediated inhibition of FAK activity detected here might serve as a mechanism to antagonize virus replication. A schematic model of the possible role of viral protein phosphorylation on virus replication is shown in Fig. 28.

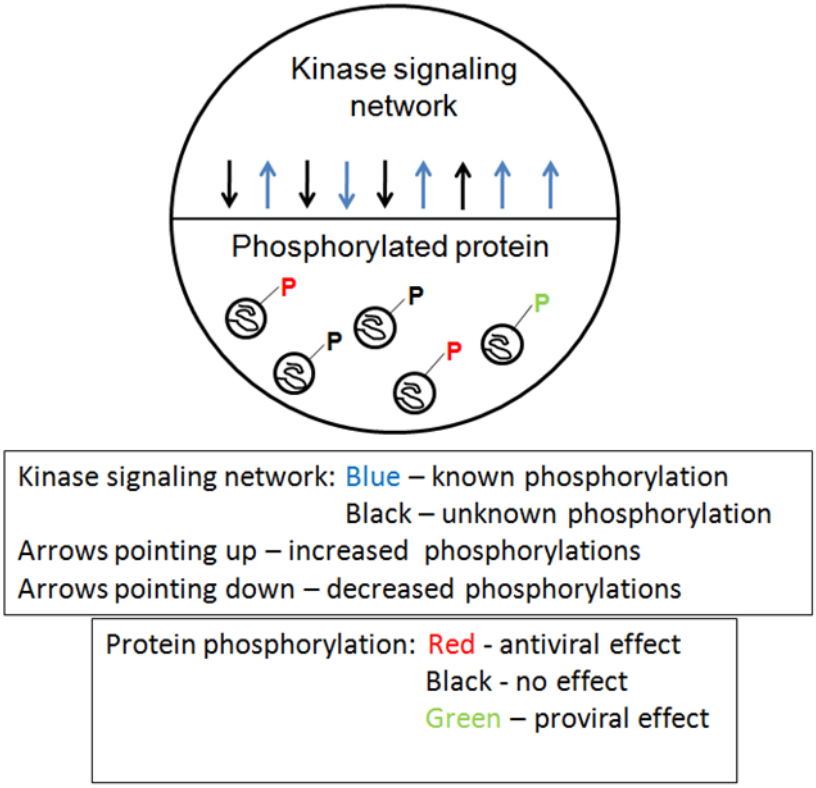

Figure 28: Schematic model of the functional relevance of IAV-regulated phosphorylations. The upper part of the figure represents the host cell kinase signaling network. Arrows pointing up or down indicate increased or decreased phosphorylations, the blue color indicates a known and black color indicates unknown implication in IAV replication. Lower part of the figure shows the effect of protein phosphorylation on virus replication. Some phosphorylations have no effects (black color), some have anti-viral effects (red color) and some have proviral effects (green color) on virus replication.

In summary, the phosphoproteomic screen performed in this study has revealed IAV-mediated regulation of several kinases and allowed the identification of host cell signaling networks. The elimination of proviral signaling circuits will be the prerequisite for the identification of inhibitory compounds to interfere with IAV propagation in the future.

5. Summary

This work is splitted in two parts, which both address the role of the IAV genotype for the function of NF-κB and host cell signaling networks. As a model system for different IAV genotypes I used an avian SC35 virus which infects avian but nu murine cells and its mouse-adapted variant SC35M which infects both avian and murine cells.

In the first part the role of NF-κB for IAV infection was investigated, as the literature did not provide a clear picture. Murine MLE-15 cells were used to perturb NF-κBsignaling either at the level of activating kinases or at the level of transcription activation. CRISPR-Cas9-mediated genome engineering was used to generate cells depleted in either the NEMO scaffold protein (and thus defective in IKK activation) or in the NF-κB DNA-binding and transactivating p65 subunit. While NF-κB was not affecting replication of SC35M, the deletion of NF-κB activity increased replication of the non-adapted SC35 virus. This antiviral effect was most noticeable upon infection of cells with low virus titers as they usually occur during the initiation phase of the IAV infection. The defect in NF-κB signaling resulted in decreased IAV-triggered phosphorylation of IRF3 and expression of the antiviral cytokine IFNβ. Reassortant viruses were generated by reverse genetics system to identify the viral proteins responsible for NF-κB dependency. SC35 viruses containing the NA segment from SC35M were completely inert to the inhibitory effect of NF-κB, highlighting the importance of the viral genotype for susceptibility to the antiviral function of NF-κB.

The second part of this study was performed to identify new host cell signaling pathways by a phosphoproteomic approach. MLE-15 cells were infected either with SC35 or SC35M and time dependent changes in the phophoproteome of MLE-15 cells were recorded by label-free quantitative phosphoproteome analysis. These experiments revealed thousands of IAV-regulated phosphorylation events. While approximately one-half of the induced

phosphorylations were triggered by both viruses, only one-third of the down-regulatedphosphorylations were co-regulated by SC35 and SC35M. Gene ontology and KEGG analyses revealed the overrepresentation of several pathways including those regulating cell adhesion, actin remodeling, and cytoskeleton organization. IAV-regulated kinases were identified by the occurrence of IAV-dependent changes in the activation loop and also by identification and analysis of common phosphorylation motifs, which allow the prediction of responsible kinases. These approaches disclosed the IAV-mediated regulation of FAK and inhibition of this kinase with pre-clinically used inhibitor Defactinib interfered with IAV replication. In addition, novel phosphorylation sites on IAV-encoded proteins were discovered. The functional analysis of selected phospho-sites showed that some phosphorylations serve to interfere with the enzymatic function of the viral proteins, thus providing an example for a novel antiviral signaling mechanism. Other phosphorylations supported the enzymatic function of viral proteins, opening new avenues for the therapeutic interference with IAV replication.

6. Zusammenfassung

Diese Arbeit besteht aus zwei Teilen, welche beide die Effekte des IAV Genotyps auf die Funktion von NF-κB und andere Signalwege in Wirtszellen adressieren. Als Modellsystem für verschiedene IAV Genotypen diente zum einen das aviäre SC35 Virus, welches erfolgreich aviäre Zellen infizieren kann und zum anderen die an murine Zellen adaptierte Variante SC35M, welches sowohl aviäre als auch murine Zellen infiziert.

Im ersten Teil der Arbeit wurde zunächst die Rolle von NF-κB für IAV Infektionen analysiert, da die Literatur kein klares Bild lieferte. Murine MLE-15 Zellen wurden verwendet, um den NF-κB Signalweg entweder auf Ebene der Kinaseaktivierung oder auf Ebene der Transkriptionsaktivierung funktionsunfähig zu machen. Durch CRISPR-Cas9-vermittelte Genom-Editierung wurden Zellen generiert, welche entweder das Gerüstprotein NEMO nicht mehr synthetisieren (und somit eine IKK-Aktivierung verhindert wird) oder in welchen die NF-κB Untereinheit p65, welche für die Bindung an die DNA und Transaktivierung essentiell ist, fehlt. Während NF-κB die Replikation von SC35M nicht beeinflusste, hatte eine Blockierung des NF-κB Signalweges eine gesteigerte Replikation des nicht-adaptierten Virus SC35 zur Folge. Dieser antivirale Effekt konnte am deutlichsten in Zellen mit niedrigem Titer beobachtet werden, da diese normalerweise in der Initiationsphase von IAV-Infektionen auftreten. Des Weiteren resultiert ein Defekt des NF-κB Signalwegs in verminderter IAV-abhängiger Phosphorylierung sowie Expression des antiviralen Zytokins IFNβ. Reassortanten der Viren wurden mittels reverser Genetik generiert um die viralen Proteine, welche für die NF-κB-Abhängigkeit verantwortlich sind, zu identifizieren. SC35 Viren, welche das NA Segment von SC35m enthalten, blieben vom inhibitorischen Effekt von NF-κB gänzlich unbeeinflusst, was die Wichtigkeit des viralen Genotyps für die Anfälligkeit der Viren gegenüber der antiviralen Funktion von NF-κB verdeutlicht.

Der zweite Teil der Arbeit diente der Identifizierung neuer Signalwege in der Wirtszelle mithilfe einer Phosphoproteom-Analyse. MLE-15 Zellen wurden entweder mit SC35 oder SC35M infiziert und zeitabhängige Veränderungen des Phosphoproteoms dieser Zellen mittels quantitativer, *label*-freier Phosphoproteomanalyse erfasst. Diese Experimente erlaubten die Identifizierung von tausenden IAV-regulierte Phosphorylierungen in den MLE-15 Zellen. Während ungefäht die Hälfte aller induzierten Phosphorylierungen von SC35 und SC35M hervorgerufen wurden, wurde lediglich ein Drittel der heruntergeregelten Phosphorylierungen von SC35 und SC35M ko-reguliert. Gen-Ontologie und KEGG-Analysen zeigten eine Überrepräsentation einiger Signalwege welche beispielsweise Zelladhäsion, Aktin-Remodellierung und die Organisation des Zytoskeletts regulieren. IAV-regulierte Kinasen wurden durch zwei unterschiedliche Ansätze identifiziert: Zum Einen durch das Auftreten IAV-abhängiger Veränderungen in der Aktivierungsschleife, zum anderen durch die Identifizierung von Phosphorylierungs-Motiven und den dazugehörigen Kinasen. Diese Vorgehensweise enthüllte eine IAV-vermittelte Regulation von FAK und funktionelle Studien zeigten, dass die Inhibition der Kinase durch den in prä-klinischen Studien verwendeten Inhibitor Defactinib mit der IAV-Replikation interferiert. Des Weiteren konnten bisher unbekannte Phosphorylierungsstellen von IAV-kodierten Proteinen erstmals beschrieben werden. Funktionale Analysen einiger Phosphorylierungsstellen zeigten, dass einige Phosphorylierungen mit der enzymatischen Funktion einiger viraler Proteine interferieren, was einen Beweis für neuartige antivirale Mechanismen liefert. Andere Phosphorylierungen hingegen unterstützen die enzymatische Funktion viraler Proteine, was neue Wege für therapeutische Interferenz mit der IAV-Replikation eröffnet.

7 References

Ayllon, J., and Garcia-Sastre, A. (2015). The NS1 protein: a multitasking virulence factor. Current topics in microbiology and immunology *386*, 73-107.

Bain, J., Plater, L., Elliott, M., Shpiro, N., Hastie, C.J., McLauchlan, H., Klevernic, I., Arthur, J.S., Alessi, D.R., and Cohen, P. (2007). The selectivity of protein kinase inhibitors: a further update. The Biochemical journal *408*, 297-315.

Banerjee, I., Miyake, Y., Nobs, S.P., Schneider, C., Horvath, P., Kopf, M., Matthias, P., Helenius, A., and Yamauchi, Y. (2014). Influenza A virus uses the aggresome processing machinery for host cell entry. Science *346*, 473-477.

Barnwal, B., Mok, C.K., Wu, J., Diwakar, M.K., Gupta, G., Zeng, Q., Chow, V.T., Song, J., Yuan, Y.A., and Tan, Y.J. (2015). A monoclonal antibody binds to threonine 49 in the non-structural 1 protein of influenza A virus and interferes with its ability to modulate viral replication. Antiviral research *116*, 55-61.

Bernasconi, D., Amici, C., La Frazia, S., Ianaro, A., and Santoro, M.G. (2005). The IkappaB kinase is a key factor in triggering influenza A virus-induced inflammatory cytokine production in airway epithelial cells. The Journal of biological chemistry *280*, 24127-24134.

Borgeling, Y., Schmolke, M., Viemann, D., Nordhoff, C., Roth, J., and Ludwig, S. (2014). Inhibition of p38 mitogen-activated protein kinase impairs influenza virus-induced primary and secondary host gene responses and protects mice from lethal H5N1 infection. The Journal of biological chemistry *289*, 13-27.

Boulo, S., Akarsu, H., Ruigrok, R.W., and Baudin, F. (2007). Nuclear traffic of influenza virus proteins and ribonucleoprotein complexes. Virus research *124*, 12-21.

Braakman, I., Hoover-Litty, H., Wagner, K.R., and Helenius, A. (1991). Folding of influenza hemagglutinin in the endoplasmic reticulum. The Journal of cell biology *114*, 401-411.

Brass, A.L., Huang, I.C., Benita, Y., John, S.P., Krishnan, M.N., Feeley, E.M., Ryan, B.J., Weyer, J.L., van der Weyden, L., Fikrig, E., *et al.* (2009). The IFITM proteins mediate cellular resistance to influenza A H1N1 virus, West Nile virus, and dengue virus. Cell *139*, 1243-1254.

Bulek, K., Liu, C., Swaidani, S., Wang, L., Page, R.C., Gulen, M.F., Herjan, T., Abbadi, A., Qian, W., Sun, D., *et al.* (2011). The inducible kinase IKKi is required for IL-17-dependent signaling associated with neutrophilia and pulmonary inflammation. Nature immunology *12*, 844-852.

Bush, R.M., Bender, C.A., Subbarao, K., Cox, N.J., and Fitch, W.M. (1999). Predicting the evolution of human influenza A. Science *286*, 1921-1925.

Cargnello, M., and Roux, P.P. (2011). Activation and function of the MAPKs and their substrates, the MAPK-activated protein kinases. Microbiology and molecular biology reviews : MMBR *75*, 50-83.

Carpten, J.D., Faber, A.L., Horn, C., Donoho, G.P., Briggs, S.L., Robbins, C.M., Hostetter, G., Boguslawski, S., Moses, T.Y., Savage, S., *et al.* (2007). A transforming mutation in the pleckstrin homology domain of AKT1 in cancer. Nature *448*, 439-444.

Carr, C.M., and Kim, P.S. (1993). A spring-loaded mechanism for the conformational change of influenza hemagglutinin. Cell *73*, 823-832.

Carrat, F., Vergu, E., Ferguson, N.M., Lemaitre, M., Cauchemez, S., Leach, S., and Valleron, A.J. (2008). Time lines of infection and disease in human influenza: a review of volunteer challenge studies. American journal of epidemiology *167*, 775-785.

Carrillo, B., Choi, J.M., Bornholdt, Z.A., Sankaran, B., Rice, A.P., and Prasad, B.V. (2014). The influenza A virus protein NS1 displays structural polymorphism. Journal of virology *88*, 4113-4122.

Castellano, E., and Downward, J. (2011). RAS Interaction with PI3K: More Than Just Another Effector Pathway. Genes & cancer *2*, 261-274.

Chariot, A. (2009). The NF-kappaB-independent functions of IKK subunits in immunity and cancer. Trends in cell biology *19*, 404-413.

Chen, B.J., Leser, G.P., Jackson, D., and Lamb, R.A. (2008). The influenza virus M2 protein cytoplasmic tail interacts with the M1 protein and influences virus assembly at the site of virus budding. Journal of virology *82*, 10059-10070.

Chen, Z.J. (2005). Ubiquitin signalling in the NF-kappaB pathway. Nature cell biology *7*, 758-765.

Cheng, A., Wong, S.M., and Yuan, Y.A. (2009). Structural basis for dsRNA recognition by NS1 protein of influenza A virus. Cell research *19*, 187-195.

Chou, Y.C., Lai, M.M., Wu, Y.C., Hsu, N.C., Jeng, K.S., and Su, W.C. (2015). Variations in genome-wide RNAi screens: lessons from influenza research. Journal of clinical bioinformatics *5*, 2.

Ciampor, F., Thompson, C.A., Grambas, S., and Hay, A.J. (1992). Regulation of pH by the M2 protein of influenza A viruses. Virus research *22*, 247-258.

Cohen, P. (2002). The origins of protein phosphorylation. Nature cell biology *4*, E127-130.

Colman, P.R. (1998). KG Nicholson, RG Webster, AJ Hay Textbook of Influenza 9.

Cong, L., Ran, F.A., Cox, D., Lin, S., Barretto, R., Habib, N., Hsu, P.D., Wu, X., Jiang, W., Marraffini, L.A., *et al.*(2013). Multiplex genome engineering using CRISPR/Cas systems. Science *339*, 819-823.

Crescenzo-Chaigne, B., and van der Werf, S. (2007). Rescue of influenza C virus from recombinant DNA. Journal of virology *81*, 11282-11289.

Cuadrado, A., and Nebreda, A.R. (2010). Mechanisms and functions of p38 MAPK signalling. The Biochemical journal *429*, 403-417.

Dapat, C., Saito, R., Suzuki, H., and Horigome, T. (2014). Quantitative phosphoproteomic analysis of host responses in human lung epithelial (A549) cells during influenza virus infection. Virus research *179*, 53-63.

Das, T.P., Suman, S., Alatassi, H., Ankem, M.K., and Damodaran, C. (2016). Inhibition of AKT promotes FOXO3a-dependent apoptosis in prostate cancer. Cell death & disease *7*, e2111.

Desselberger, U., Racaniello, V.R., Zazra, J.J., and Palese, P. (1980). The 3' and 5'-terminal sequences of influenza A, B and C virus RNA segments are highly conserved and show partial inverted complementarity. Gene *8*, 315-328.

Dhand, R., Hiles, I., Panayotou, G., Roche, S., Fry, M.J., Gout, I., Totty, N.F., Truong, O., Vicendo, P., Yonezawa, K., *et al.* (1994). PI 3-kinase is a dual specificity enzyme: autoregulation by an intrinsic protein-serine kinase activity. The EMBO journal *13*, 522-533.

Dias, A., Bouvier, D., Crepin, T., McCarthy, A.A., Hart, D.J., Baudin, F., Cusack, S., and Ruigrok, R.W. (2009). The cap-snatching endonuclease of influenza virus polymerase resides in the PA subunit. Nature *458*, 914-918.

DiDonato, J.A., Hayakawa, M., Rothwarf, D.M., Zandi, E., and Karin, M. (1997). A cytokine-responsive IkappaB kinase that activates the transcription factor NF-kappaB. Nature *388*, 548-554.

Diehl, N., and Schaal, H. (2013). Make yourself at home: viral hijacking of the PI3K/Akt signaling pathway. Viruses *5*, 3192-3212.

Domingues, P., Golebiowski, F., Tatham, M.H., Lopes, A.M., Taggart, A., Hay, R.T., and Hale, B.G. (2015). Global Reprogramming of Host SUMOylation during Influenza Virus Infection. Cell reports *13*, 1467-1480.

Ehrhardt, C., Marjuki, H., Wolff, T., Nurnberg, B., Planz, O., Pleschka, S., and Ludwig, S. (2006). Bivalent role of the phosphatidylinositol-3-kinase (PI3K) during influenza virus infection and host cell defence. Cell Microbiol *8*, 1336-1348.

Ehrhardt, C., Ruckle, A., Hrincius, E.R., Haasbach, E., Anhlan, D., Ahmann, K., Banning, C., Reiling, S.J., Kuhn, J., Strobl, S., *et al.* (2013). The NF-kappaB inhibitor SC75741 efficiently blocks influenza virus propagation and confers a high barrier for development of viral resistance. Cell Microbiol *15*, 1198-1211.

Ehrhardt, C., Wolff, T., Pleschka, S., Planz, O., Beermann, W., Bode, J.G., Schmolke, M., and Ludwig, S. (2007). Influenza A virus NS1 protein activates the PI3K/Akt pathway to mediate antiapoptotic signaling responses. Journal of virology *81*, 3058-3067.

Elbahesh, H., Cline, T., Baranovich, T., Govorkova, E.A., Schultz-Cherry, S., and Russell, C.J. (2014). Novel roles of focal adhesion kinase in cytoplasmic entry and replication of influenza A viruses. Journal of virology *88*, 6714-6728.

Ersahin, T., Tuncbag, N., and Cetin-Atalay, R. (2015). The PI3K/AKT/mTOR interactive pathway. Molecular bioSystems *11*, 1946-1954.

Ferguson, L., Eckard, L., Epperson, W.B., Long, L.P., Smith, D., Huston, C., Genova, S., Webby, R., and Wan, X.F. (2015). Influenza D virus infection in Mississippi beef cattle. Virology *486*, 28-34.

Flory, E., Kunz, M., Scheller, C., Jassoy, C., Stauber, R., Rapp, U.R., and Ludwig, S. (2000). Influenza virus-induced NF-kappaB-dependent gene expression is mediated by overexpression of viral proteins and involves oxidative radicals and activation of IkappaB kinase. The Journal of biological chemistry *275*, 8307-8314.

Fodor, E., and Smith, M. (2004). The PA subunit is required for efficient nuclear accumulation of the PB1 subunit of the influenza A virus RNA polymerase complex. Journal of virology *78*, 9144-9153.

Gabriel, G., Dauber, B., Wolff, T., Planz, O., Klenk, H.D., and Stech, J. (2005). The viral polymerase mediates adaptation of an avian influenza virus to a mammalian host. Proceedings of the National Academy of Sciences of the United States of America *102*, 18590-18595.

Gabriel, G., Garn, H., Wegmann, M., Renz, H., Herwig, A., Klenk, H.D., and Stech, J. (2008). The potential of a protease activation mutant of a highly pathogenic avian influenza virus for a pandemic live vaccine. Vaccine *26*, 956-965.

Gabriel, G., Klingel, K., Planz, O., Bier, K., Herwig, A., Sauter, M., and Klenk, H.D. (2009). Spread of infection and lymphocyte depletion in mice depends on polymerase of influenza virus. The American journal of pathology *175*, 1178-1186.

Gao, S., Song, L., Li, J., Zhang, Z., Peng, H., Jiang, W., Wang, Q., Kang, T., Chen, S., and Huang, W. (2012a). Influenza A virus-encoded NS1 virulence factor protein inhibits innate immune response by targeting IKK. Cell Microbiol *14*, 1849-1866.

Gao, W., Sun, W., Qu, B., Cardona, C.J., Powell, K., Wegner, M., Shi, Y., and Xing, Z. (2012b). Distinct regulation of host responses by ERK and JNK MAP kinases in swine macrophages infected with pandemic (H1N1) 2009 influenza virus. PloS one *7*, e30328.

Garnett, M.J., and Marais, R. (2004). Guilty as charged: B-RAF is a human oncogene. Cancer cell *6*, 313-319.

Garten, R.J., Davis, C.T., Russell, C.A., Shu, B., Lindstrom, S., Balish, A., Sessions, W.M., Xu, X., Skepner, E., Deyde, V., *et al.* (2009). Antigenic and genetic characteristics of swine-origin 2009 A(H1N1) influenza viruses circulating in humans. Science *325*, 197-201.

Goulet, M.L., Olagnier, D., Xu, Z., Paz, S., Belgnaoui, S.M., Lafferty, E.I., Janelle, V., Arguello, M., Paquet, M., Ghneim, K., *et al.* (2013). Systems analysis of a RIG-I agonist inducing broad spectrum inhibition of virus infectivity. PLoS pathogens *9*, e1003298.

Grumont, R.J., and Gerondakis, S. (2000). Rel induces interferon regulatory factor 4 (IRF-4) expression in lymphocytes: modulation of interferon-regulated gene expression by rel/nuclear factor kappaB. The Journal of experimental medicine *191*, 1281-1292.

Guilligay, D., Tarendeau, F., Resa-Infante, P., Coloma, R., Crepin, T., Sehr, P., Lewis, J., Ruigrok, R.W., Ortin, J., Hart, D.J., *et al.* (2008). The structural basis for cap binding by influenza virus polymerase subunit PB2. Nature structural & molecular biology *15*, 500-506.

Haasbach, E., Reiling, S.J., Ehrhardt, C., Droebner, K., Ruckle, A., Hrincius, E.R., Leban, J., Strobl, S., Vitt, D., Ludwig, S., *et al.* (2013). The NF-kappaB inhibitor SC75741 protects mice against highly pathogenic avian influenza A virus. Antiviral research *99*, 336-344.

Halder, U.C., Bhowmick, R., Roy Mukherjee, T., Nayak, M.K., and Chawla-Sarkar, M. (2013). Phosphorylation drives an apoptotic protein to activate antiapoptotic genes: paradigm of influenza A matrix 1 protein function. The Journal of biological chemistry *288*, 14554-14568.

Hale, B.G., Knebel, A., Botting, C.H., Galloway, C.S., Precious, B.L., Jackson, D., Elliott, R.M., and Randall, R.E. (2009). CDK/ERK-mediated phosphorylation of the human influenza A virus NS1 protein at threonine-215. Virology *383*, 6-11.

Hale, B.G., Randall, R.E., Ortin, J., and Jackson, D. (2008). The multifunctional NS1 protein of influenza A viruses. The Journal of general virology *89*, 2359-2376.

Handschick, K., Beuerlein, K., Jurida, L., Bartkuhn, M., Muller, H., Soelch, J., Weber, A., Dittrich-Breiholz, O., Schneider, H., Scharfe, M., *et al.*(2014). Cyclin-dependent kinase 6 is a chromatin-bound cofactor for NF-kappaB-dependent gene expression. Molecular cell *53*, 193-208.

Hao, L., Sakurai, A., Watanabe, T., Sorensen, E., Nidom, C.A., Newton, M.A., Ahlquist, P., and Kawaoka, Y. (2008). Drosophila RNAi screen identifies host genes important for influenza virus replication. Nature *454*, 890-893.

Hayden, M.S., and Ghosh, S. (2012). NF-kappaB, the first quarter-century: remarkable progress and outstanding questions. Genes & development *26*, 203-234.

Hemmings, B.A., and Restuccia, D.F. (2012). PI3K-PKB/Akt pathway. Cold Spring Harbor perspectives in biology *4*, a011189.

Hinz, M., and Scheidereit, C. (2014). The IkappaB kinase complex in NF-kappaB regulation and beyond. EMBO reports *15*, 46-61.

Hirata, N., Suizu, F., Matsuda-Lennikov, M., Edamura, T., Bala, J., and Noguchi, M. (2014). Inhibition of Akt kinase activity suppresses entry and replication of influenza virus. Biochemical and biophysical research communications *450*, 891-898.

Hiscott, J., Kwon, H., and Genin, P. (2001). Hostile takeovers: viral appropriation of the NF-kappaB pathway. The Journal of clinical investigation *107*, 143-151.

Hoffmann, E., Krauss, S., Perez, D., Webby, R., and Webster, R.G. (2002a). Eight-plasmid system for rapid generation of influenza virus vaccines. Vaccine *20*, 3165-3170.

Hoffmann, E., Mahmood, K., Yang, C.F., Webster, R.G., Greenberg, H.B., and Kemble, G. (2002b). Rescue of influenza B virus from eight plasmids. Proceedings of the National Academy of Sciences of the United States of America *99*, 11411-11416.

Hoffmann, E., Neumann, G., Kawaoka, Y., Hobom, G., and Webster, R.G. (2000). A DNA transfection system for generation of influenza A virus from eight plasmids. Proceedings of the National Academy of Sciences of the United States of America *97*, 6108-6113.

Hoffmann, E., Stech, J., Guan, Y., Webster, R.G., and Perez, D.R. (2001). Universal primer set for the full-length amplification of all influenza A viruses. Archives of virology *146*, 2275-2289.

Hsiang, T.Y., Zhou, L., and Krug, R.M. (2012). Roles of the phosphorylation of specific serines and threonines in the NS1 protein of human influenza A viruses. Journal of virology *86*, 10370-10376.

Huang, D.B., Vu, D., Cassiday, L.A., Zimmerman, J.M., Maher, L.J., 3rd, and Ghosh, G. (2003a). Crystal structure of NF-kappaB (p50)2 complexed to a high-affinity RNA aptamer. Proceedings of the National Academy of Sciences of the United States of America *100*, 9268-9273.

Huang, Q., Sivaramakrishna, R.P., Ludwig, K., Korte, T., Bottcher, C., and Herrmann, A. (2003b). Early steps of the conformational change of influenza virus hemagglutinin to a fusion active state: stability and energetics of the hemagglutinin. Biochimica et biophysica acta *1614*, 3-13.

Huang, T.T., Wuerzberger-Davis, S.M., Wu, Z.H., and Miyamoto, S. (2003c). Sequential modification of NEMO/IKKgamma by SUMO-1 and ubiquitin mediates NF-kappaB activation by genotoxic stress. Cell *115*, 565-576.

Huang, X., Liu, T., Muller, J., Levandowski, R.A., and Ye, Z. (2001). Effect of influenza virus matrix protein and viral RNA on ribonucleoprotein formation and nuclear export. Virology *287*, 405-416.

Humphrey, S.J., James, D.E., and Mann, M. (2015). Protein Phosphorylation: A Major Switch Mechanism for Metabolic Regulation. Trends in endocrinology and metabolism: TEM *26*, 676-687.

Hutchinson, E.C., Denham, E.M., Thomas, B., Trudgian, D.C., Hester, S.S., Ridlova, G., York, A., Turrell, L., and Fodor, E. (2012). Mapping the phosphoproteome of influenza A and B viruses by mass spectrometry. PLoS pathogens *8*, e1002993.

Hutchinson, E.C., and Fodor, E. (2013). Transport of the influenza virus genome from nucleus to nucleus. Viruses *5*, 2424-2446.

Ito, T. (2000). Interspecies transmission and receptor recognition of influenza A viruses. Microbiology and immunology *44*, 423-430.

Iwanaszko, M., and Kimmel, M. (2015). NF-kappaB and IRF pathways: cross-regulation on target genes promoter level. BMC genomics *16*, 307.

Iyoda, K., Sasaki, Y., Horimoto, M., Toyama, T., Yakushijin, T., Sakakibara, M., Takehara, T., Fujimoto, J., Hori, M., Wands, J.R., *et al.* (2003). Involvement of the p38 mitogen-activated protein kinase cascade in hepatocellular carcinoma. Cancer *97*, 3017-3026.

Jacob, T., Van den Broeke, C., and Favoreel, H.W. (2011). Viral serine/threonine protein kinases. Journal of virology *85*, 1158-1173.

Jagger, B.W., Wise, H.M., Kash, J.C., Walters, K.A., Wills, N.M., Xiao, Y.L., Dunfee, R.L., Schwartzman, L.M., Ozinsky, A., Bell, G.L., *et al.* (2012). An overlapping protein-coding region in influenza A virus segment 3 modulates the host response. Science *337*, 199-204.

Jiang, S., Li, R., Du, L., and Liu, S. (2010). Roles of the hemagglutinin of influenza A virus in viral entry and development of antiviral therapeutics and vaccines. Protein & cell *1*, 342-354.

Jin, J., Hu, H., Li, H.S., Yu, J., Xiao, Y., Brittain, G.C., Zou, Q., Cheng, X., Mallette, F.A., Watowich, S.S., *et al.* (2014). Noncanonical NF-kappaB pathway controls the production of type I interferons in antiviral innate immunity. Immunity *40*, 342-354.

Johnson, G.L., and Nakamura, K. (2007). The c-jun kinase/stress-activated pathway: regulation, function and role in human disease. Biochimica et biophysica acta *1773*, 1341-1348.

Julkunen, I., Melen, K., Nyqvist, M., Pirhonen, J., Sareneva, T., and Matikainen, S. (2000). Inflammatory responses in influenza A virus infection. Vaccine *19 Suppl 1*, S32-37.

Juozapaitis, M., and Antoniukas, L. (2007). [Influenza virus]. Medicina *43*, 919-929.

Jureka, A.S., Kleinpeter, A.B., Cornilescu, G., Cornilescu, C.C., and Petit, C.M. (2015). Structural Basis for a Novel Interaction between the NS1 Protein Derived from the 1918 Influenza Virus and RIG-I. Structure *23*, 2001-2010.

Karin, M., Yamamoto, Y., and Wang, Q.M. (2004). The IKK NF-kappa B system: a treasure trove for drug development. Nature reviews Drug discovery *3*, 17-26.

Karlas, A., Machuy, N., Shin, Y., Pleissner, K.P., Artarini, A., Heuer, D., Becker, D., Khalil, H., Ogilvie, L.A., Hess, S., *et al.* (2010). Genome-wide RNAi screen identifies human host factors crucial for influenza virus replication. Nature *463*, 818-822.

Kathum, O.A., Schrader, T., Anhlan, D., Nordhoff, C., Liedmann, S., Pande, A., Mellmann, A., Ehrhardt, C., Wixler, V., and Ludwig, S. (2016). Phosphorylation of influenza A virus NS1 protein at threonine 49 suppresses its interferon antagonistic activity. Cell Microbiol *18*, 784-791.

Kato, Y., Kravchenko, V.V., Tapping, R.I., Han, J., Ulevitch, R.J., and Lee, J.D. (1997). BMK1/ERK5 regulates serum-induced early gene expression through transcription factor MEF2C. The EMBO journal *16*, 7054-7066.

Kawakami, E., Watanabe, T., Fujii, K., Goto, H., Watanabe, S., Noda, T., and Kawaoka, Y. (2011). Strand-specific real-time RT-PCR for distinguishing influenza vRNA, cRNA, and mRNA. Journal of virological methods *173*, 1-6.

Kawaoka (2007). virology. *chapter 32*.

Keshet, Y., and Seger, R. (2010). The MAP kinase signaling cascades: a system of hundreds of components regulates a diverse array of physiological functions. Methods in molecular biology *661*, 3-38.

Killip, M.J., Fodor, E., and Randall, R.E. (2015). Influenza virus activation of the interferon system. Virus research *209*, 11-22.

Kochs, G., Garcia-Sastre, A., and Martinez-Sobrido, L. (2007). Multiple anti-interferon actions of the influenza A virus NS1 protein. Journal of virology *81*, 7011-7021.

Konig, R., Stertz, S., Zhou, Y., Inoue, A., Hoffmann, H.H., Bhattacharyya, S., Alamares, J.G., Tscherne, D.M., Ortigoza, M.B., Liang, Y., *et al.* (2010). Human host factors required for influenza virus replication. Nature *463*, 813-817.

Kriete, A., and Mayo, K.L. (2009). Atypical pathways of NF-kappaB activation and aging. Experimental gerontology *44*, 250-255.

Krumbholz, A., Philipps, A., Oehring, H., Schwarzer, K., Eitner, A., Wutzler, P., and Zell, R. (2011). Current knowledge on PB1-F2 of influenza A viruses. Medical microbiology and immunology *200*, 69-75.

Kujime, K., Hashimoto, S., Gon, Y., Shimizu, K., and Horie, T. (2000). p38 mitogen-activated protein kinase and c-jun-NH2-terminal kinase regulate RANTES production by influenza virus-infected human bronchial epithelial cells. Journal of immunology *164*, 3222-3228.

Kumakura, M., Kawaguchi, A., and Nagata, K. (2015). Actin-myosin network is required for proper assembly of influenza virus particles. Virology *476*, 141-150.

Kumar, N., Xin, Z.T., Liang, Y., Ly, H., and Liang, Y. (2008). NF-kappaB signaling differentially regulates influenza virus RNA synthesis. Journal of virology *82*, 9880-9889.

Lamb, R.a.R.K. (2001). Orthomyoxyviridae: the viruses and their replication., Vol 4th.

Landry, C.R., Levy, E.D., and Michnick, S.W. (2009). Weak functional constraints on phosphoproteomes. Trends in genetics : TIG *25*, 193-197.

Lee, D.C., Cheung, C.Y., Law, A.H., Mok, C.K., Peiris, M., and Lau, A.S. (2005). p38 mitogen-activated protein kinase-dependent hyperinduction of tumor necrosis factor alpha expression in response to avian influenza virus H5N1. Journal of virology *79*, 10147-10154.

Lee, J.D., Ulevitch, R.J., and Han, J. (1995). Primary structure of BMK1: a new mammalian map kinase. Biochemical and biophysical research communications *213*, 715-724.

Lemmon, M.A., and Schlessinger, J. (2010). Cell signaling by receptor tyrosine kinases. Cell *141*, 1117-1134.

Levy, E.D., Michnick, S.W., and Landry, C.R. (2012). Protein abundance is key to distinguish promiscuous from functional phosphorylation based on evolutionary information. Philosophical transactions of the Royal Society of London Series B, Biological sciences *367*, 2594-2606.

Li, C., and Chen, H. (2014). Enhancement of influenza virus transmission by gene reassortment. Current topics in microbiology and immunology *385*, 185-204.

Li, S.Q., Orlich, M., and Rott, R. (1990). Generation of seal influenza virus variants pathogenic for chickens, because of hemagglutinin cleavage site changes. Journal of virology *64*, 3297-3303.

Li, Z.W., Chu, W., Hu, Y., Delhase, M., Deerinck, T., Ellisman, M., Johnson, R., and Karin, M. (1999). The IKKbeta subunit of IkappaB kinase (IKK) is essential for nuclear factor kappaB activation and prevention of apoptosis. The Journal of experimental medicine *189*, 1839-1845.

Libermann, T.A., and Baltimore, D. (1990). Activation of interleukin-6 gene expression through the NF-kappa B transcription factor. Molecular and cellular biology *10*, 2327-2334.

Lienhard, G.E. (2008). Non-functional phosphorylations? Trends in biochemical sciences *33*, 351-352.

Ludwig, S., Ehrhardt, C., Neumeier, E.R., Kracht, M., Rapp, U.R., and Pleschka, S. (2001). Influenza virus-induced AP-1-dependent gene expression requires activation of the JNK signaling pathway. The Journal of biological chemistry *276*, 10990-10998.

Ludwig, S., Planz, O., Pleschka, S., and Wolff, T. (2003). Influenza-virus-induced signaling cascades: targets for antiviral therapy? Trends in molecular medicine *9*, 46-52.

Ludwig, S., Pleschka, S., Planz, O., and Wolff, T. (2006). Ringing the alarm bells: signalling and apoptosis in influenza virus infected cells. Cell Microbiol *8*, 375-386.

Luo, R., Fang, L., Jin, H., Wang, D., An, K., Xu, N., Chen, H., and Xiao, S. (2014). Label-free quantitative phosphoproteomic analysis reveals differentially regulated proteins and pathway in PRRSV-infected pulmonary alveolar macrophages. Journal of proteome research *13*, 1270-1280.

Ma, J., Shen, H., Liu, Q., Bawa, B., Qi, W., Duff, M., Lang, Y., Lee, J., Yu, H., Bai, J., *et al.* (2015). Pathogenicity and transmissibility of novel reassortant H3N2 influenza viruses with 2009 pandemic H1N1 genes in pigs. Journal of virology *89*, 2831-2841.

Ma, W., Brenner, D., Wang, Z., Dauber, B., Ehrhardt, C., Hogner, K., Herold, S., Ludwig, S., Wolff, T., Yu, K., *et al.*(2010a). The NS segment of an H5N1 highly pathogenic avian influenza virus (HPAIV) is sufficient to alter replication efficiency, cell tropism, and host range of an H7N1 HPAIV. Journal of virology *84*, 2122-2133.

Ma, W., Kahn, R.E., Richt, J.A., (2009). The pig as a mixing vessel for influenza viruses: Human and veterinary implications. J Mol Genet Med *3(1): 158–166*.

Ma, W., Lager, K.M., Vincent, A.L., Janke, B.H., Gramer, M.R., and Richt, J.A. (2009). The role of swine in the generation of novel influenza viruses. Zoonoses and public health *56*, 326-337.

Ma, W., Vincent, A.L., Lager, K.M., Janke, B.H., Henry, S.C., Rowland, R.R., Hesse, R.A., and Richt, J.A. (2010b). Identification and characterization of a highly virulent triple reassortant H1N1 swine influenza virus in the United States. Virus genes *40*, 28-36.

Maelfait, J., Roose, K., Bogaert, P., Sze, M., Saelens, X., Pasparakis, M., Carpentier, I., van Loo, G., and Beyaert, R. (2012). A20 (Tnfaip3) deficiency in myeloid cells protects against influenza A virus infection. PLoS pathogens *8*, e1002570.

Manz, B., Schwemmle, M., and Brunotte, L. (2013). Adaptation of avian influenza A virus polymerase in mammals to overcome the host species barrier. Journal of virology *87*, 7200-7209.

Marc, D., Barbachou, S., and Soubieux, D. (2013). The RNA-binding domain of influenzavirus non-structural protein-1 cooperatively binds to virus-specific RNA sequences in a structure-dependent manner. Nucleic acids research *41*, 434-449.

Matlin, K.S., Reggio, H., Helenius, A., and Simons, K. (1981). Infectious entry pathway of influenza virus in a canine kidney cell line. The Journal of cell biology *91*, 601-613.

Mazur, I., Wurzer, W.J., Ehrhardt, C., Pleschka, S., Puthavathana, P., Silberzahn, T., Wolff, T., Planz, O., and Ludwig, S. (2007). Acetylsalicylic acid (ASA) blocks influenza virus propagation via its NF-kappaB-inhibiting activity. Cell Microbiol *9*, 1683-1694.

Mbalaviele, G., Sommers, C.D., Bonar, S.L., Mathialagan, S., Schindler, J.F., Guzova, J.A., Shaffer, A.F., Melton, M.A., Christine, L.J., Tripp, C.S., *et al.* (2009). A novel, highly selective, tight binding IkappaB kinase-2 (IKK-2) inhibitor: a tool to correlate IKK-2 activity to the fate and functions of the components of the nuclear factor-kappaB pathway in arthritis-relevant cells and animal models. The Journal of pharmacology and experimental therapeutics *329*, 14-25.

McSkimming, D.I., Rasheed, K., and Kannan, N. (2017). Classifying kinase conformations using a machine learning approach. BMC bioinformatics *18*, 86.

Medina, R.A., and Garcia-Sastre, A. (2011). Influenza A viruses: new research developments. Nature reviews Microbiology *9*, 590-603.

Min, J.Y., Li, S., Sen, G.C., and Krug, R.M. (2007). A site on the influenza A virus NS1 protein mediates both inhibition of PKR activation and temporal regulation of viral RNA synthesis. Virology *363*, 236-243.

Morrison, D.K. (2012). MAP kinase pathways. Cold Spring Harbor perspectives in biology *4*.

Mostafa, A., Kanrai, P., Petersen, H., Ibrahim, S., Rautenschlein, S., and Pleschka, S. (2015). Efficient generation of recombinant influenza A viruses employing a new approach to overcome the genetic instability of HA segments. PloS one *10*, e0116917.

Muhlbauer, D., Dzieciolowski, J., Hardt, M., Hocke, A., Schierhorn, K.L., Mostafa, A., Muller, C., Wisskirchen, C., Herold, S., Wolff, T., *et al.*(2015). Influenza virus-induced caspase-dependent enlargement of nuclear pores promotes nuclear export of viral ribonucleoprotein complexes. Journal of virology *89*, 6009-6021.

Muramoto, Y., Noda, T., Kawakami, E., Akkina, R., and Kawaoka, Y. (2013). Identification of novel influenza A virus proteins translated from PA mRNA. Journal of virology *87*, 2455-2462.

Muramoto, Y., Shoemaker, J.E., Le, M.Q., Itoh, Y., Tamura, D., Sakai-Tagawa, Y., Imai, H., Uraki, R., Takano, R., Kawakami, E., *et al.* (2014). Disease severity is associated with differential gene expression at the early and late phases of infection in nonhuman primates infected with different H5N1 highly pathogenic avian influenza viruses. Journal of virology *88*, 8981-8997.

Nacken, W., Anhlan, D., Hrincius, E.R., Mostafa, A., Wolff, T., Sadewasser, A., Pleschka, S., Ehrhardt, C., and Ludwig, S. (2014). Activation of c-jun N-terminal kinase upon influenza A virus (IAV) infection is independent of pathogen-related receptors but dependent on amino acid sequence variations of IAV NS1. Journal of virology *88*, 8843-8852.

Nan, Y., Nan, G., and Zhang, Y.J. (2014). Interferon induction by RNA viruses and antagonism by viral pathogens. Viruses *6*, 4999-5027.

Nayak, D.P., Balogun, R.A., Yamada, H., Zhou, Z.H., and Barman, S. (2009). Influenza virus morphogenesis and budding. Virus research *143*, 147-161.

Nayak, D.P., Hui, E.K., and Barman, S. (2004). Assembly and budding of influenza virus. Virus research *106*, 147-165.

Neri, L.M., Borgatti, P., Capitani, S., and Martelli, A.M. (2002). The nuclear phosphoinositide 3-kinase/AKT pathway: a new second messenger system. Biochimica et biophysica acta *1584*, 73-80.

Nicolson, C., Major, D., Wood, J.M., and Robertson, J.S. (2005). Generation of influenza vaccine viruses on Vero cells by reverse genetics: an H5N1 candidate vaccine strain produced under a quality system. Vaccine *23*, 2943-2952.

Nimmerjahn, F., Dudziak, D., Dirmeier, U., Hobom, G., Riedel, A., Schlee, M., Staudt, L.M., Rosenwald, A., Behrends, U., Bornkamm, G.W., *et al.*(2004). Active NF-kappaB signalling is a prerequisite for influenza virus infection. The Journal of general virology *85*, 2347-2356.

Nolen, B., Taylor, S., and Ghosh, G. (2004). Regulation of protein kinases; controlling activity through activation segment conformation. Molecular cell *15*, 661-675.

Oberstein, A., Perlman, D.H., Shenk, T., and Terry, L.J. (2015). Human cytomegalovirus pUL97 kinase induces global changes in the infected cell phosphoproteome. Proteomics *15*, 2006-2022.

Ohman, T., Soderholm, S., Paidikondala, M., Lietzen, N., Matikainen, S., and Nyman, T.A. (2015). Phosphoproteome characterization reveals that Sendai virus infection activates mTOR signaling in human epithelial cells. Proteomics *15*, 2087-2097.

Oliveira, A.P., and Sauer, U. (2012). The importance of post-translational modifications in regulating Saccharomyces cerevisiae metabolism. FEMS yeast research *12*, 104-117.

Ozaki, H., Govorkova, E.A., Li, C., Xiong, X., Webster, R.G., and Webby, R.J. (2004). Generation of high-yielding influenza A viruses in African green monkey kidney (Vero) cells by reverse genetics. Journal of virology *78*, 1851-1857.

Ozawa, M., and Kawaoka, Y. (2011). Taming influenza viruses. Virus research *162*, 8-11.

Pahl, H.L., and Baeuerle, P.A. (1995). Expression of influenza virus hemagglutinin activates transcription factor NF-kappa B. Journal of virology *69*, 1480-1484.

Palese, P., and Young, J.F. (1982). Variation of influenza A, B, and C viruses. Science *215*, 1468-1474.

Paterson, D., and Fodor, E. (2012). Emerging roles for the influenza A virus nuclear export protein (NEP). PLoS pathogens *8*, e1003019.

Peyssonnaux, C., Provot, S., Felder-Schmittbuhl, M.P., Calothy, G., and Eychene, A. (2000). Induction of postmitotic neuroretina cell proliferation by distinct Ras downstream signaling pathways. Molecular and cellular biology *20*, 7068-7079.

Pinto, L.H., and Lamb, R.A. (2006). The M2 proton channels of influenza A and B viruses. The Journal of biological chemistry *281*, 8997-9000.

Pinto, R., Herold, S., Cakarova, L., Hoegner, K., Lohmeyer, J., Planz, O., and Pleschka, S. (2011). Inhibition of influenza virus-induced NF-kappaB and Raf/MEK/ERK activation can reduce both virus titers and cytokine expression simultaneously in vitro and in vivo. Antiviral research *92*, 45-56.

Pleschka, S. (2008). RNA viruses and the mitogenic Raf/MEK/ERK signal transduction cascade. Biological chemistry *389*, 1273-1282.

Pleschka, S. (2013). Overview of influenza viruses. Current topics in microbiology and immunology *370*, 1-20.

Pleschka, S., Jaskunas, R., Engelhardt, O.G., Zurcher, T., Palese, P., and Garcia-Sastre, A. (1996). A plasmid-based reverse genetics system for influenza A virus. Journal of virology *70*, 4188-4192.

Pleschka, S., Wolff, T., Ehrhardt, C., Hobom, G., Planz, O., Rapp, U.R., and Ludwig, S. (2001). Influenza virus propagation is impaired by inhibition of the Raf/MEK/ERK signalling cascade. Nature cell biology *3*, 301-305.

Plotkin, J.B., and Dushoff, J. (2003). Codon bias and frequency-dependent selection on the hemagglutinin epitopes of influenza A virus. Proceedings of the National Academy of Sciences of the United States of America *100*, 7152-7157.

Popova, T.G., Turell, M.J., Espina, V., Kehn-Hall, K., Kidd, J., Narayanan, A., Liotta, L., Petricoin, E.F., 3rd, Kashanchi, F., Bailey, C., *et al.* (2010). Reverse-phase phosphoproteome analysis of signaling pathways induced by Rift valley fever virus in human small airway epithelial cells. PloS one *5*, e13805.

Portela, A., and Digard, P. (2002). The influenza virus nucleoprotein: a multifunctional RNA-binding protein pivotal to virus replication. The Journal of general virology *83*, 723-734.

Qi, M., and Elion, E.A. (2005). MAP kinase pathways. Journal of cell science *118*, 3569-3572.

Raman, M., Chen, W., and Cobb, M.H. (2007). Differential regulation and properties of MAPKs. Oncogene *26*, 3100-3112.

Razani, B., Reichardt, A.D., and Cheng, G. (2011). Non-canonical NF-kappaB signaling activation and regulation: principles and perspectives. Immunological reviews *244*, 44-54.

Reddy, R.H., Kim, H., Cha, S., Lee, B., and Kim, Y.J. (2017). Structure-Based Virtual Screening of Protein Tyrosine Phosphatase Inhibitors: Significance, Challenges, and Solutions. Journal of microbiology and biotechnology *27*, 878-895.

Rincon, M., and Davis, R.J. (2009). Regulation of the immune response by stress-activated protein kinases. Immunological reviews *228*, 212-224.

Roberts, K.L., Manicassamy, B., and Lamb, R.A. (2015). Influenza A virus uses intercellular connections to spread to neighboring cells. Journal of virology *89*, 1537-1549.

Roux, P.P., and Thibault, P. (2013). The coming of age of phosphoproteomics--from large data sets to inference of protein functions. Molecular & cellular proteomics : MCP *12*, 3453-3464.

Rust, M.J., Lakadamyali, M., Zhang, F., and Zhuang, X. (2004). Assembly of endocytic machinery around individual influenza viruses during viral entry. Nature structural & molecular biology *11*, 567-573.

Sarkar, S.N., Peters, K.L., Elco, C.P., Sakamoto, S., Pal, S., and Sen, G.C. (2004). Novel roles of TLR3 tyrosine phosphorylation and PI3 kinase in double-stranded RNA signaling. Nature structural & molecular biology *11*, 1060-1067.

Scheeff, E.D., Eswaran, J., Bunkoczi, G., Knapp, S., and Manning, G. (2009). Structure of the pseudokinase VRK3 reveals a degraded catalytic site, a highly conserved kinase fold, and a putative regulatory binding site. Structure *17*, 128-138.

Scheiblauer, H., Kendal, A.P., and Rott, R. (1995). Pathogenicity of influenza A/Seal/Mass/1/80 virus mutants for mammalian species. Archives of virology *140*, 341-348.

Scheidereit, C. (2006). IkappaB kinase complexes: gateways to NF-kappaB activation and transcription. Oncogene *25*, 6685-6705.

Schmitz, M.L., Kracht, M., and Saul, V.V. (2014). The intricate interplay between RNA viruses and NF-kappaB. Biochimica et biophysica acta *1843*, 2754-2764.

Schramp, M., Hedman, A., Li, W., Tan, X., and Anderson, R. (2012). PIP kinases from the cell membrane to the nucleus. Sub-cellular biochemistry *58*, 25-59.

Schwartz, D., and Gygi, S.P. (2005). An iterative statistical approach to the identification of protein phosphorylation motifs from large-scale data sets. Nature biotechnology *23*, 1391-1398.

Shapira, S.D., Gat-Viks, I., Shum, B.O., Dricot, A., de Grace, M.M., Wu, L., Gupta, P.B., Hao, T., Silver, S.J., Root, D.E., *et al.* (2009). A physical and regulatory map of host-influenza interactions reveals pathways in H1N1 infection. Cell *139*, 1255-1267.

Sharma, K., D'Souza, R.C., Tyanova, S., Schaab, C., Wisniewski, J.R., Cox, J., and Mann, M. (2014). Ultradeep human phosphoproteome reveals a distinct regulatory nature of Tyr and Ser/Thr-based signaling. Cell reports *8*, 1583-1594.

Shaul, Y.D., and Seger, R. (2007). The MEK/ERK cascade: from signaling specificity to diverse functions. Biochimica et biophysica acta *1773*, 1213-1226.

Shaw, M.L.a.P., P (2013). Orthomyxoviridae. Lippincott Williams & Wilkins *6th*.

Shi, Y., Wu, Y., Zhang, W., Qi, J., and Gao, G.F. (2014). Enabling the 'host jump': structural determinants of receptor-binding specificity in influenza A viruses. Nature reviews Microbiology *12*, 822-831.

Skehel, J.J., and Wiley, D.C. (2000). Receptor binding and membrane fusion in virus entry: the influenza hemagglutinin. Annual review of biochemistry *69*, 531-569.

Skehel, J.J., and Wiley, D.C. (2002). Influenza haemagglutinin. Vaccine *20 Suppl 2*, S51-54.

Smith, A.E., and Helenius, A. (2004). How viruses enter animal cells. Science *304*, 237-242.

Smith, W., Manch, M.D.,Andrewes, C.H., Lond, M.D., Laidlaw, P.P., Camb, B.C. (1933). A VIRUS OBTAINED FROM INFLUENZA PATIENTS. The Lancet *222*, 3.

Stahl, J.A., Chavan, S.S., Sifford, J.M., MacLeod, V., Voth, D.E., Edmondson, R.D., and Forrest, J.C. (2013). Phosphoproteomic analyses reveal signaling pathways that facilitate lytic gammaherpesvirus replication. PLoS pathogens *9*, e1003583.

Stark, G.R., Kerr, I.M., Williams, B.R., Silverman, R.H., and Schreiber, R.D. (1998). How cells respond to interferons. Annual review of biochemistry *67*, 227-264.

Stegmann, T., Morselt, H.W., Scholma, J., and Wilschut, J. (1987). Fusion of influenza virus in an intracellular acidic compartment measured by fluorescence dequenching. Biochimica et biophysica acta *904*, 165-170.

Steinhauer, D.A. (1999). Role of hemagglutinin cleavage for the pathogenicity of influenza virus. Virology *258*, 1-20.

Stetson, D.B., and Medzhitov, R. (2006). Type I interferons in host defense. Immunity *25*, 373-381.

Stokes, M.P., Farnsworth, C.L., Moritz, A., Silva, J.C., Jia, X., Lee, K.A., Guo, A., Polakiewicz, R.D., and Comb, M.J. (2012). PTMScan direct: identification and quantification of peptides from critical signaling proteins by immunoaffinity enrichment coupled with LC-MS/MS. Molecular & cellular proteomics : MCP *11*, 187-201.

Subbarao, K., Chen, H., Swayne, D., Mingay, L., Fodor, E., Brownlee, G., Xu, X., Lu, X., Katz, J., Cox, N., *et al.* (2003). Evaluation of a genetically modified reassortant H5N1 influenza A virus vaccine candidate generated by plasmid-based reverse genetics. Virology *305*, 192-200.

Sugrue, R.J., Bahadur, G., Zambon, M.C., Hall-Smith, M., Douglas, A.R., and Hay, A.J. (1990). Specific structural alteration of the influenza haemagglutinin by amantadine. The EMBO journal *9*, 3469-3476.

Sui, B., Bamba, D., Weng, K., Ung, H., Chang, S., Van Dyke, J., Goldblatt, M., Duan, R., Kinch, M.S., and Li, W.B. (2009). The use of Random Homozygous Gene Perturbation to identify novel host-oriented targets for influenza. Virology *387*, 473-481.

Sulzmaier, F.J., Jean, C., and Schlaepfer, D.D. (2014). FAK in cancer: mechanistic findings and clinical applications. Nature reviews Cancer *14*, 598-610.

Talon, J., Horvath, C.M., Polley, R., Basler, C.F., Muster, T., Palese, P., and Garcia-Sastre, A. (2000a). Activation of interferon regulatory factor 3 is inhibited by the influenza A virus NS1 protein. Journal of virology *74*, 7989-7996.

Talon, J., Salvatore, M., O'Neill, R.E., Nakaya, Y., Zheng, H., Muster, T., Garcia-Sastre, A., and Palese, P. (2000b). Influenza A and B viruses expressing altered NS1 proteins: A vaccine approach. Proceedings of the National Academy of Sciences of the United States of America *97*, 4309-4314.

Taubenberger, J.K., and Kash, J.C. (2011). Insights on influenza pathogenesis from the grave. Virus research *162*, 2-7.

Tauber, S., Ligertwood, Y., Quigg-Nicol, M., Dutia, B.M., and Elliott, R.M. (2012). Behaviour of influenza A viruses differentially expressing segment 2 gene products in vitro and in vivo. The Journal of general virology *93*, 840-849.

Trifonov, V., Khiabanian, H., and Rabadan, R. (2009). Geographic dependence, surveillance, and origins of the 2009 influenza A (H1N1) virus. The New England journal of medicine *361*, 115-119.

Tripodi, F., Nicastro, R., Reghellin, V., and Coccetti, P. (2015). Post-translational modifications on yeast carbon metabolism: Regulatory mechanisms beyond transcriptional control. Biochimica et biophysica acta *1850*, 620-627.

Tuna, N., Karabay, O., and Yahyaoglu, M. (2012). Comparison of efficacy and safety of oseltamivir and zanamivir in pandemic influenza treatment. Indian journal of pharmacology *44*, 780-783.

Turrell, L., Hutchinson, E.C., Vreede, F.T., and Fodor, E. (2015). Regulation of influenza A virus nucleoprotein oligomerization by phosphorylation. Journal of virology *89*, 1452-1455.

Vanhaesebroeck, B., Ali, K., Bilancio, A., Geering, B., and Foukas, L.C. (2005). Signalling by PI3K isoforms: insights from gene-targeted mice. Trends in biochemical sciences *30*, 194-204.

Vincent, A.L., Ma, W., Lager, K.M., Gramer, M.R., Richt, J.A., and Janke, B.H. (2009). Characterization of a newly emerged genetic cluster of H1N1 and H1N2 swine influenza virus in the United States. Virus genes *39*, 176-185.

Vlastaridis, P., Kyriakidou, P., Chaliotis, A., Van de Peer, Y., Oliver, S.G., and Amoutzias, G.D. (2017). Estimating the total number of phosphoproteins and phosphorylation sites in eukaryotic proteomes. GigaScience *6*, 1-11.

Wang, C., Deng, L., Hong, M., Akkaraju, G.R., Inoue, J., and Chen, Z.J. (2001). TAK1 is a ubiquitin-dependent kinase of MKK and IKK. Nature *412*, 346-351.

Wang, J., Basagoudanavar, S.H., Wang, X., Hopewell, E., Albrecht, R., Garcia-Sastre, A., Balachandran, S., and Beg, A.A. (2010). NF-kappa B RelA subunit is crucial for early IFN-beta expression and resistance to RNA virus replication. Journal of immunology *185*, 1720-1729.

Wang, S., Zhao, Z., Bi, Y., Sun, L., Liu, X., and Liu, W. (2013). Tyrosine 132 phosphorylation of influenza A virus M1 protein is crucial for virus replication by controlling the nuclear import of M1. Journal of virology *87*, 6182-6191.

Wang, X., Hussain, S., Wang, E.J., Wang, X., Li, M.O., Garcia-Sastre, A., and Beg, A.A. (2007). Lack of essential role of NF-kappa B p50, RelA, and cRel subunits in virus-induced type 1 IFN expression. Journal of immunology *178*, 6770-6776.

Wang, X., Li, M., Zheng, H., Muster, T., Palese, P., Beg, A.A., and Garcia-Sastre, A. (2000). Influenza A virus NS1 protein prevents activation of NF-kappaB and induction of alpha/beta interferon. Journal of virology *74*, 11566-11573.

Wang, Y., Zhou, J., Ruan, C., and Du, Y. (2012). Inhibition of type I interferon production via suppressing IKK-gamma expression: a new strategy for counteracting host antiviral defense by influenza A viruses? Journal of proteome research *11*, 217-223.

Watanabe, T., Watanabe, S., and Kawaoka, Y. (2010). Cellular networks involved in the influenza virus life cycle. Cell host & microbe *7*, 427-439.

Wendel, I., Rubbenstroth, D., Doedt, J., Kochs, G., Wilhelm, J., Staeheli, P., Klenk, H.D., and Matrosovich, M. (2015). The avian-origin PB1 gene segment facilitated replication and transmissibility of the H3N2/1968 pandemic influenza virus. Journal of virology *89*, 4170-4179.

Whittaker, G., Bui, M., and Helenius, A. (1996). Nuclear trafficking of influenza virus ribonuleoproteins in heterokaryons. Journal of virology *70*, 2743-2756.

Wilson, I.A., Skehel, J.J., and Wiley, D.C. (1981). Structure of the haemagglutinin membrane glycoprotein of influenza virus at 3 A resolution. Nature *289*, 366-373.

Wise, H.M., Hutchinson, E.C., Jagger, B.W., Stuart, A.D., Kang, Z.H., Robb, N., Schwartzman, L.M., Kash, J.C., Fodor, E., Firth, A.E., *et al.* (2012). Identification of a novel splice variant form of the influenza A virus M2 ion channel with an antigenically distinct ectodomain. PLoS pathogens *8*, e1002998.

Wojcechowskyj, J.A., Didigu, C.A., Lee, J.Y., Parrish, N.F., Sinha, R., Hahn, B.H., Bushman, F.D., Jensen, S.T., Seeholzer, S.H., and Doms, R.W. (2013). Quantitative phosphoproteomics reveals extensive cellular reprogramming during HIV-1 entry. Cell host & microbe *13*, 613-623.

Woronicz, J.D., Gao, X., Cao, Z., Rothe, M., and Goeddel, D.V. (1997). IkappaB kinase-beta: NF-kappaB activation and complex formation with IkappaB kinase-alpha and NIK. Science *278*, 866-869.

Wright, P.F., Neumann, G. and Kawaoka, Y. (2013). Orthomyxoviruses.

Wurzer, W.J., Ehrhardt, C., Pleschka, S., Berberich-Siebelt, F., Wolff, T., Walczak, H., Planz, O., and Ludwig, S. (2004). NF-kappaB-dependent induction of tumor necrosis factor-related apoptosis-inducing ligand (TRAIL) and Fas/FasL is crucial for efficient influenza virus propagation. The Journal of biological chemistry *279*, 30931-30937.

Wurzer, W.J., Planz, O., Ehrhardt, C., Giner, M., Silberzahn, T., Pleschka, S., and Ludwig, S. (2003). Caspase 3 activation is essential for efficient influenza virus propagation. The EMBO journal *22*, 2717-2728.

Xiao, H., Killip, M.J., Staeheli, P., Randall, R.E., and Jackson, D. (2013). The human interferon-induced MxA protein inhibits early stages of influenza A virus infection by retaining the incoming viral genome in the cytoplasm. Journal of virology *87*, 13053-13058.

Yamaguchi, H., and Wang, H.G. (2001). The protein kinase PKB/Akt regulates cell survival and apoptosis by inhibiting Bax conformational change. Oncogene *20*, 7779-7786.

Yamaoka, S., Courtois, G., Bessia, C., Whiteside, S.T., Weil, R., Agou, F., Kirk, H.E., Kay, R.J., and Israel, A. (1998). Complementation cloning of NEMO, a component of the IkappaB kinase complex essential for NF-kappaB activation. Cell *93*, 1231-1240.

Yen, H.L., Hoffmann, E., Taylor, G., Scholtissek, C., Monto, A.S., Webster, R.G., and Govorkova, E.A. (2006). Importance of neuraminidase active-site residues to the neuraminidase inhibitor resistance of influenza viruses. Journal of virology *80*, 8787-8795.

Zhang, L., Wang, J.C., Hou, L., Cao, P.R., Wu, L., Zhang, Q.S., Yang, H.Y., Zang, Y., Ding, J.P., and Li, J. (2015). Functional Role of Histidine in the Conserved His-x-Asp Motif in the Catalytic Core of Protein Kinases. Scientific reports *5*, 10115.

Zhang, Y., and Dong, C. (2007). Regulatory mechanisms of mitogen-activated kinase signaling. Cellular and molecular life sciences : CMLS *64*, 2771-2789.

Zhirnov, O.P., Syrtsev, V.V., Vorob'eva, I.V., and Klenk, H.D. (2008). [Site-directed modification of caspase cleavage site regions in avian influenza virus proteins]. Voprosy virusologii *53*, 16-21.

Acknowledgement

Writing down words would never be enough to express my gratitude to the people I name here. However as it is the only way I can express my feelings, I make an honest effort to bring those names together and also recapitulate that without them this work would have but remained a dream.

I thank Prof. Dr. M. Lienhard Schmitz for being an amazing positive influence on my ambitions, for having the patience to listen through my numerous project related problems and offering instant tips to resolve them and for being such a supportive supervisor. He was the one who completed my transition from a scientific amateur to a worldly-wise scientific researcher.

In Prof. Dr. Stephan Pleschka, I found a wonderful supervisor cum advisor cum scientific-North Star who motivated me to go that extra mile to publish and proceed even in the face of immense adversity at times. Thank you for being there for me whenever I needed.

A very special thanks for Prof. Michael U. Martin for being my doctor father and reviewer for my work and to Prof. Dr. Reinhard Dammann for kindly consenting to examine the defense session.

A sincere thank goes to Prof. Dr. Michael Kracht for his suggestions and inputs in my publications and to Axel Weber for bioinformatic analyses of my work. In the institute of biochemistry and institute of medical virology, I was lucky enough to have come across some great colleagues to all of whom I offer my sincere most thanks for everything that they did. Thank you Vera Saul, Markus Seibert, Olesja Ritter, Tabea Riedlinger, Julia Busch, Nelli Ens, Jana Haas, Ann-Christin Beitel, Georgette Stovall, Jan Hagenbucher, Mattias Riedl, Ebru Erogan, Julia Dzieciolowski, Pumaree Kanrai, Ahmed Elsayed, Christin Müller for

creating such a comfortable and friendly atmosphere in the lab. A big thanks to Ines Höfliger, for her unfailing ability to help whenever required. Away from blood-related family, some people made life so much easier. To Hilda Stekman, Alfonso Rodriguez, Julian Rodriguez, Lisa Dieterle, Francesca Ferrante, Dino Benedetto, Roxana Solga, Gosia Sotomska, Aleksandra Turkiewicz, Irina Kuznetsova and Virginia Friedrichs I say special thank you. Virginia Friedrichs you deserve a special mention for being my personal translator at times. Without you all it was not an easy journey.

I want to thank to my family specially to my Ma for always being there for me. The struggle of her life and her believe in me no matter what, keep me motivating towards big achievements. I think I was smart enough at the age of 14 to choose the right person for my life. Thank you dear husband for being a strong support system and emotional outlet for all these years. THANK YOU!